

Figure 57. NGC 3998: a barred lenticular galaxy with a Seyfert AGN and nuclear dust (Knapp et al. 1996). Despite its large stellar velocity dispersion, this galaxy does not have a partially depleted core. Gutiérrez et al. (2011) identified a bar at $R_{\text{maj}} \lesssim 8''$, a ring between $30'' \lesssim R_{\text{maj}} \lesssim 50''$, and an antitruncation in the light profile of the disk at $R_{\text{maj}} \sim 122''$. Laurikainen et al. (2010) found that NGC 3998 features a weak bar at $R_{\text{maj}} < 8''$, a bright lens at $R_{\text{maj}} < 15''$, and a weak bump in the surface brightness profile at $R_{\text{maj}} \sim 40''$. We see three distinct peaks in the ellipticity profile. The first two peaks occur at $R_{\text{maj}} \sim 7''$ and $R_{\text{maj}} \sim 15''$, and they correspond to a weak bar and to a faint oval component, respectively. These components are fit with two Ferrer functions. The third peak at $R_{\text{maj}} \sim 35''$ coincides with a bump in the surface brightness profile and is produced by a ring. The AGN component is modeled with a Gaussian profile.

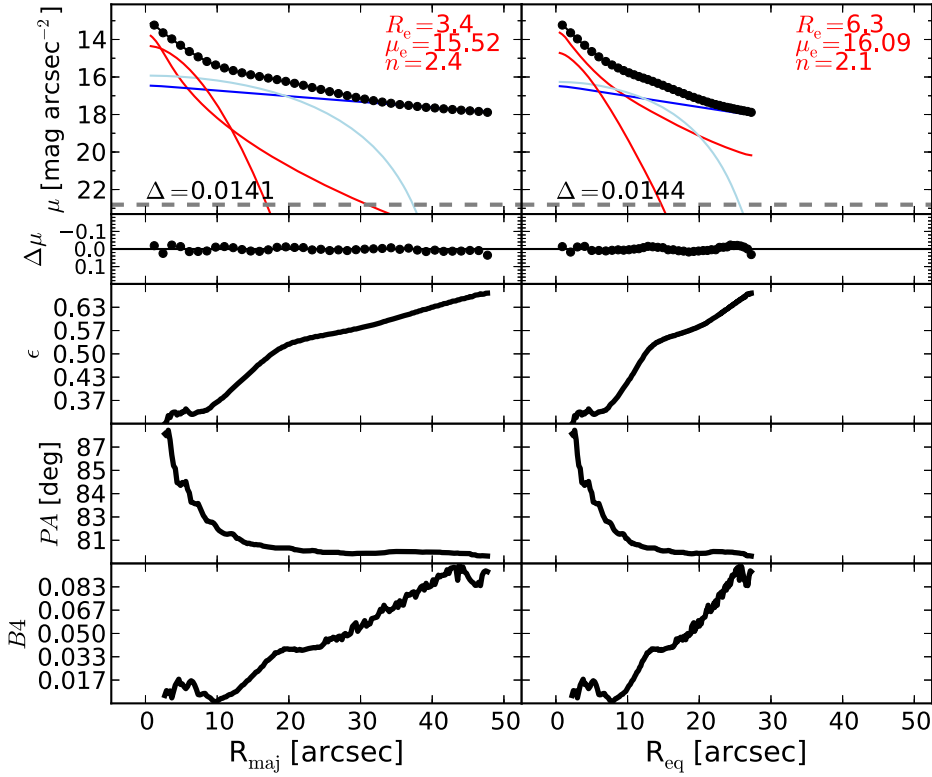


Figure 58. NGC 4026: an edge-on lenticular galaxy with a nuclear stellar disk (with size $\lesssim 0''.5$; Lledo et al. 2010). The unsharp mask reveals the presence of a bar ($R_{\text{maj}} \lesssim 30''$) and a disky component embedded in the bulge that is responsible for the peak at $R_{\text{maj}} \sim 5''$ in the B_4 profile. The disky component can also be recognized in the velocity map (ATLAS^{3D}). The bar is fit with a Ferrer function and the inner disk with a low- n Sérsic profile. We do not model the nuclear component to avoid degeneracies.

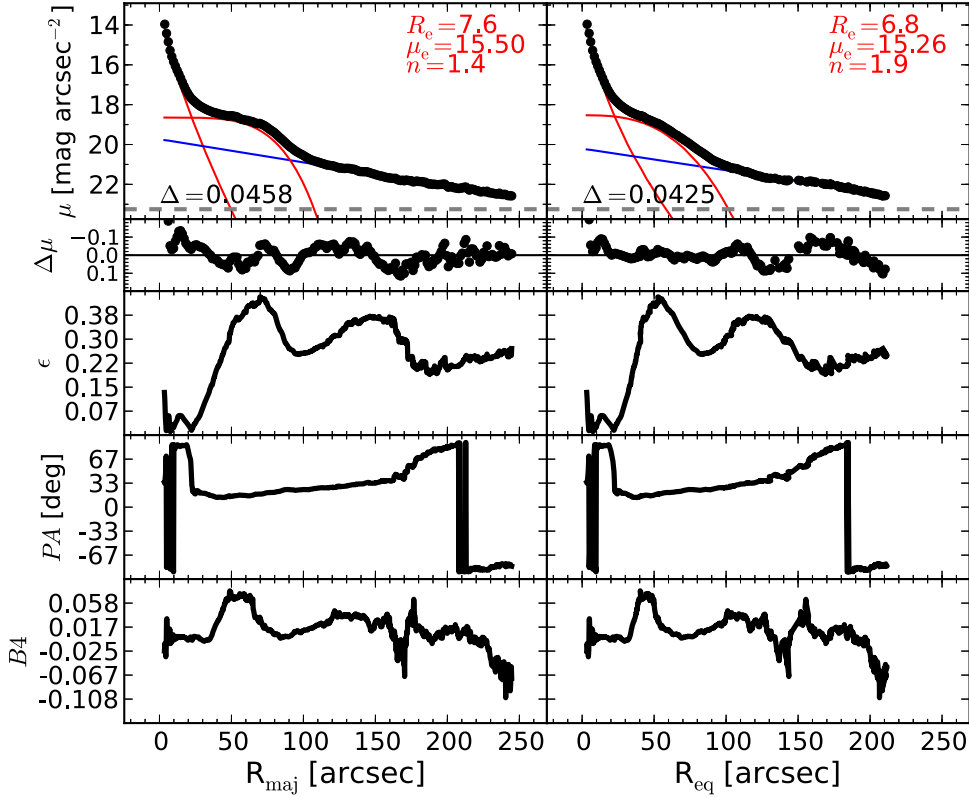


Figure 59. NGC 4151: a face-on barred spiral galaxy that hosts a Seyfert AGN (Véron-Cetty & Véron 2006) and circumnuclear dust (Pott et al. 2010). The nucleus of this galaxy is very bright, and the IRAF task `ellipse` fails at fitting the isophotes within $R_{\text{maj}} < 4''$; thus, our light profile starts at $R_{\text{maj}} \sim 4''$. The bar is fit with a low- n Sérsic profile.

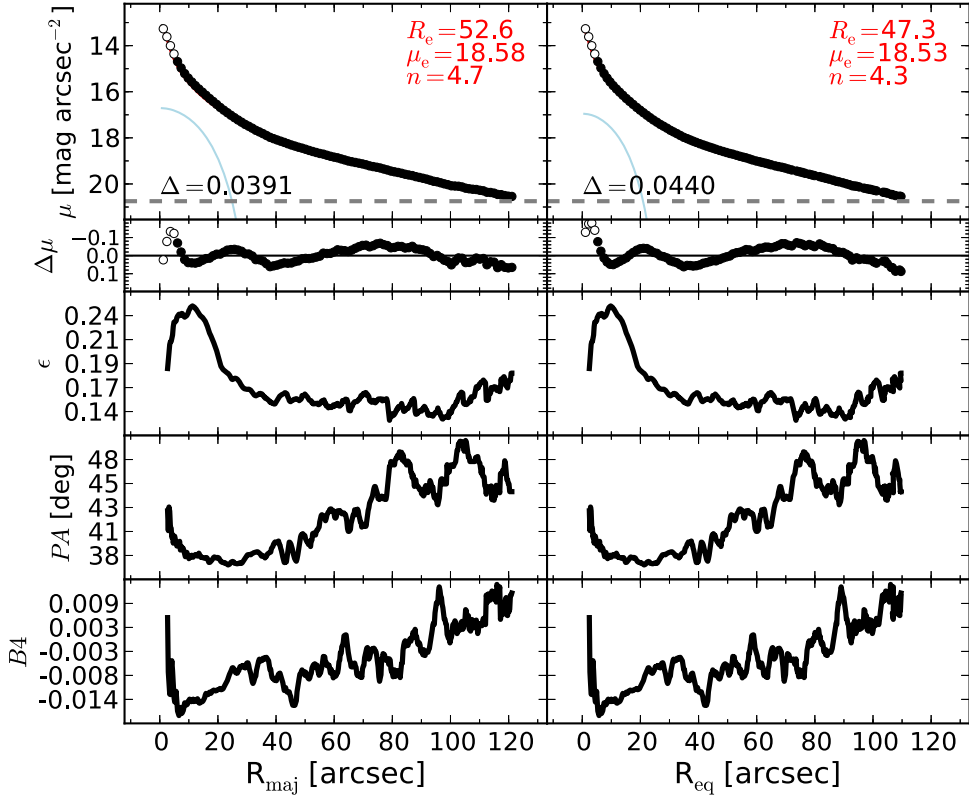


Figure 60. NGC 4261: an elliptical galaxy with a LINER nucleus (Véron-Cetty & Véron 2006) and a dusty nuclear disk (Tran et al. 2001). The galaxy features an unresolved partially depleted core (Rusli et al. 2013a). The ellipticity profile has a peak at $R_{\text{maj}} \sim 10''$, revealing the presence of an embedded component, which we model with a Ferrer function. The data within the innermost $6''$ are excluded from the fit.

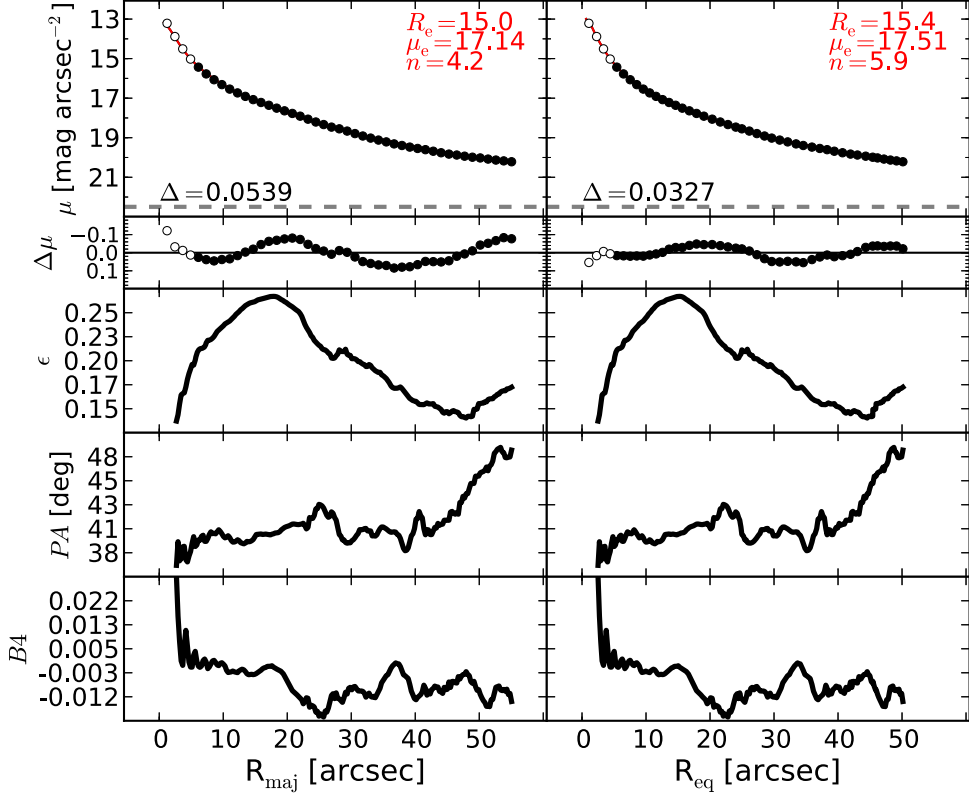


Figure 61. NGC 4291: an elliptical galaxy with an unresolved partially depleted core (Rusli et al. 2013a). After excluding the data within the innermost $6''$ from the fit, we observe that NGC 4291 can be reasonably well modeled with a Sérsic profile.

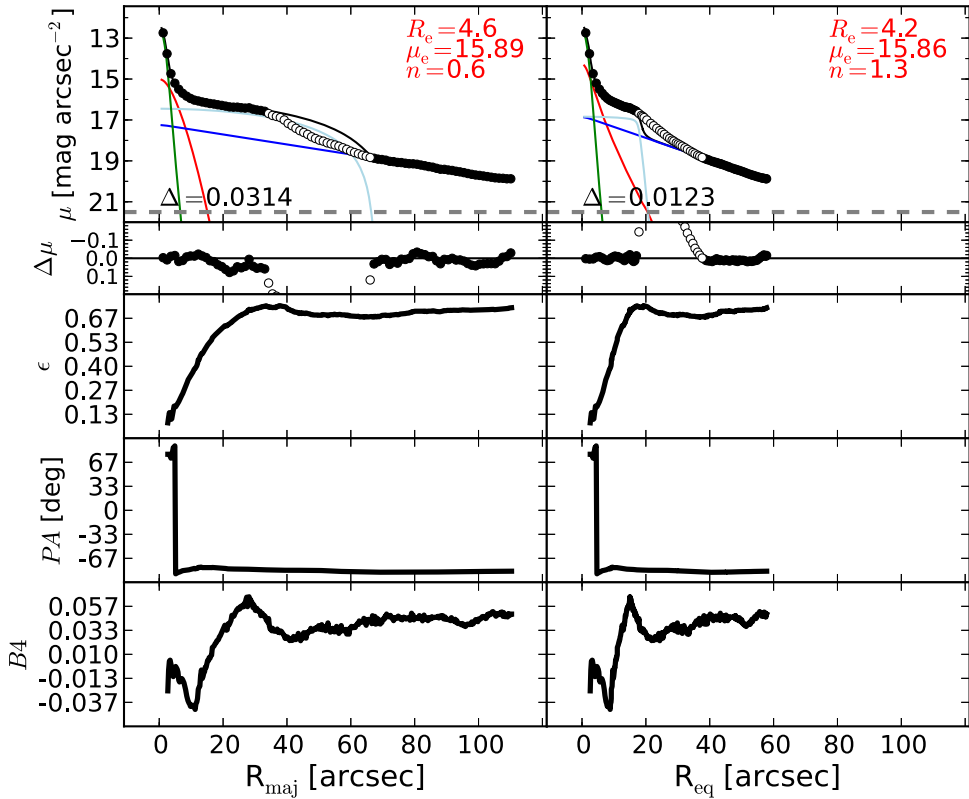


Figure 62. NGC 4388: an edge-on spiral galaxy with a Seyfert AGN (Véron-Cetty & Véron 2006) and copious nuclear dust (Martini et al. 2003). The peaks at $R_{\text{maj}} \sim 30''$ in the ellipticity and $B4$ profiles signal the presence of a bar. The data between $35'' \lesssim R_{\text{maj}} \lesssim 65''$ are excluded from the fit. The AGN component is fit with a Gaussian profile.

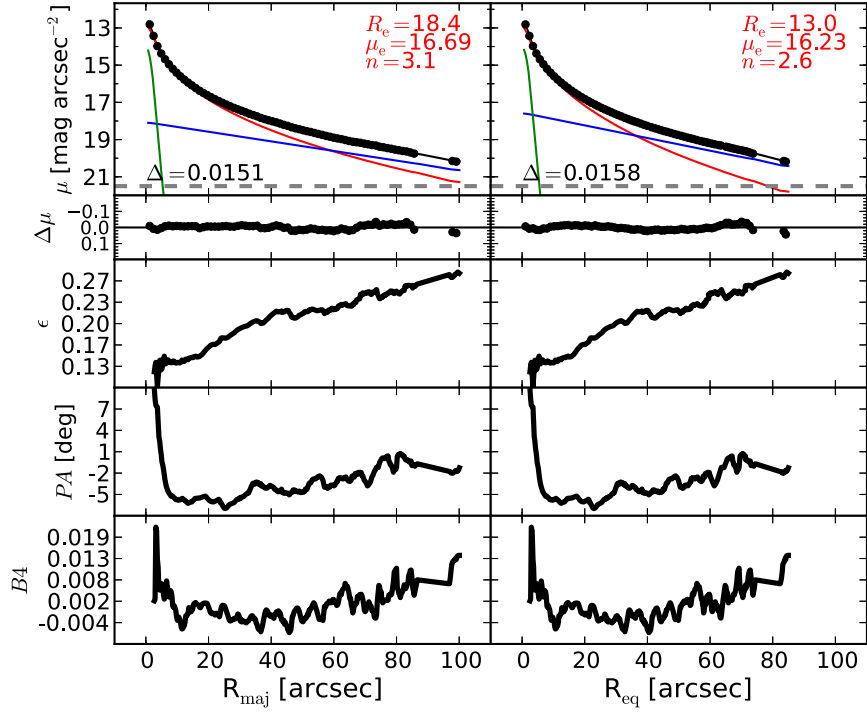


Figure 63. NGC 4459: a lenticular galaxy, whose disk profile has been reported to have an antitruncation at $R_{\text{maj}} \sim 119''$ (Gutiérrez et al. 2011). The ellipticity constantly increases across the entire observed radial range ($R_{\text{maj}} \lesssim 100''$). This is an indication that, going from the galaxy center to the outskirts, the disk component becomes increasingly more important over the spheroidal component. However, the lack of a plateau in the ellipticity profile at large radii implies that at $R_{\text{maj}} \sim 100''$ the contribution from the bulge is still significant compared to that of the disk. We note that the antitruncation reported by Gutiérrez et al. (2011) could be an artificial feature produced by the transition from the Sérsic bulge to the exponential disk. According to their analysis of the surface brightness profile of NGC 4459 (their Figure 14), the contribution from the disk completely overcomes that of the bulge beyond $R_{\text{maj}} \gtrsim 60''$. In the surface brightness profile, they identified two exponential declines with different scale lengths (the first between $60'' \lesssim R_{\text{maj}} \lesssim 110''$, and the second beyond $R_{\text{maj}} \gtrsim 120''$). However, we checked that in the radial range $60'' \lesssim R_{\text{maj}} \lesssim 110''$ the surface brightness profile is not a perfect exponential, but presents a curvature. This can be securely assessed only by fitting the data within the mentioned radial range with a single exponential function and plotting the residuals; if the residuals betray a curvature, the data cannot be accommodated by a single exponential function. According to our decomposition, the disk of NGC 4459 starts dominating beyond $R_{\text{maj}} \gtrsim 100''$. The exponential function of our model seems to nicely match the “second” exponential decline identified by Gutiérrez et al. (2011). We do not find evidence for any embedded components in our data. A nuclear light excess is modeled with a Gaussian profile.

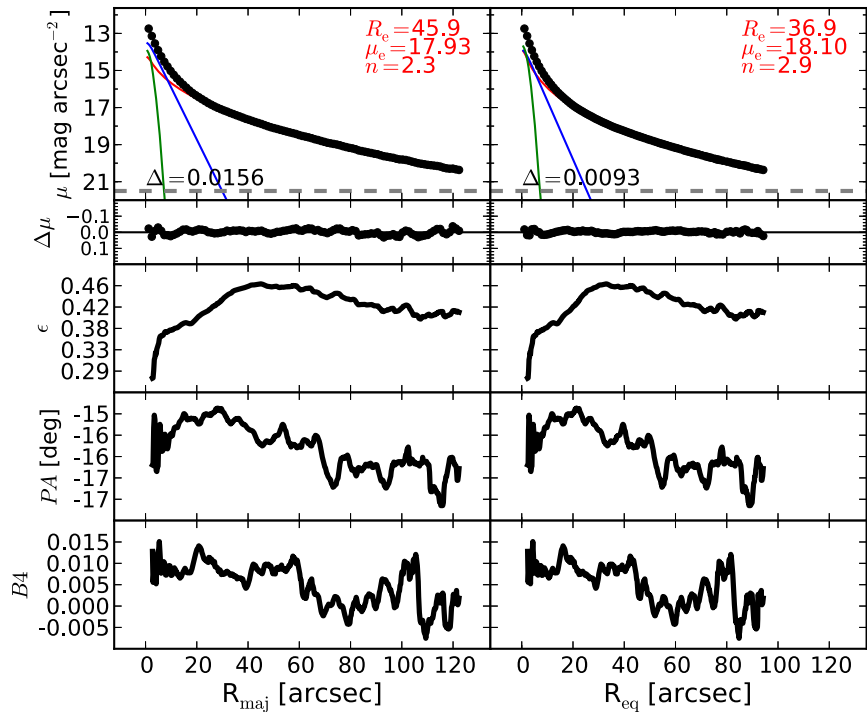


Figure 64. NGC 4473: an elliptical galaxy with an embedded disk (Ledo et al. 2010). The disk is clearly visible in the velocity map (ATLAS^{3D}, SLUGGS). We account for a nuclear excess of light by adding a narrow Gaussian function to the model.

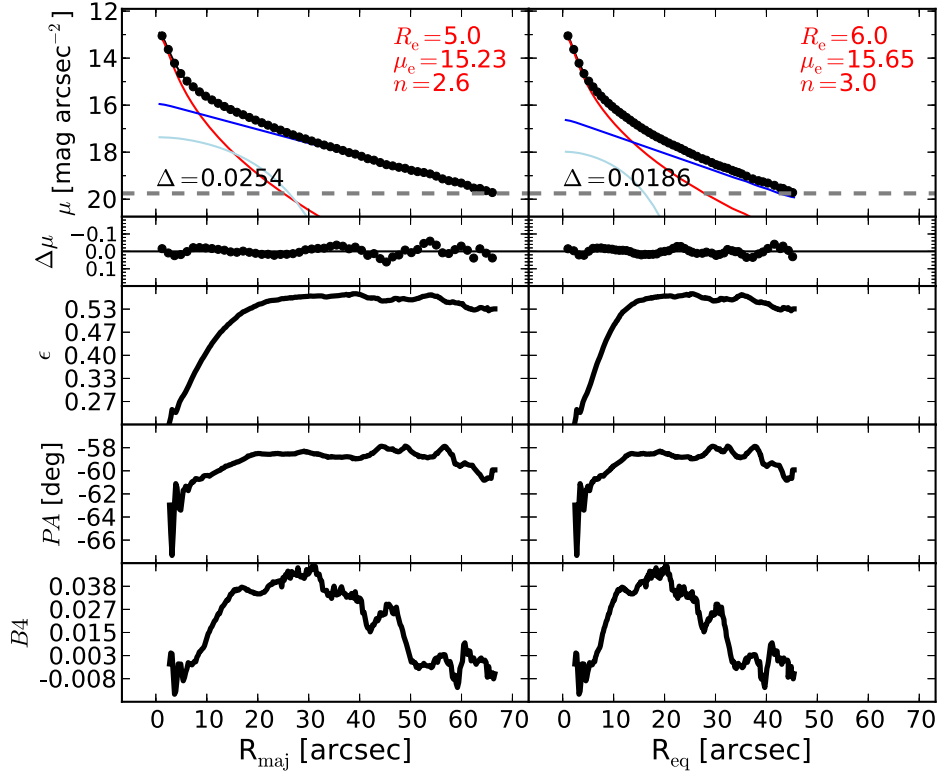


Figure 65. NGC 4564: an edge-on lenticular galaxy. In the unsharp mask, one can glimpse an oval structure extending out to $R_{\text{maj}} \lesssim 15''$ (see the peak in the $B4$ profile). Fitting NGC 4564 with a Sérsic + exponential model produces poor residuals. However, the addition of a Ferrer function to the model dramatically improves the fit and smoothes the residuals.

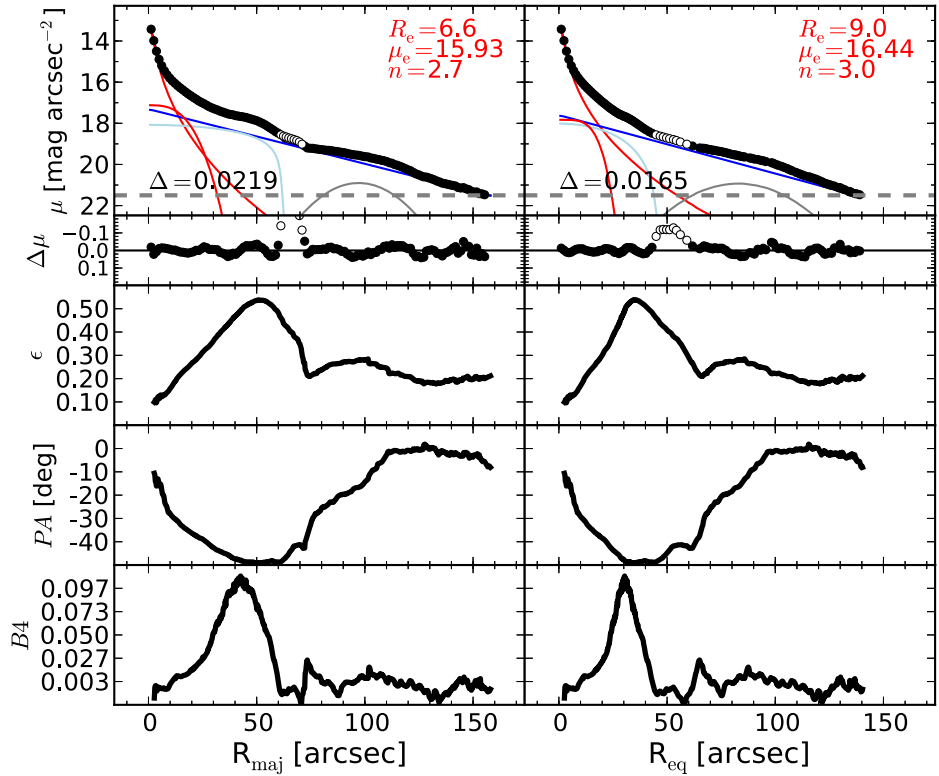


Figure 66. NGC 4596: an edge-on barred lenticular galaxy. The morphology of this galaxy is quite complex. The bar extends out to $R_{\text{maj}} \lesssim 50''$ and concludes in two evident ansae. The large-scale disk features a wide ring that is responsible for the curvature in the light profile observed within $60'' \lesssim R_{\text{maj}} \lesssim 130''$ (see also Comerón et al. 2014). An additional embedded disk component ($R_{\text{maj}} \lesssim 15''$) can be recognized in the $B4$ profile and in the velocity map. The bump in the light profile within $60'' \lesssim R_{\text{maj}} \lesssim 70''$ corresponds to the ansae of the bar, and this data range is therefore excluded from the fit. The large-scale bar is fit with a Ferrer function and the inner disk with a low- n Sérsic profile.

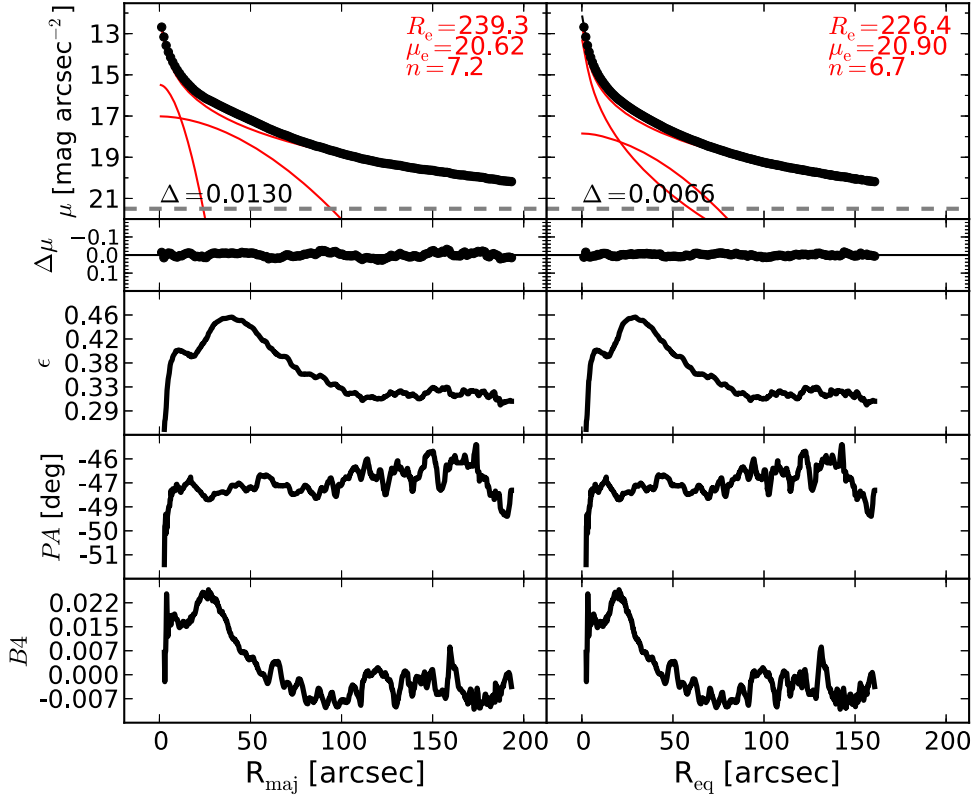


Figure 67. NGC 4697: an elliptical galaxy with an embedded disk (Scorza & Bender 1995). The velocity map (ATLAS^{3D}, SLUGGS) and the unsharp mask of NGC 4697 clearly show the presence of an intermediate-size disk embedded in the galaxy's spheroidal component. However, the ellipticity profile presents two peaks. The peak at $R_{\text{maj}} \sim 40''$ corresponds to the intermediate-size embedded disk just mentioned, while the peak at $R_{\text{maj}} \sim 10''$ pertains to a smaller inner disk. After testing different decomposition models, in which we fit the two embedded disks with different functions (exponential, Sérsic, Ferrer), while always describing the main spheroidal component with a Sérsic profile, we noticed that the spheroid parameters do not significantly vary among the various decompositions. Our preferred model for NGC 4697 consists of a Sérsic bulge + two Sérsic inner disks.

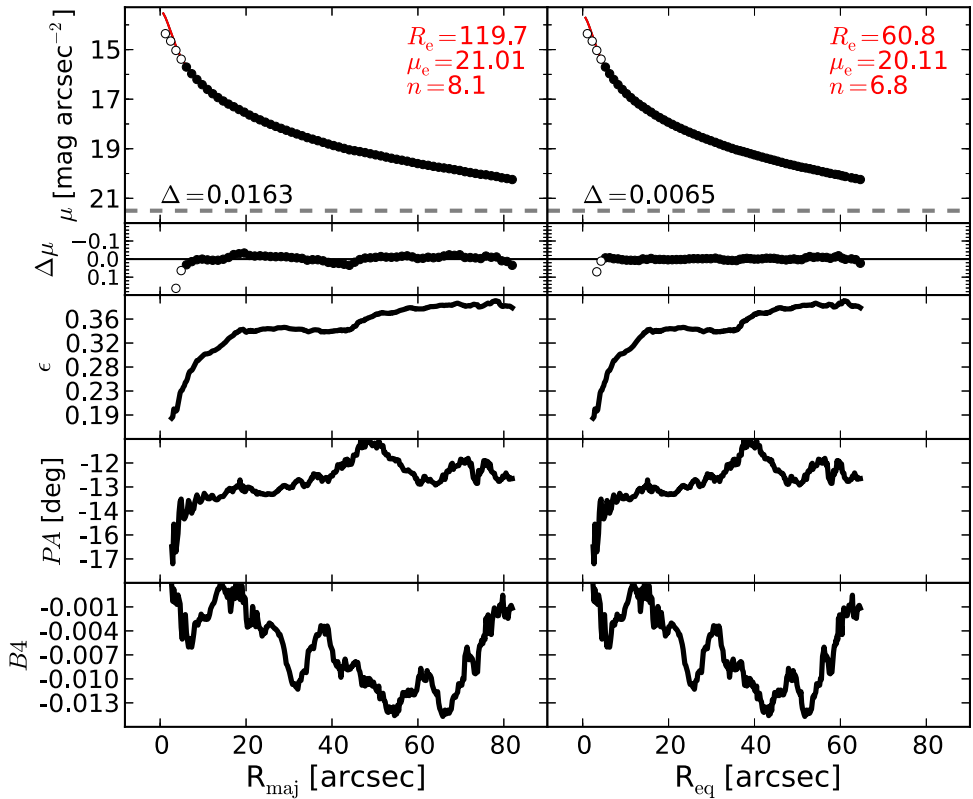


Figure 68. NGC 4889: the brightest member of the Coma Cluster, an elliptical galaxy with an unresolved partially depleted core (Rusli et al. 2013a). We exclude the innermost $6''$ from the fit and successfully model the galaxy with a single Sérsic profile.

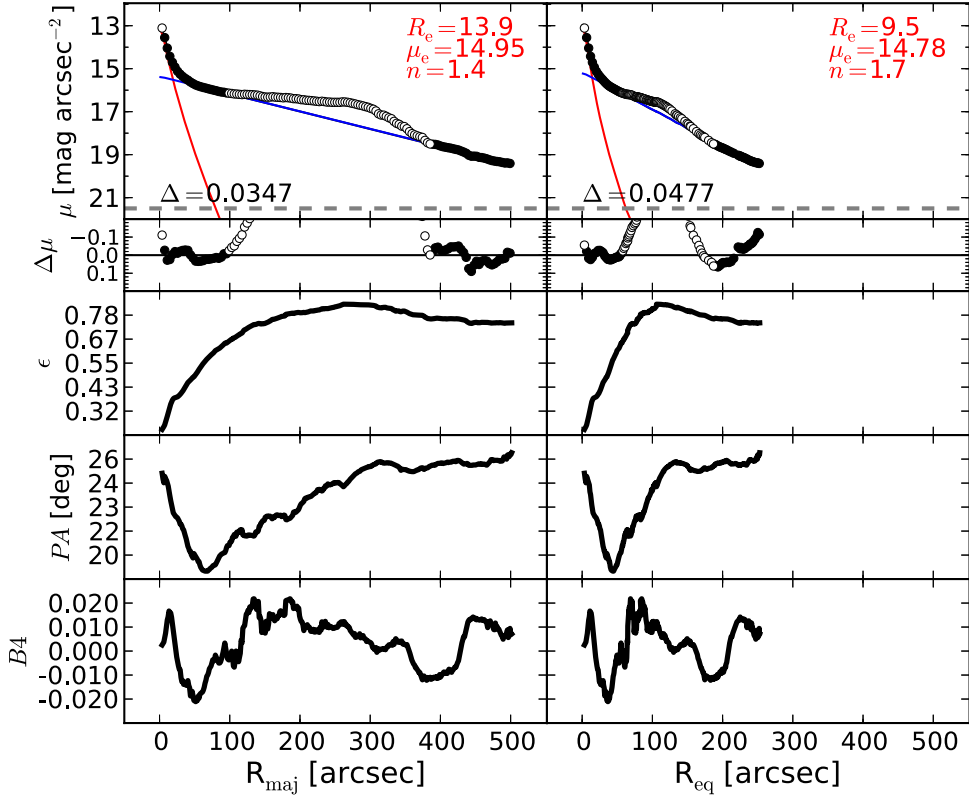


Figure 69. NGC 4945: an edge-on, dusty spiral galaxy that hosts a Seyfert AGN (Lin et al. 2011). The light profile has an obvious bump that can be ascribed to the bar. This bump cannot be easily modeled with a Ferrer function or with a Sérsic profile; thus, we exclude the data in the range $100'' \lesssim R_{\text{maj}} \sim 400''$ from the fit. We also exclude the data within the innermost $6.''4$ owing to the contribution from the AGN.

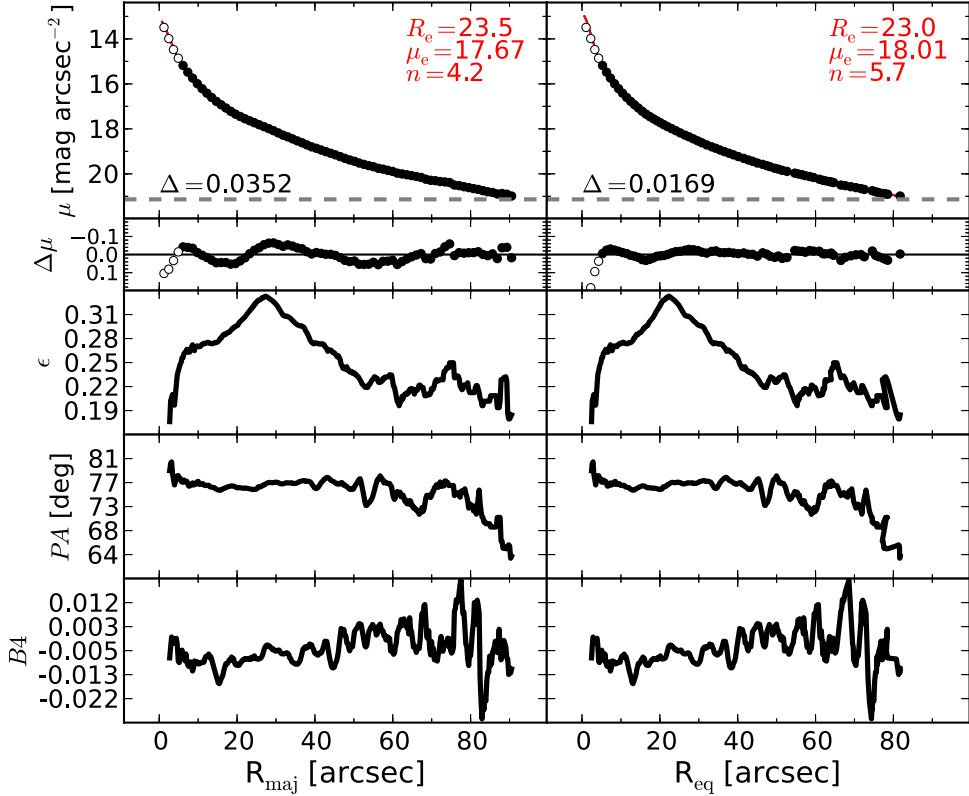


Figure 70. NGC 5077: an elliptical galaxy with an unresolved partially depleted core (Trujillo et al. 2004). We mask the data within the innermost $6.''1$ and fit the galaxy with a Sérsic profile.

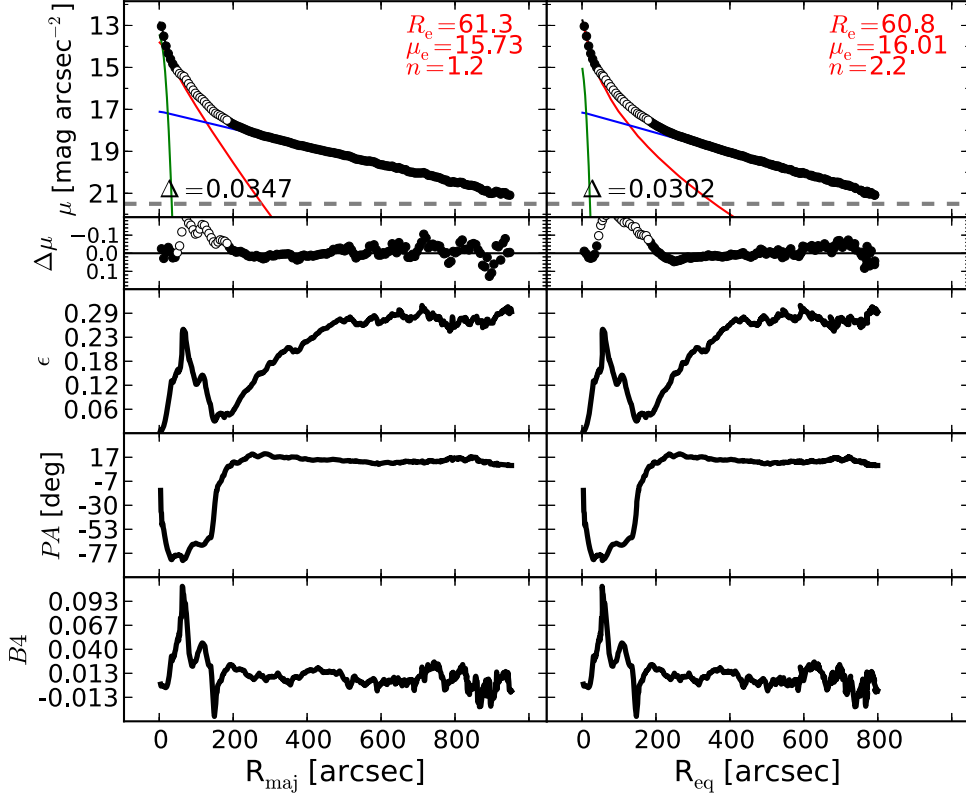


Figure 71. NGC 5128: a merging system. The data within $50'' \lesssim R_{\text{maj}} \lesssim 200''$ are excluded from the fit.

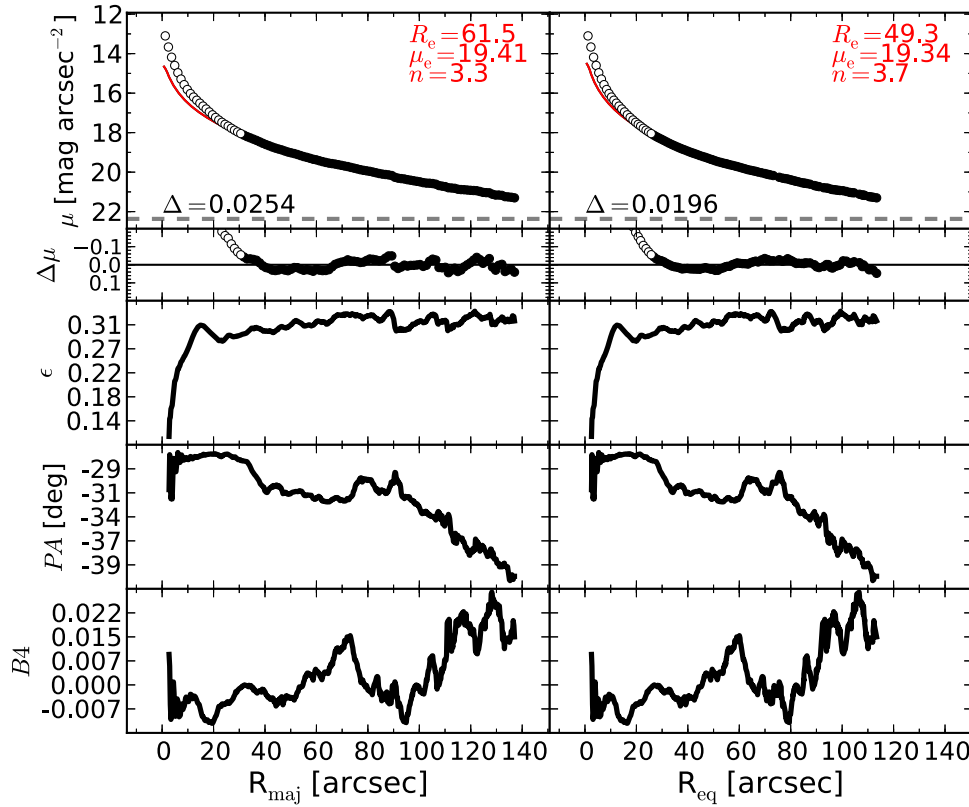


Figure 72. NGC 5576: an elliptical galaxy with a disturbed morphology. The isophotal parameters suggest the presence of an embedded disk ($R_{\text{maj}} \lesssim 20''$), but attempts to account for such a component were unsuccessful. The data within $R_{\text{maj}} \lesssim 36''$ are excluded from the fit, and the galaxy is modeled with a Sérsic profile.

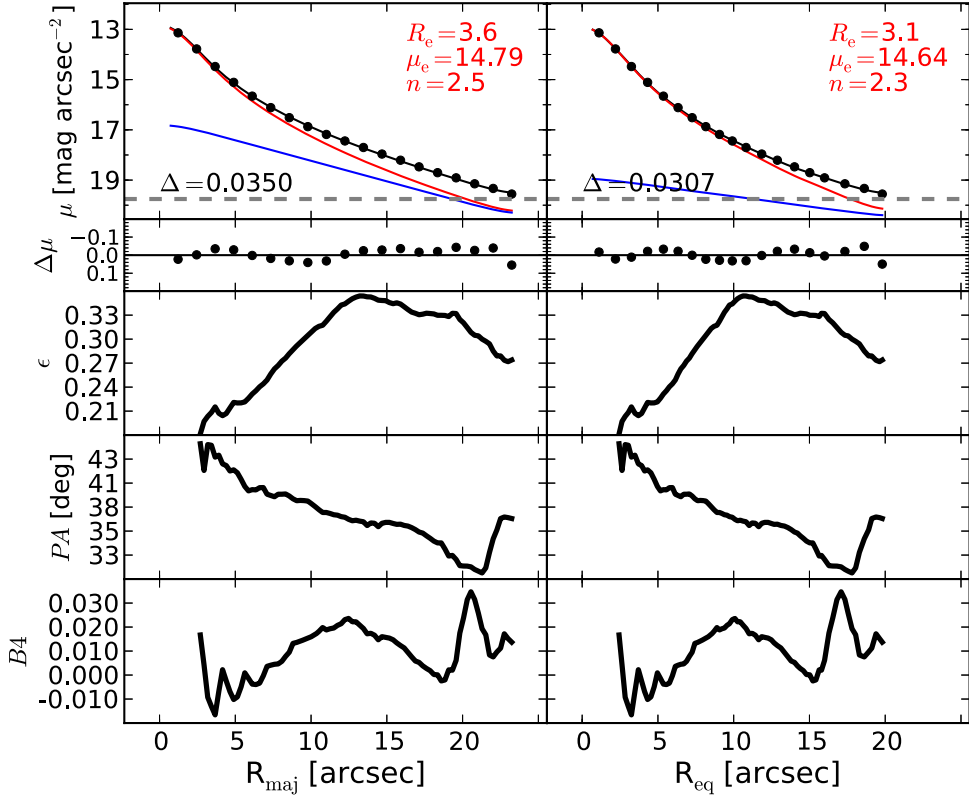


Figure 73. NGC 5845: a lenticular galaxy. From the unsharp mask and the velocity map (ATLAS^{3D}), we identify a disk, but it is not clear whether the disk is large scale or intermediate scale. The ellipticity profile has a peak at $R_{\text{maj}} \sim 13''$, which suggests that the disk is indeed intermediate scale, i.e., it does not dominate at large radii.

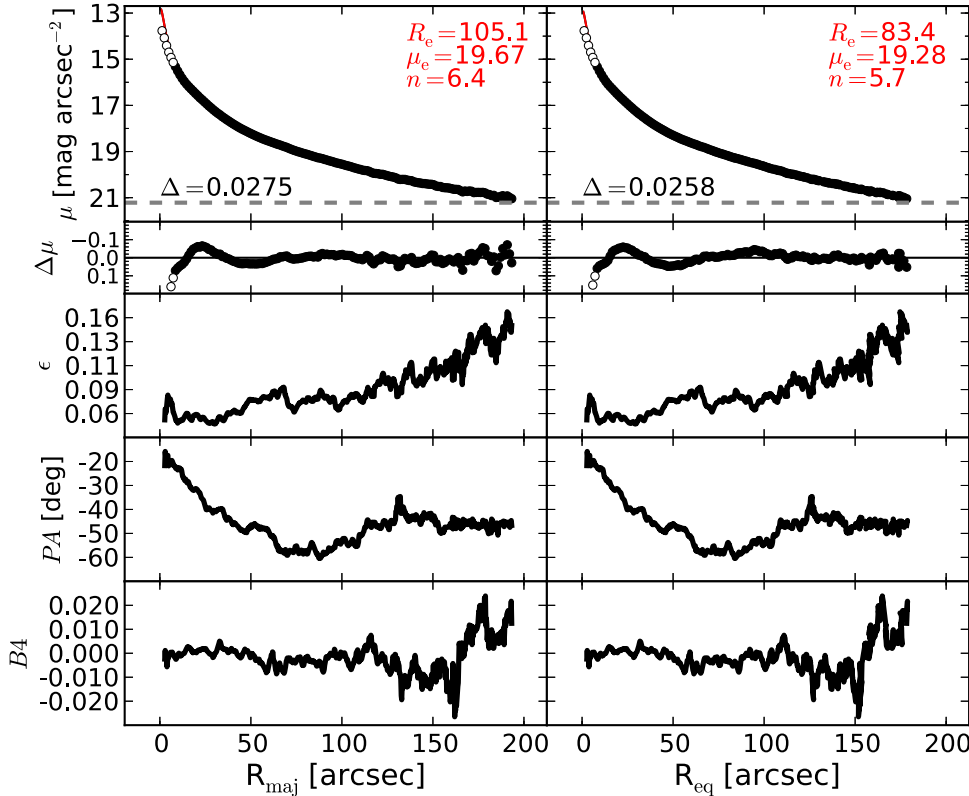


Figure 74. NGC 5846: an elliptical galaxy with an unresolved partially depleted core (Rusli et al. 2013a). This galaxy has a LINER nucleus (Carrillo et al. 1999) and filamentary nuclear dust (Tran et al. 2001). It also displays a strong isophotal twist between its center and $R_{\text{maj}} \sim 70''$. The light profile presents a slight bump at $R_{\text{maj}} \sim 20''$. However, the isophotal parameters, the unsharp mask, and the velocity map (ATLAS^{3D}) lack clear evidence for an embedded component. We thus model NGC 5846 with a single Sérsic profile, after masking the data within the innermost $6''$.

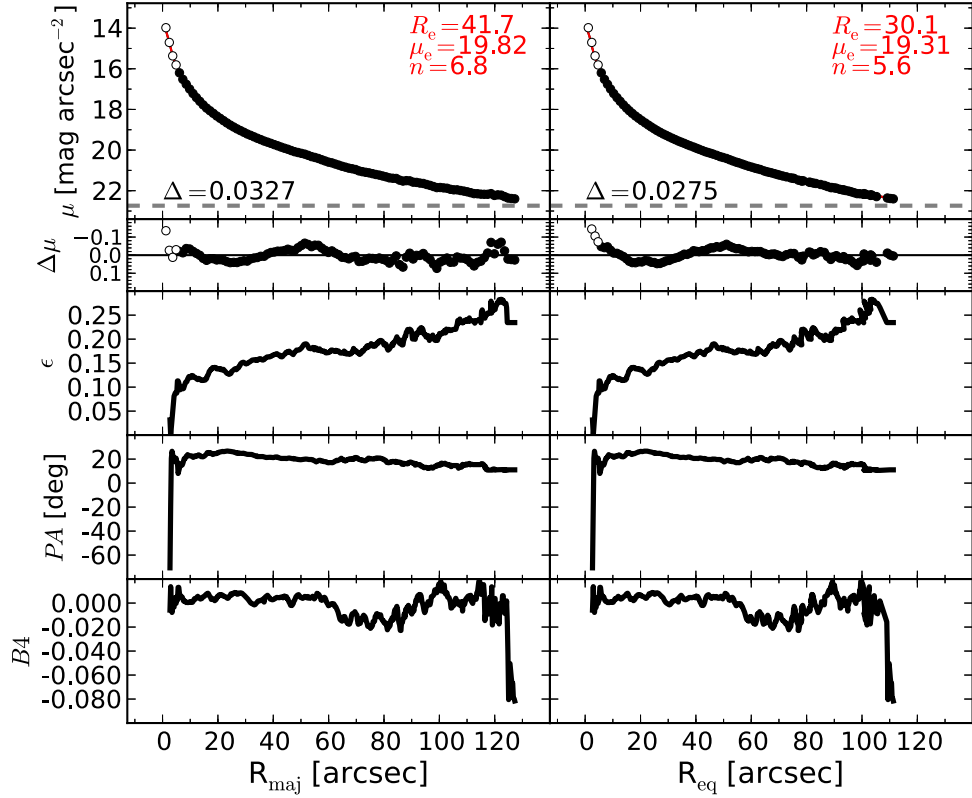


Figure 75. NGC 6251: an elliptical galaxy. Its large stellar velocity dispersion suggests the presence of a partially depleted core. The galaxy features a nuclear disk of dust (Ferrarese & Ford 1999) and a Seyfert AGN (Panessa & Bassani 2002). We mask the data within the innermost $6''.1$. A single Sérsic profile provides a good description of this galaxy.

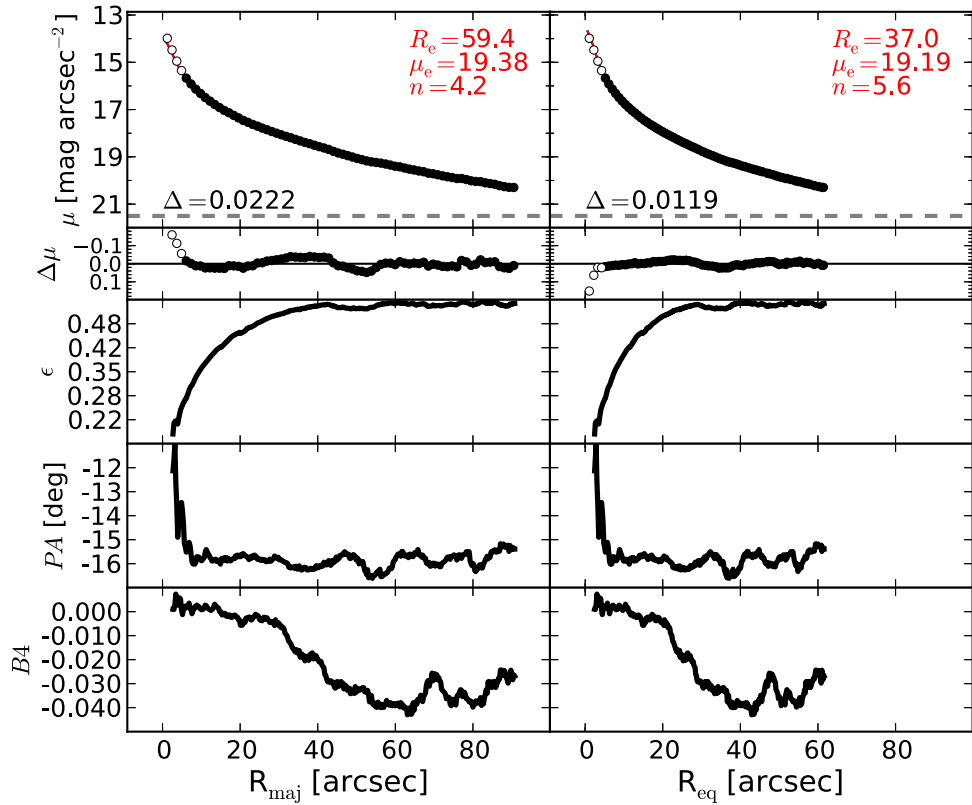


Figure 76. NGC 7052: an elliptical galaxy with an unresolved partially depleted core (Quillen et al. 2000). We mask the data within the innermost $6''.1$ and model the galaxy with a single Sérsic profile.

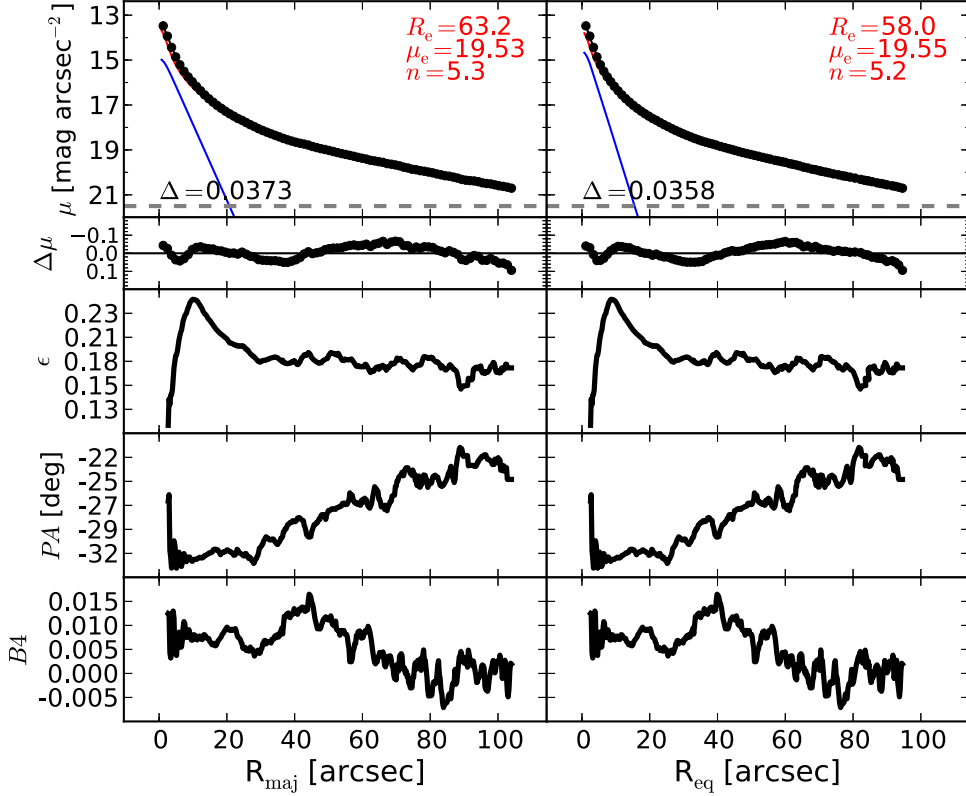


Figure 77. NGC 7619: an elliptical galaxy with an unresolved partially depleted core (Rusli et al. 2013a). We identified an embedded disk signaled by the peak at $R_{\text{maj}} \sim 10''$ in the ellipticity profile. The velocity map of this galaxy confirms the presence of a fast-rotating component (J. Falcon-Barroso 2015, private communication). We note that the residuals obtained from our bulge + inner-disk model do not suggest the presence of a partially depleted core.

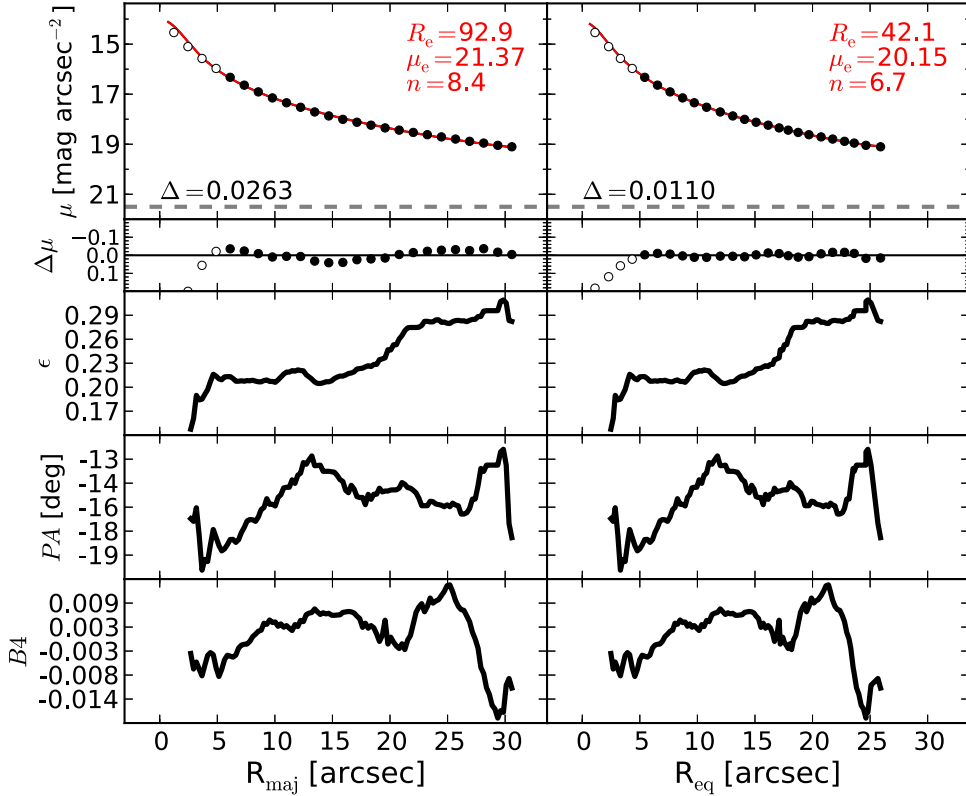


Figure 78. NGC 7768: an elliptical galaxy with an unresolved partially depleted core (Rusli et al. 2013a). The image of NGC 7768 is corrupted by a saturated star, which lies close to the galaxy. The sky background is not constant across the image. To be safe, we fit only the data within the innermost $R_{\text{maj}} \lesssim 30''$, where the contribution from the background is negligible. The data within $R_{\text{maj}} < 6.''1$ are excluded from the fit.

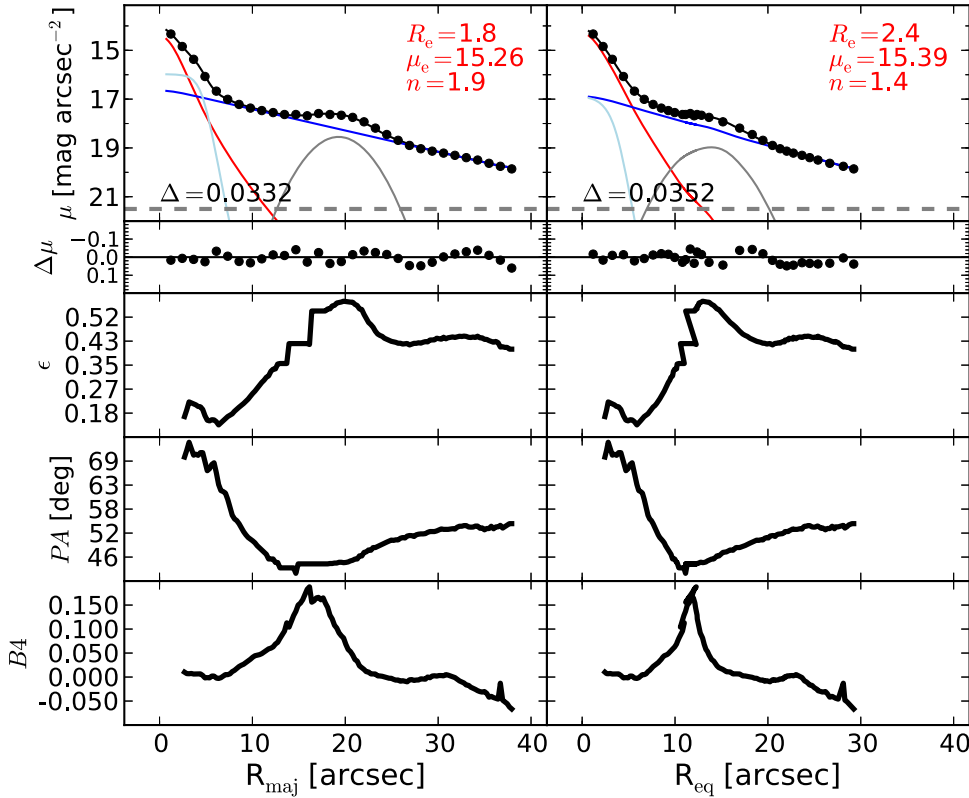


Figure 79. UGC 03789: a face-on spiral galaxy, featuring a ring ($R_{\text{maj}} \sim 20''$) and a nuclear bar ($R_{\text{maj}} \lesssim 4''$), which can be seen in the unsharp mask and produces corresponding peaks in the ellipticity and PA profiles. The bar is fit with a Ferrer function.

galaxy light profiles; therefore, their models implicitly include “m-n” or “m-c.” In the table caption, we comment on the most significant discrepancies between our results and those obtained by the other studies.

G.S. acknowledges the invaluable support received from Alessandro Marconi, Eleonora Sani, and Leslie Hunt in the early stages of this research. G.S. warmly thanks Chieng Peng, Peter Erwin, Luca Cortese, Giuseppe Gavazzi, Bililign Dullo, Paolo Bonfini, Elisabete Lima Da Cunha, and Gonzalo Diaz for useful discussion. We thank the anonymous referee for their thorough review and highly appreciate the comments and suggestions, which significantly contributed to improving the quality of the publication. This research was supported by Australian Research Council funding through grants DP110103509 and FT110100263. This work is based on observations made with the IRAC instrument (Fazio et al. 2004) on board the *Spitzer Space Telescope*, which is operated by the Jet Propulsion Laboratory, California Institute of Technology, under a contract with NASA. This research has made use of the GOLDMine database (Gavazzi et al. 2003) and the NASA/IPAC Extragalactic Database (NED), which is operated by the Jet Propulsion Laboratory, California Institute of Technology, under contract with the National Aeronautics and Space Administration.

APPENDIX 1D ANALYTICAL FUNCTIONS

Here we provide the mathematical expressions of the analytical functions used to model the observed surface brightness profiles, $\mu(R)$, of galaxies. The projected galactic

radius, R , corresponds to the distance of the isophotes from the galaxy center (along either the major or equivalent axis).

The Sérsic (1963, 1968) model is a three-parameter function of the following form:

$$\mu_{\text{Sérsic}}(\mu_e, R_e, n; R) = \mu_e + \frac{2.5 b_n}{\ln(10)} \left[\left(\frac{R}{R_e} \right)^{1/n} - 1 \right], \quad (5)$$

(Caon et al. 1993; Andredakis et al. 1995; Graham & Driver 2005), where μ_e is the surface brightness at the effective radius R_e that encloses half of the total light from the model. The Sérsic index n is the parameter that measures the curvature of the radial light profile, and b_n is a scalar value defined in terms of the Sérsic index n such that

$$\Gamma(2n) = 2\gamma(2n, b_n), \quad (6)$$

where Γ is the complete gamma function (Ciotti 1991) and γ is the incomplete gamma function defined by

$$\gamma(2n, x) = \int_0^x e^{-t} t^{2n-1} dt. \quad (7)$$

The exponential model is a special case ($n = 1$) of the Sérsic model. It can therefore be written as a two-parameter function such that

$$\mu_{\text{exponential}}(\mu_0, h; R) = \mu_0 + \frac{2.5}{\ln(10)} \left(\frac{R}{h} \right), \quad (8)$$

where μ_0 is the central surface brightness and h is the scale length equal to $R_e/1.678$.

The Gaussian model is another special case ($n = 0.5$) of the Sérsic model, and thus also a two-parameter function of the

following form:

$$\mu_{\text{Gaussian}}(\mu_0, \text{FWHM}; R) = \mu_0 + \frac{2.5}{\ln(10)} \left[\frac{R^2}{2(\text{FWHM}/2.355)^2} \right], \quad (9)$$

where μ_0 is the central surface brightness and FWHM is the full width at half-maximum of the Gaussian profile.

The Moffat (1969) model is a three-parameter function that can be expressed as

$$\mu_{\text{Moffat}}(\mu_0, \alpha, \beta; R) = \mu_0 - 2.5 \log \left[1 + \left(\frac{R}{\alpha} \right)^2 \right]^{-\beta}, \quad (10)$$

where μ_0 is the central surface brightness, α is related to the FWHM through

$$\text{FWHM} = 2\alpha\sqrt{2^{1/\beta} - 1}, \quad (11)$$

and β regulates the shape of the profile at large radii.

The Ferrer model is a four-parameter function defined as

$$\begin{aligned} \mu_{\text{Ferrer}}(\mu_0, R_{\text{out}}, \alpha, \beta; R) \\ = \begin{cases} \mu_0 - 2.5 \log \left[1 - \left(\frac{R}{R_{\text{out}}} \right)^{2-\beta} \right]^{\alpha} & \text{for } R < R_{\text{out}}, \\ +\infty & \text{for } R \geq R_{\text{out}} \end{cases} \end{aligned} \quad (12)$$

where μ_0 is the central surface brightness, α controls the sharpness of the truncation, β is related to the central slope, and R_{out} is the outer radial limit within which the function is defined.

The symmetric Gaussian ring is a three-parameter function of the following form:

$$\begin{aligned} \mu_{\text{Gaussian}}(\mu_0, R_0, \text{FWHM}; R) \\ = \mu_0 + \frac{2.5}{\ln(10)} \left[\frac{(R - R_0)^2}{2(\text{FWHM}/2.355)^2} \right], \end{aligned} \quad (13)$$

where μ_0 and FWHM have the same meaning as in Equation (9), and R_0 is the radius at which the Gaussian profile is centered.

REFERENCES

- Andredakis, Y. C., Peletier, R. F., & Balcells, M. 1995, *MNRAS*, **275**, 874
 Arnold, J. A., Romanowsky, A. J., Brodie, J. P., et al. 2011, *ApJL*, **736**, L26
 Arnold, J. A., Romanowsky, A. J., Brodie, J. P., et al. 2014, *ApJ*, **791**, 80
 Athanassoula, E., & Beaton, R. L. 2006, *MNRAS*, **370**, 1499
 Beaton, R. L., Majewski, S. R., Guhathakurta, P., et al. 2007, *ApJL*, **658**, L91
 Beifiori, A., Courteau, S., Corsini, E. M., & Zhu, Y. 2012, *MNRAS*, **419**, 2497
 Bender, R. 1990, *A&A*, **229**, 441
 Caon, N., Capaccioli, M., & D'Onofrio, M. 1993, *MNRAS*, **265**, 1013
 Capaccioli, M. 1987, in IAU Symp. 127, Structure and Dynamics of Elliptical Galaxies, ed. P. T. de Zeeuw, **47**
 Cappellari, M., Emsellem, E., Krajnović, D., et al. 2011, *MNRAS*, **413**, 813
 Cappellari, M., Verolme, E. K., van der Marel, R. P., et al. 2002, *ApJ*, **578**, 787
 Carrillo, R., Masegosa, J., Dultzin-Hacyan, D., & Ordoñez, R. 1999, RMxAA, **35**, 187
 Carter, D. 1987, *ApJ*, **312**, 514
 Ciambur, B. C. 2015, arXiv:1507.02691
 Ciotti, L. 1991, *A&A*, **249**, 99
 Comastri, A., Gilli, R., Marconi, A., Risaliti, G., & Salvati, M. 2015, arXiv:1501.03620
 Comerón, S., Elmegreen, B. G., Salo, H., et al. 2012, *ApJ*, **759**, 98
 Comerón, S., Knapen, J. H., Beckman, J. E., et al. 2010, *MNRAS*, **402**, 2462
 Comerón, S., Salo, H., Laurikainen, E., et al. 2014, *A&A*, **562**, A121
 Contini, T., Consideré, S., & Davoust, E. 1998, *A&AS*, **130**, 285
 de Vaucouleurs, G., de Vaucouleurs, A., Corwin, H. G., Jr., et al. 1991, Third Reference Catalogue of Bright Galaxies. Vol. I: Explanations and References. Vol. II: Data for Galaxies Between 0^h and 12^h. Vol. III: Data for Galaxies Between 12^h and 24^h
 Diaz, A. I., Prieto, M. A., & Wamsteker, W. 1988, *A&A*, **195**, 53
 D'Onofrio, M., Zaggia, S. R., Longo, G., Caon, N., & Capaccioli, M. 1995, *A&A*, **296**, 319
 Dressler, A. 1989, in IAU Symp. 134, Active Galactic Nuclei, ed. D. E. Osterbrock, & J. S. Miller, **217**
 Dullo, B. T., & Graham, A. W. 2013, arXiv:1310.5867
 Dullo, B. T., & Graham, A. W. 2014, *MNRAS*, **444**, 2700
 Elmegreen, B. G., & Elmegreen, D. M. 1985, *ApJ*, **288**, 438
 Elmegreen, D. M., Chromey, F. R., & Johnson, C. O. 1995, *AJ*, **110**, 2102
 Elmegreen, D. M., Elmegreen, B. G., & Eberwein, K. S. 2002, *ApJ*, **564**, 234
 Emsellem, E., Cappellari, M., Krajnović, D., et al. 2011, *MNRAS*, **414**, 888
 Erwin, P. 2004, *A&A*, **415**, 941
 Erwin, P. 2015, *ApJ*, **799**, 226
 Erwin, P., Beckman, J. E., & Pohlen, M. 2005, *ApJL*, **626**, L81
 Erwin, P., Beltrán, J. C. V., Graham, A. W., & Beckman, J. E. 2003, *ApJ*, **597**, 929
 Erwin, P., & Debattista, V. P. 2013, *MNRAS*, **431**, 3060
 Erwin, P., & Gadotti, D. A. 2012, *AdAst*, **2012**, 4
 Erwin, P., Gutiérrez, L., & Beckman, J. E. 2012, *ApJL*, **744**, L11
 Erwin, P., Pohlen, M., & Beckman, J. E. 2008, *AJ*, **135**, 20
 Erwin, P., & Sparke, L. S. 2003, *ApJS*, **146**, 299
 Fazio, G. G., Hora, J. L., Allen, L. E., et al. 2004, *ApJS*, **154**, 10
 Ferrarese, L., Côté, P., Jordán, A., et al. 2006, *ApJS*, **164**, 334
 Ferrarese, L., & Ford, H. C. 1999, *ApJ*, **515**, 583
 Ferrarese, L., & Merritt, D. 2000, *ApJL*, **539**, L9
 Fisher, D. B., & Drory, N. 2010, *ApJ*, **716**, 942
 Fontanot, F., Monaco, P., & Shankar, F. 2015, *MNRAS*, **453**, 4112
 Forbes, D. A., Brodie, J. P., & Huchra, J. 1997, *AJ*, **113**, 887
 Forbes, D. A., Franx, M., & Illingworth, G. D. 1994, *ApJL*, **428**, L49
 Franx, M., & Illingworth, G. D. 1988, *ApJL*, **327**, L55
 Gadotti, D. A. 2008, *MNRAS*, **384**, 420
 Gadotti, D. A., & de Souza, R. E. 2006, *ApJS*, **163**, 270
 Gadotti, D. A., & Sánchez-Janssen, R. 2012, *MNRAS*, **423**, 877
 Gavazzi, G., Boselli, A., Donati, A., Franzetti, P., & Scodéglio, M. 2003, *A&A*, **400**, 451
 Gebhardt, K., Bender, R., Bower, G., et al. 2000, *ApJL*, **539**, L13
 Graham, A. W. 2015, arXiv:1501.02937
 Graham, A. W., Colless, M. M., Busarello, G., Zaggia, S., & Longo, G. 1998, *A&AS*, **133**, 325
 Graham, A. W., & Driver, S. P. 2005, *PASA*, **22**, 118
 Graham, A. W., & Driver, S. P. 2007a, *ApJ*, **655**, 77
 Graham, A. W., & Driver, S. P. 2007b, *MNRAS*, **380**, L15
 Graham, A. W., Driver, S. P., Allen, P. D., & Liske, J. 2007, *MNRAS*, **378**, 198
 Graham, A. W., Dullo, B. T., & Savorgnan, G. A. D. 2015, *ApJ*, **804**, 32
 Graham, A. W., Erwin, P., Caon, N., & Trujillo, I. 2001, *ApJL*, **563**, L11
 Graham, A. W., Erwin, P., Trujillo, I., & Asensio Ramos, A. 2003, *AJ*, **125**, 2951
 Graham, A. W., & Guzmán, R. 2003, *AJ*, **125**, 2936
 Graham, A. W., & Scott, N. 2013, *ApJ*, **764**, 151
 Graham, A. W., & Scott, N. 2015, *ApJ*, **798**, 54
 Greenhill, L. J., Booth, R. S., Ellingsen, S. P., et al. 2003, *ApJ*, **590**, 162
 Grillmair, C. J., Faber, S. M., Lauer, T. R., et al. 1994, *AJ*, **108**, 102
 Gutiérrez, L., Erwin, P., Aladro, R., & Beckman, J. E. 2011, *AJ*, **142**, 145
 Häring, N., & Rix, H.-W. 2004, *ApJL*, **604**, L89
 Haynes, M. P., Giovanelli, R., Salzer, J. J., et al. 1999, *AJ*, **117**, 1668
 Jardel, J. R., Gebhardt, K., Shen, J., et al. 2011, *ApJ*, **739**, 21
 Jedrzejewski, R. I. 1987, *MNRAS*, **226**, 747
 Jun, H. D., & Im, M. 2008, *ApJL*, **678**, L97
 Khachikian, E. Y., & Weedman, D. W. 1974, *ApJ*, **192**, 581
 Kim, T., Gadotti, D. A., Sheth, K., et al. 2014, *ApJ*, **782**, 64
 Kim, T., Sheth, K., Gadotti, D. A., et al. 2015, *ApJ*, **799**, 99
 King, I. R., & Minkowski, R. 1966, *ApJ*, **143**, 1002
 Knapp, G. R., Rupen, M. P., Fich, M., Harper, D. A., & Wynn-Williams, C. G. 1996, *A&A*, **315**, L75
 Kormendy, J., & Gebhardt, K. 2001, in AIP Conf. Ser. 586, 20th Texas Symp. on Relativistic Astrophysics, ed. J. C. Wheeler, & H. Martel (Melville, NY: AIP), **363**

- Kormendy, J., & Richstone, D. 1995, *ARA&A*, **33**, 581
- Krajnović, D., Alatalo, K., Blitz, L., et al. 2013, *MNRAS*, **432**, 1768
- Krajnović, D., Emsellem, E., Cappellari, M., et al. 2011, *MNRAS*, **414**, 2923
- Laor, A., Fiore, F., Elvis, M., Wilkes, B. J., & McDowell, J. C. 1997, *ApJ*, **477**, 93
- Läske, R., Ferrarese, L., & van de Ven, G. 2014a, *ApJ*, arXiv:1311.1530
- Läske, R., Ferrarese, L., van de Ven, G., & Shankar, F. 2014b, *ApJ*, arXiv:1311.1531
- Laurikainen, E., Salo, H., & Buta, R. 2005, *MNRAS*, **362**, 1319
- Laurikainen, E., Salo, H., Buta, R., Knapen, J. H., & Comerón, S. 2010, *MNRAS*, **405**, 1089
- ledo, H. R., Sarzi, M., Dotti, M., Khochfar, S., & Morelli, L. 2010, *MNRAS*, **407**, 969
- Lin, L.-H., Taam, R. E., Yen, D. C. C., Muller, S., & Lim, J. 2011, *ApJ*, **731**, 15
- Magorrian, J., Tremaine, S., Richstone, D., et al. 1998, *AJ*, **115**, 2285
- Makovoz, D., & Marleau, F. R. 2005, *PASP*, **117**, 1113
- Marconi, A., & Hunt, L. K. 2003, *ApJL*, **589**, L21
- Martini, P., Regan, M. W., Mulchaey, J. S., & Pogge, R. W. 2003, *ApJS*, **146**, 353
- Moffat, A. F. J. 1969, *A&A*, **3**, 455
- Morrison, H., Caldwell, N., Schiavon, R. P., et al. 2011, *ApJL*, **726**, L9
- Muñoz-Mateos, J. C., Sheth, K., Gil de Paz, A., et al. 2013, *ApJ*, **771**, 59
- Munoz-Tunon, C., Prieto, M., Beckman, J., & Cepa, J. 1989, *Ap&SS*, **156**, 301
- Nieto, J.-L., Bender, R., Arnaud, J., & Surma, P. 1991, *A&A*, **244**, L25
- Nowak, N., Thomas, J., Erwin, P., et al. 2010, *MNRAS*, **403**, 646
- Panessa, F., & Bassani, L. 2002, *A&A*, **394**, 435
- Pastrav, B. A., Popescu, C. C., Tuffs, R. J., & Sansom, A. E. 2013a, *A&A*, **553**, A80
- Pastrav, B. A., Popescu, C. C., Tuffs, R. J., & Sansom, A. E. 2013b, *A&A*, **557**, A137
- Peeples, M. S., & Martini, P. 2006, *ApJ*, **652**, 1097
- Peng, C. Y., Ho, L. C., Impey, C. D., & Rix, H.-W. 2002, *AJ*, **124**, 266
- Peng, C. Y., Ho, L. C., Impey, C. D., & Rix, H.-W. 2010, *AJ*, **139**, 2097
- Pott, J.-U., Malkan, M. A., Elitzur, M., et al. 2010, *ApJ*, **715**, 736
- Quillen, A. C., Bower, G. A., & Stritzinger, M. 2000, *ApJS*, **128**, 85
- Ravindranath, S., Ho, L. C., Peng, C. Y., Filippenko, A. V., & Sargent, W. L. W. 2001, *AJ*, **122**, 653
- Richings, A. J., Uttley, P., & Körding, E. 2011, *MNRAS*, **415**, 2158
- Richstone, D., Ajhar, E. A., Bender, R., et al. 1998, *Natur*, **395**, A14
- Rix, H.-W., & White, S. D. M. 1990, *ApJ*, **362**, 52
- Rix, H.-W., & White, S. D. M. 1992, *MNRAS*, **254**, 389
- Rusli, S. P., Erwin, P., Saglia, R. P., et al. 2013a, *AJ*, **146**, 160
- Rusli, S. P., Thomas, J., Erwin, P., et al. 2011, *MNRAS*, **410**, 1223
- Rusli, S. P., Thomas, J., Saglia, R. P., et al. 2013b, *AJ*, **146**, 45
- Salucci, P., Szuszkiewicz, E., Monaco, P., & Danese, L. 1999, *MNRAS*, **307**, 637
- Sani, E., Marconi, A., Hunt, L. K., & Risaliti, G. 2011, *MNRAS*, **413**, 1479
- Savorgnan, G., Graham, A. W., Marconi, A., et al. 2013, *MNRAS*, **434**, 387
- Savorgnan, G. A. D., & Graham, A. W. 2015a, *MNRAS*, submitted
- Savorgnan, G. A. D., & Graham, A. W. 2015b, *MNRAS*, **446**, 2330
- Schaye, J., Crain, R. A., Bower, R. G., et al. 2015, *MNRAS*, **446**, 521
- Scorza, C., & Bender, R. 1990, *A&A*, **235**, 49
- Scorza, C., & Bender, R. 1995, *A&A*, **293**, 20
- Scott, N., Davies, R. L., Houghton, R. C. W., et al. 2014, *MNRAS*, **441**, 274
- Sérsic, J. L. 1963, *BAAA*, **6**, 41
- Sérsic, J. L. 1968, *Atlas de Galaxias Australes*
- Shankar, F. 2009, *NewAR*, **53**, 57
- Shankar, F. 2013, *CQGra*, **30**, 244001
- Sheth, K., Regan, M., Hinz, J. L., et al. 2010, *PASP*, **122**, 1397
- Simões Lopes, R. D., Storchi-Bergmann, T., de Fátima Saraiva, M., & Martini, P. 2007, *ApJ*, **655**, 718
- Tran, H. D., Tsvetanov, Z., Ford, H. C., et al. 2001, *AJ*, **121**, 2928
- Trujillo, I., Erwin, P., Asensio Ramos, A., & Graham, A. W. 2004, *AJ*, **127**, 1917
- Trujillo, I., Graham, A. W., & Caon, N. 2001, *MNRAS*, **326**, 869
- Véron-Cetty, M.-P., & Véron, P. 2006, *A&A*, **455**, 773
- Vika, M., Driver, S. P., Cameron, E., Kelvin, L., & Robotham, A. 2012, *MNRAS*, **419**, 2264
- Wadadekar, Y., Robbason, B., & Kembhavi, A. 1999, *ApJ*, **117**, 1219
- Whitmore, B. C., Lucas, R. A., McElroy, D. B., et al. 1990, *AJ*, **100**, 1489
- Worley, G. 1994, *ApJS*, **95**, 107
- Yee, H. K. C. 1992, in ASP Conf. Ser. 31, Relationships between Active Galactic Nuclei and Starburst Galaxies, ed. A. V. Filippenko (San Francisco, CA: ASP), 417

4

$$M_{\text{BH}} - L_{\text{gal}}, M_{\text{BH}} - L_{\text{sph}} \text{ and } M_{\text{BH}} - M_{*,\text{sph}}$$

In Chapter 3, reliable and accurate multicomponent decompositions were presented for 66 galaxies, our final sample, out of the 75 belonging to the initial sample. These 66 galaxies currently constitute the largest sample to date with reliable and homogeneous (i.e. derived in a systematic and consistent manner) structural decompositions that can be used to investigate correlations between directly measured black hole masses and host galaxy parameters.

This Chapter is dedicated to the analysis of three black hole mass correlations: the $M_{\text{BH}} - L_{\text{gal}}$, $M_{\text{BH}} - L_{\text{sph}}$ and $M_{\text{BH}} - M_{*,\text{sph}}$ relations. Four principal questions will be addressed.

1. Is the $M_{\text{BH}} - L_{\text{sph}}$ relation more fundamental than the $M_{\text{BH}} - L_{\text{gal}}$ relation (e.g. Kormendy & Ho 2013), or are they equally important (e.g. Läsker et al. 2014b)?
2. Graham & Scott (2013) identified two different sequences of spheroids in the $M_{\text{BH}} - L_{\text{sph}}$ diagram, namely Sérsic and core-Sérsic. However, their bulge luminosities were not derived from individual galaxy decompositions, but they were inferred from observed, total galaxy magnitudes through a mean statistical correction. Do we recover their result here, using the present dataset?
3. Does the quality of the present dataset allow us to identify any (additional) substructure in the three diagrams under study?
4. Some studies have distinguished pseudo-bulges and classical bulges according to their Sérsic index, and claimed that in the $M_{\text{BH}} - L_{\text{sph}}$ diagram pseudo-bulges are offset from the correlation defined by classical bulges. Here we test this result with our data.

A robust linear regression analysis is crucial for the study of black hole mass correlations. In particular, more emphasis is typically given to the slope rather than the intercept of scaling relations, because the slope is the parameter that theoretical models (currently) predict¹. Several studies (e.g. Tremaine et al. 2002; Graham 2007; Tundo et al. 2007; Graham 2016b) have pointed out inconsistencies between the values of the slope measured by different groups for the same correlation. These discrepancies can arise from the use of different galaxy samples, selection biases, or the statistical techniques used to perform the linear regression analysis.

In the following analysis, we will make use of three linear regression routines: the BCES code from Akritas & Bershady (1996), the FITEXY routine (Press et al., 1992), as modified by Tremaine et al. (2002), and the Bayesian estimator `linmix_err` (Kelly, 2007). Albeit its remarkable computational speed, the BCES estimator is not reliable in case of poor number statistics of the galaxy sample analysed, or when at least one low-precision measurement is included in the dataset, or if the mean square of the uncertainties associated with the independent variable is comparable to the variance of the distribution of the independent variable (Tremaine et al., 2002). When any of these circumstances occur, the modified FITEXY routine and the Bayesian estimator `linmix_err` perform better than the BCES routine (Tremaine et al., 2002; Novak et al., 2006; Park et al., 2012). All of these three estimators take into account the intrinsic scatter of a correlation, but only the FITEXY and the `linmix_err` codes allow one to measure it. The interest in measuring the intrinsic scatter of black hole mass scaling relations relies on the assumption that the galaxy parameter associated with the smallest intrinsic residual variance has the best chance of being causally correlated to the black hole mass.

The remainder of this Chapter comprises the published version of the paper “Supermassive Black Holes and Their Host Spheroids. II. The Red and Blue Sequence in the $M_{\text{BH}} - M_{*,\text{sph}}$ Diagram” by G. A. D. Savorgnan et al., as it appears in Volume 817 of the *The Astrophysical Journal*.

¹However, more and more attention is being paid to the intercept of black hole mass scaling relations, which plays a major role for the prediction of cosmic gravitational waves background from SMBH binary coalescence (e.g. Shannon et al. 2015; Shankar et al. 2016), the derivation of the SMBH mass function and space density, or the calibration of the reverberation mapping virial factor.



SUPERMASSIVE BLACK HOLES AND THEIR HOST SPHEROIDS. II. THE RED AND BLUE SEQUENCE IN THE $M_{\text{BH}}-M_{*,\text{sph}}$ DIAGRAM

GIULIA A. D. SAVORGNAN¹, ALISTER W. GRAHAM¹, ALESSANDRO MARCONI², AND ELEONORA SANI³

¹ Centre for Astrophysics and Supercomputing, Swinburne University of Technology, Hawthorn, Victoria 3122, Australia; gsavorgn@astro.swin.edu.au

² Dipartimento di Fisica e Astronomia, Università di Firenze, via G. Sansone 1, I-50019 Sesto Fiorentino, Firenze, Italy

³ European Southern Observatory, Alonso de Cordova, Vitacura 3107, Santiago, Chile

Received 2015 July 17; accepted 2015 November 23; published 2016 January 19

ABSTRACT

In our first paper, we performed a detailed (i.e., bulge, disks, bars, spiral arms, rings, halo, nucleus, etc.) decomposition of 66 galaxies, with directly measured black hole masses, M_{BH} , imaged at 3.6 μm with *Spitzer*. Our sample is the largest to date and, for the first time, the decompositions were checked for consistency with the galaxy kinematics. We present correlations between M_{BH} and the host spheroid (and galaxy) luminosity, L_{sph} (and L_{gal}), and also stellar mass, $M_{*,\text{sph}}$. While most previous studies have used galaxy samples that were overwhelmingly dominated by high-mass, early-type galaxies, our sample includes 17 spiral galaxies, half of which have $M_{\text{BH}} < 10^7 M_{\odot}$, and allows us to better investigate the poorly studied low-mass end of the $M_{\text{BH}}-M_{*,\text{sph}}$ correlation. The bulges of early-type galaxies follow $M_{\text{BH}} \propto M_{*,\text{sph}}^{1.04 \pm 0.10}$ and define a tight *red sequence* with intrinsic scatter $\epsilon_{(M_{\text{BH}}|M_{*,\text{sph}})} = 0.43 \pm 0.06$ dex and a median $M_{\text{BH}}/M_{*,\text{sph}}$ ratio of $0.68 \pm 0.04\%$, i.e., a $\pm 2\sigma$ range of 0.1%–5%. At the low-mass end, the bulges of late-type galaxies define a much steeper *blue sequence*, with $M_{\text{BH}} \propto M_{*,\text{sph}}^{2-3}$ and $M_{\text{BH}}/M_{*,\text{sph}}$ equal to 0.02% at $M_{\text{BH}} \approx 10^6 M_{\odot}$. We additionally report that (1) our Sérsic galaxy sample follows $M_{\text{BH}} \propto M_{*,\text{sph}}^{1.48 \pm 0.20}$, a less steep sequence than previously reported; (2) bulges with Sérsic index $n_{\text{sph}} < 2$, argued by some to be pseudo-bulges, are not offset to lower M_{BH} from the correlation defined by the current bulge sample with $n_{\text{sph}} > 2$; and (3) L_{sph} and L_{gal} correlate equally well with M_{BH} , in terms of intrinsic scatter, only for early-type galaxies—once reasonable numbers of spiral galaxies are included, the correlation with L_{sph} is better than that with L_{gal} .

Key words: black hole physics – galaxies: bulges – galaxies: elliptical and lenticular, cD – galaxies: evolution – galaxies: structure

1. INTRODUCTION

A quarter of a century ago, Dressler (1989) foresaw a “rough scaling of black hole mass with the mass of the spheroidal component” of galaxies, as suggested by the sequence of five galaxies (M87, M104, M31, M32, and the Milky Way). Yee (1992) then announced a linear relation between what was effectively black hole mass and galaxy mass for high-luminosity, bulge-dominated, early-type galaxies radiating near the Eddington limit. This “rough scaling” was a premature version of the early correlations between black hole mass, M_{BH} , and host spheroid luminosity, L_{sph} , and also host spheroid mass, M_{sph} (Kormendy & Richstone 1995; Magorrian et al. 1998; Marconi & Hunt 2003; Häring & Rix 2004). These initial studies were dominated by high-mass, early-type galaxies, for which they too reported a quasi-linear $M_{\text{BH}}-M_{\text{sph}}$ relation. Subsequent studies of the $M_{\text{BH}}-L_{\text{sph}}$ and $M_{\text{BH}}-M_{\text{sph}}$ diagrams (Ferrarese & Ford 2005; Graham 2007; Lauer et al. 2007a; Gültekin et al. 2009; Sani et al. 2011; Beifiori et al. 2012; Erwin & Gadotti 2012; van den Bosch et al. 2012; Vika et al. 2012; Kormendy & Ho 2013; McConnell & Ma 2013) continued to use galaxy samples dominated by high-mass, early-type systems with $M_{\text{BH}} \gtrsim 0.5 \times 10^8 M_{\odot}$, and they too recovered a near-linear relation. However, the consensus about a linear $M_{\text{BH}}-M_{\text{sph}}$ correlation was not unanimous. Some studies had reported a slope steeper than one, or noticed that the low-mass spheroids were offset to the right of (or below) the relation traced by the high-mass spheroids (Laor 1998, 2001; Wandel 1999; Ryan et al. 2007). Graham (2012), Graham & Scott (2013), and Scott et al. (2013) found two distinct trends in

the $M_{\text{BH}}-L_{\text{sph}}$ and $M_{\text{BH}}-M_{\text{sph}}$ diagrams: a linear and a super-quadratic correlation at the high- and low-mass ends, respectively.⁴ Recently, Läsker et al. (2014a; 2014b) derived 2.2 μm bulge luminosities for 35 galaxies (among which only four were classified as spiral galaxies), and reported a slope below unity for their $M_{\text{BH}}-L_{\text{sph}}$ relation. They also claimed that the black hole mass correlates equally well with the total galaxy luminosity as it does with the bulge luminosity.

The $M_{\text{BH}}-L_{\text{sph}}$ relation for early-type (elliptical + lenticular) galaxies can be predicted by combining two other correlations that involve the bulge stellar velocity dispersion, σ . One of these is the $M_{\text{BH}}-\sigma$ relation (Ferrarese & Merritt 2000; Gebhardt et al. 2000), which can be described with a single power law ($M_{\text{BH}} \propto \sigma^{5-6}$) over a wide range in velocity dispersion (70–350 km s^{-1} , e.g., Graham et al. 2011; McConnell et al. 2011; Graham & Scott 2013). The other is the $L_{\text{sph}}-\sigma$ relation, which has long been known to be a “double power law,” with $L_{\text{sph}} \propto \sigma^{5-6}$ at the luminous end⁵ (Schechter 1980; Malumuth & Kirshner 1981; Lauer et al. 2007b; von der Linden et al. 2007; Liu et al. 2008) and $L_{\text{sph}} \propto \sigma^2$ at intermediate and faint luminosities (Davies et al. 1983; Held et al. 1992; de Rijcke et al. 2005; Matković & Guzmán 2005; Balcells et al. 2007; Chilingarian et al. 2008; Forbes et al. 2008; Cody et al. 2009; Tortora et al. 2009; Kourkchi

⁴ Readers interested in an extensive review about the early discovery and successive improvements of these correlations should consult Graham (2016).

⁵ Recent work has the $M_{\text{BH}}-\sigma$ correlation as steep as $M_{\text{BH}} \propto \sigma^{6.5}$ (Savorgnan & Graham 2015) and the high-luminosity end of the $L_{\text{sph}}-\sigma$ correlation as steep as $L_{\text{sph}} \propto \sigma^8$ (Montero-Dorta et al. 2015).

et al. 2012). The change in slope of the $L_{\text{sph}}-\sigma$ relation occurs at $M_B \approx -20.5$ mag, corresponding to $\sigma \approx 200 \text{ km s}^{-1}$. The $M_{\text{BH}}-L_{\text{sph}}$ relation should, therefore, be better described by a “broken,” rather than a single, power law: with $M_{\text{BH}} \propto L_{\text{sph}}^{2.5}$ at the low-luminosity end, and $M_{\text{BH}} \propto L_{\text{sph}}^1$ at the high-luminosity end. Due to the scatter in the $M_{\text{BH}}-L_{\text{sph}}$ (or $M_{\text{BH}}-M_{\text{sph}}$) diagram, studies that have not sufficiently probed below $M_{\text{BH}} \approx 10^7 M_\odot$ can easily miss the change in slope occurring at $M_{\text{BH}} \approx 10^{(8\pm1)} M_\odot$, and erroneously recover a single log-linear relation.

When Graham (2012) pointed out this overlooked inconsistency between these linear and bent relations, he identified two different populations of galaxies, namely the core-Sérsic spheroids (Graham et al. 2003; Trujillo et al. 2004) and the Sérsic spheroids⁶, and attributed the change in slope (from super-quadratic to linear) to their different formation mechanisms. In this scenario, core-Sérsic spheroids are built in dry merger events where the black hole and the bulge grow at the same pace, increasing their mass in lock steps ($M_{\text{BH}} \propto L_{\text{sph}}^1$), whereas Sérsic spheroids originate from gas-rich processes in which the mass of the black hole increases more rapidly than the mass of its host spheroid ($M_{\text{BH}} \propto L_{\text{sph}}^{2.5}$).

Graham & Scott (2013, hereafter GS13) and Scott et al. (2013) presented separate power-law linear regressions for the Sérsic and core-Sérsic spheroids in the $M_{\text{BH}}-L_{\text{sph}}$ and $M_{\text{BH}}-M_{*,\text{sph}}$ (spheroid stellar mass) diagrams, probing down to $M_{\text{BH}} \approx 10^6 M_\odot$. To obtain their dust-corrected *bulge* magnitudes, they did not perform bulge/disk decompositions, but converted the *B*-band and *K_S*-band observed, total galaxy magnitudes into bulge magnitudes using a mean statistical bulge-to-total ratio based on each object’s morphological type and disk inclination.⁷ These mean statistical bulge-to-total ratios were obtained from the results of two-component (Sérsic-bulge/exponential-disk) decompositions in the literature. Here we investigate in more detail the $M_{\text{BH}}-L_{\text{sph}}$ and $M_{\text{BH}}-M_{*,\text{sph}}$ diagrams using state-of-the-art galaxy decompositions (Savorgnan & Graham 2015, hereafter Paper I) for galaxies with directly measured black hole masses. Our galaxies are large and nearby, which allows us to perform accurate multicomponent decompositions (instead of simple bulge/disk decompositions). Our decompositions were performed on 3.6 μm *Spitzer* satellite imagery, which is an excellent proxy for the stellar mass, superior to the *K*-band (Sheth et al. 2010, and references therein). Nine of our galaxies have $M_{\text{BH}} \lesssim 10^7 M_\odot$, which allows us to better constrain the slope of the correlation at the low-mass end. Furthermore, our galaxy sample includes 17 spiral galaxies, representing a notable improvement over past studies dominated by early-type galaxies. In a forthcoming paper, we will explore the relation between the black hole mass and the bulge dynamical mass, $M_{\text{dyn},\text{sph}} \propto R_e \sigma^2$, and address the issue of a black hole fundamental plane.

2. DATA

Our galaxy sample (see Table 1) consists of 66 objects for which a dynamical measurement of the black hole mass had been tabulated in the literature (by GS13 or Rusli et al. 2013) at

⁶ Core-Sérsic spheroids have partially depleted cores relative to their outer Sérsic light profile, whereas Sérsic spheroids have no central deficit of stars.

⁷ While this resulted in individual bulge magnitudes not being exactly correct, their large sample size allowed them to obtain a reasonable $M_{\text{BH}}-L_{\text{sph}}$ relation for the ensemble.

the time that we started this project, and for which we were able to obtain useful spheroid parameters from 3.6 μm *Spitzer* satellite imagery.

Spheroid magnitudes were derived from our state-of-the-art galaxy decompositions, which take into account bulge, disks, spiral arms, bars, rings, halo, extended or unresolved nuclear source, and partially depleted core. Kinematical information (Emsellem et al. 2011; Arnold et al. 2014; Scott et al. 2014) was used to confirm the presence of rotationally supported disk components in most early-type (elliptical + lenticular) galaxies, and to identify their extent (intermediate-scale disks that are fully embedded in the bulge, or large-scale disks that encase the bulge and dominate the light at large radii). It is worth stressing that, contrary to common knowledge, the majority of “elliptical” galaxies contain disks, i.e., they are not single-component spheroidal systems. Paper I presents the data set used here, including details about the data reduction process and the galaxy modeling technique that we developed. It also discusses how we estimated the uncertainties⁸ on the bulge magnitudes and presents the individual 66 galaxy decompositions, along with a comparison and discussion of past decompositions.

Bulge luminosities⁹ (Table 1) from Paper I were converted into stellar masses using a constant 3.6 μm mass-to-light ratio, $\Gamma_{3.6} = 0.6$ (Meidt et al. 2014). We additionally explored a more sophisticated way to compute mass-to-light ratios, using the color- $\Gamma_{3.6}$ relation published by Meidt et al. (2014), their Equation (4), which allows one to estimate $\Gamma_{3.6}$ of a galaxy from its [3.6]–[4.5] color. Individual [3.6]–[4.5] colors¹⁰ were taken from Peletier et al. (2012, column 8 of their Table 1) when available for our galaxies, or were estimated from the bulge stellar velocity dispersion, σ , using the color- σ relation presented by Peletier et al. (2012, their Figure 6). We found that the range in [3.6]–[4.5] color is small (0.06 mag), and thus the range in $\Gamma_{3.6}$ is also small (0.04). After checking that using a single $\Gamma_{3.6} = 0.6$, independent of [3.6]–[4.5] color, does not significantly affect the results of our analysis, we decided to use individual, color-dependent mass-to-light ratios.

For each galaxy, the total luminosity (or galaxy luminosity, L_{gal}) is the sum of the luminosities of all its sub-components. Due to the complexity of their modeling, four galaxies (see Table 1, column 7) had their galaxy luminosities

⁸ By comparing, for each of our galaxies, the measurements of the bulge magnitude obtained by different authors with that obtained by us, we estimated the uncertainties on the bulge magnitudes, in effect taking into account systematic errors. Systematic errors include incorrect sky subtraction, inaccurate masking of contaminating sources, imprecise description of the PSF, erroneous choice of model components (for example, when failing to identify a galaxy subcomponent and thus omitting it in the model, or when describing a galaxy sub-component with an inadequate function), the radial extent of the surface brightness profile and one’s sampling of this. Most of these factors are not included in popular two-dimensional (2D) fitting codes which report only the statistical errors associated with their fitted parameters. In fact, when performing multicomponent decomposition of high signal-to-noise images of nearby—therefore, well spatially resolved—galaxies, errors are dominated by systematics rather than Poisson noise. Unlike many papers, we believe that we have not underestimated the uncertainties associated to the bulge best-fit parameters.

⁹ Following Sani et al. (2011), absolute luminosities were calculated assuming a 3.6 μm solar absolute magnitude of 3.25 mag. Absolute luminosities were not corrected for cosmological redshift dimming (this correction would be as small as -0.02 mag for galaxies at a distance of 40 Mpc or -0.05 mag for galaxies at a distance of 100 Mpc).

¹⁰ These are integrated [3.6]–[4.5] colors, measured in a circular aperture within each galaxy’s effective radius.

Table 1
Galaxy Sample

Galaxy	Type	Core	Distance (Mpc)	M_{BH} ($10^8 M_{\odot}$)	MAG_{sph} (mag)	MAG_{gal} (mag)	[3.6]–[4.5] (mag)	$M_{*,\text{sph}}$ ($10^{10} M_{\odot}$)
(1)	(2)	(3)	(4)	(5)	(6)	(7)	(8)	(9)
IC 1459	E	yes	28.4	24^{+10}_{-10}	$-26.15^{+0.18}_{-0.11}$	-26.15 ± 0.25	-0.12	27^{+3}_{-4}
IC 2560	Sp (bar)	no?	40.7	$0.044^{+0.044}_{-0.022}$	$-22.27^{+0.66}_{-0.58}$	-24.76 ± 0.25	-0.08	$1.0^{+0.7}_{-0.5}$
IC 4296	E	yes?	40.7	11^{+2}_{-2}	$-26.35^{+0.18}_{-0.11}$	-26.35 ± 0.25	-0.12	31^{+3}_{-5}
M31	Sp (bar)	no	0.7	$1.4^{+0.9}_{-0.3}$	$-22.74^{+0.18}_{-0.11}$	-24.67 ± 0.25	-0.09	$1.5^{+0.2}_{-0.2}$
M49	E	yes	17.1	25^{+3}_{-3}	$-26.54^{+0.18}_{-0.11}$	-26.54 ± 0.25	-0.12	39^{+4}_{-6}
M59	E	no	17.8	$3.9^{+0.4}_{-0.4}$	$-25.18^{+0.18}_{-0.11}$	-25.27 ± 0.25	-0.09	14^{+2}_{-2}
M64	Sp	no?	7.3	$0.016^{+0.004}_{-0.004}$	$-21.54^{+0.18}_{-0.11}$	-24.24 ± 0.25	-0.06	$0.64^{+0.07}_{-0.10}$
M81	Sp (bar)	no	3.8	$0.74^{+0.21}_{-0.11}$	$-23.01^{+0.88}_{-0.66}$	-24.43 ± 0.25	-0.09	$1.9^{+1.6}_{-1.1}$
M84	E	yes	17.9	$9.0^{+0.9}_{-0.8}$	$-26.01^{+0.66}_{-0.58}$	-26.01 ± 0.25	-0.10	28^{+20}_{-13}
M87	E	yes	15.6	$58.0^{+3.5}_{-3.5}$	$-26.00^{+0.66}_{-0.58}$	-26.00 ± 0.25	-0.11	26^{+18}_{-12}
M89	E	yes	14.9	$4.7^{+0.5}_{-0.5}$	$-24.48^{+0.66}_{-0.58}$	-24.74 ± 0.25	-0.11	$6.3^{+4.4}_{-2.9}$
M94	Sp (bar)	no?	4.4	$0.060^{+0.014}_{-0.014}$	$-22.08^{+0.18}_{-0.11}$	≤ -23.36	-0.07	$1.00^{+0.11}_{-0.15}$
M96	Sp (bar)	no	10.1	$0.073^{+0.015}_{-0.015}$	$-22.15^{+0.18}_{-0.11}$	-24.20 ± 0.25	-0.08	$0.97^{+0.11}_{-0.15}$
M104	S0/Sp	yes	9.5	$6.4^{+0.4}_{-0.4}$	$-23.91^{+0.66}_{-0.58}$	-25.21 ± 0.25	-0.12	$3.4^{+2.4}_{-1.6}$
M105	E	yes	10.3	4^{+1}_{-1}	$-24.29^{+0.66}_{-0.58}$	-24.29 ± 0.25	-0.10	$5.6^{+3.9}_{-2.5}$
M106	Sp (bar)	no	7.2	$0.39^{+0.01}_{-0.01}$	$-21.11^{+0.18}_{-0.11}$	-24.04 ± 0.25	-0.08	$0.37^{+0.04}_{-0.06}$
NGC 0524	S0	yes	23.3	$8.3^{+2.7}_{-1.3}$	$-23.19^{+0.18}_{-0.11}$	-24.92 ± 0.25	-0.09	$2.2^{+0.2}_{-0.3}$
NGC 0821	E	no	23.4	$0.39^{+0.26}_{-0.09}$	$-24.00^{+0.88}_{-0.66}$	-24.26 ± 0.25	-0.09	$4.7^{+4.0}_{-2.6}$
NGC 1023	S0 (bar)	no	11.1	$0.42^{+0.04}_{-0.04}$	$-22.82^{+0.18}_{-0.11}$	-24.20 ± 0.25	-0.10	$1.5^{+0.2}_{-0.2}$
NGC 1300	Sp (bar)	no	20.7	$0.73^{+0.69}_{-0.35}$	$-22.06^{+0.66}_{-0.58}$	-24.16 ± 0.25	-0.10	$0.70^{+0.49}_{-0.32}$
NGC 1316	merger	no	18.6	$1.50^{+0.75}_{-0.80}$	$-24.89^{+0.66}_{-0.58}$	-26.48 ± 0.25	-0.10	$9.5^{+6.7}_{-4.3}$
NGC 1332	E/S0	no	22.3	14^{+2}_{-2}	$-24.89^{+0.88}_{-0.66}$	-24.95 ± 0.25	-0.12	$8.2^{+6.8}_{-4.5}$
NGC 1374	E	no?	19.2	$5.8^{+0.5}_{-0.5}$	$-23.68^{+0.18}_{-0.11}$	-23.70 ± 0.25	-0.09	$3.6^{+0.4}_{-0.5}$
NGC 1399	E	yes	19.4	$4.7^{+0.6}_{-0.6}$	$-26.43^{+0.18}_{-0.11}$	-26.46 ± 0.25	-0.12	33^{+4}_{-5}
NGC 2273	Sp (bar)	no	28.5	$0.083^{+0.004}_{-0.004}$	$-23.00^{+0.66}_{-0.58}$	-24.21 ± 0.25	-0.08	$2.0^{+1.4}_{-0.9}$
NGC 2549	S0 (bar)	no	12.3	$0.14^{+0.02}_{-0.13}$	$-21.25^{+0.18}_{-0.11}$	-22.60 ± 0.25	-0.10	$0.35^{+0.04}_{-0.05}$
NGC 2778	S0 (bar)	no	22.3	$0.15^{+0.09}_{-0.10}$	$-20.80^{+0.66}_{-0.58}$	-22.44 ± 0.25	-0.09	$0.25^{+0.18}_{-0.12}$
NGC 2787	S0 (bar)	no	7.3	$0.40^{+0.04}_{-0.05}$	$-20.11^{+0.66}_{-0.58}$	-22.28 ± 0.25	-0.10	$0.12^{+0.08}_{-0.05}$
NGC 2974	Sp (bar)	no	20.9	$1.7^{+0.2}_{-0.2}$	$-22.95^{+0.66}_{-0.58}$	-24.16 ± 0.25	-0.09	$1.8^{+1.3}_{-0.8}$
NGC 3079	Sp (bar)	no?	20.7	$0.024^{+0.024}_{-0.012}$	$-23.01^{+0.66}_{-0.58}$	≤ -24.45	-0.07	$2.4^{+1.7}_{-1.1}$
NGC 3091	E	yes	51.2	36^{+1}_{-2}	$-26.28^{+0.18}_{-0.11}$	-26.28 ± 0.25	-0.12	30^{+3}_{-5}
NGC 3115	E/S0	no	9.4	$8.8^{+10.0}_{-2.7}$	$-24.22^{+0.18}_{-0.11}$	-24.40 ± 0.25	-0.11	$4.9^{+0.5}_{-0.7}$
NGC 3227	Sp (bar)	no	20.3	$0.14^{+0.10}_{-0.06}$	$-21.76^{+0.66}_{-0.58}$	-24.26 ± 0.25	-0.08	$0.67^{+0.47}_{-0.31}$
NGC 3245	S0 (bar)	no	20.3	$2.0^{+0.5}_{-0.5}$	$-22.43^{+0.18}_{-0.11}$	-23.88 ± 0.25	-0.10	$1.0^{+0.1}_{-0.2}$
NGC 3377	E	no	10.9	$0.77^{+0.04}_{-0.06}$	$-23.49^{+0.66}_{-0.58}$	-23.57 ± 0.25	-0.06	$4.0^{+2.8}_{-1.8}$
NGC 3384	S0 (bar)	no	11.3	$0.17^{+0.01}_{-0.02}$	$-22.43^{+0.18}_{-0.11}$	-23.74 ± 0.25	-0.08	$1.2^{+0.1}_{-0.2}$
NGC 3393	Sp (bar)	no	55.2	$0.34^{+0.02}_{-0.02}$	$-23.48^{+0.66}_{-0.58}$	-25.29 ± 0.25	-0.10	$2.8^{+1.9}_{-1.3}$
NGC 3414	E	no	24.5	$2.4^{+0.3}_{-0.3}$	$-24.35^{+0.18}_{-0.11}$	-24.42 ± 0.25	-0.09	$6.5^{+0.7}_{-1.0}$
NGC 3489	S0/Sp (bar)	no	11.7	$0.058^{+0.008}_{-0.008}$	$-21.13^{+0.66}_{-0.58}$	-23.07 ± 0.25	-0.06	$0.42^{+0.30}_{-0.19}$
NGC 3585	E	no	19.5	$3.1^{+1.4}_{-0.6}$	$-25.52^{+0.66}_{-0.58}$	-25.55 ± 0.25	-0.10	18^{+12}_{-8}
NGC 3607	E	no	22.2	$1.3^{+0.5}_{-0.5}$	$-25.36^{+0.66}_{-0.58}$	-25.45 ± 0.25	-0.10	15^{+10}_{-7}
NGC 3608	E	yes	22.3	$2.0^{+1.1}_{-0.6}$	$-24.50^{+0.66}_{-0.58}$	-24.50 ± 0.25	-0.08	$7.8^{+5.5}_{-3.6}$
NGC 3842	E	yes	98.4	97^{+30}_{-26}	$-27.00^{+0.18}_{-0.11}$	-27.04 ± 0.25	-0.11	61^{+7}_{-9}
NGC 3998	S0 (bar)	no	13.7	$8.1^{+2.0}_{-1.9}$	$-22.32^{+0.88}_{-0.66}$	-23.53 ± 0.25	-0.12	$0.78^{+0.65}_{-0.43}$
NGC 4026	S0 (bar)	no	13.2	$1.8^{+0.6}_{-0.3}$	$-21.58^{+0.88}_{-0.66}$	-23.16 ± 0.25	-0.09	$0.50^{+0.42}_{-0.28}$
NGC 4151	Sp (bar)	no	20.0	$0.65^{+0.07}_{-0.07}$	$-23.40^{+0.66}_{-0.58}$	-24.44 ± 0.25	-0.09	$2.8^{+2.0}_{-1.3}$
NGC 4261	E	yes	30.8	5^{+1}_{-1}	$-25.72^{+0.66}_{-0.58}$	-25.76 ± 0.25	-0.12	18^{+13}_{-8}
NGC 4291	E	yes	25.5	$3.3^{+0.9}_{-2.5}$	$-24.05^{+0.66}_{-0.58}$	-24.05 ± 0.25	-0.11	$3.9^{+2.8}_{-1.8}$
NGC 4388	Sp (bar)	no?	17.0	$0.075^{+0.002}_{-0.002}$	$-21.26^{+0.88}_{-0.66}$	≤ -23.50	-0.07	$0.46^{+0.39}_{-0.26}$
NGC 4459	S0	no	15.7	$0.68^{+0.13}_{-0.13}$	$-23.48^{+0.66}_{-0.58}$	-24.01 ± 0.25	-0.09	$2.9^{+2.1}_{-1.3}$
NGC 4473	E	no	15.3	$1.2^{+0.4}_{-0.9}$	$-23.88^{+0.66}_{-0.58}$	-24.11 ± 0.25	-0.10	$3.9^{+2.7}_{-1.8}$
NGC 4564	S0	no	14.6	$0.60^{+0.03}_{-0.09}$	$-22.30^{+0.18}_{-0.11}$	-22.99 ± 0.25	-0.11	$0.82^{+0.09}_{-0.12}$
NGC 4596	S0 (bar)	no	17.0	$0.79^{+0.38}_{-0.33}$	$-22.73^{+0.18}_{-0.11}$	-24.18 ± 0.25	-0.08	$1.6^{+0.2}_{-0.2}$
NGC 4697	E	no	11.4	$1.8^{+0.2}_{-0.1}$	$-24.82^{+0.88}_{-0.66}$	-24.94 ± 0.25	-0.09	10^{+8}_{-6}
NGC 4889	E	yes	103.2	210^{+160}_{-160}	$-27.54^{+0.18}_{-0.11}$	-27.54 ± 0.25	-0.12	91^{+10}_{-14}
NGC 4945	Sp (bar)	no?	3.8	$0.014^{+0.014}_{-0.007}$	$-20.96^{+0.66}_{-0.58}$	≤ -23.79	-0.06	$0.36^{+0.26}_{-0.17}$

Table 1
(Continued)

Galaxy	Type	Core	Distance (Mpc)	M_{BH} ($10^8 M_{\odot}$)	MAG_{sph} (mag)	MAG_{gal} (mag)	[3.6]–[4.5] (mag)	$M_{*,\text{sph}}$ ($10^{10} M_{\odot}$)
(1)	(2)	(3)	(4)	(5)	(6)	(7)	(8)	(9)
NGC 5077	E	yes	41.2	$7.4^{+4.7}_{-3.0}$	$-25.45^{+0.18}_{-0.11}$	-25.45 ± 0.25	-0.11	15^{+2}_{-2}
NGC 5128	merger	no?	3.8	$0.45^{+0.17}_{-0.10}$	$-23.89^{+0.88}_{-0.66}$	-24.97 ± 0.25	-0.07	$5.0^{+4.2}_{-2.8}$
NGC 5576	E	no	24.8	$1.6^{+0.3}_{-0.4}$	$-24.44^{+0.18}_{-0.11}$	-24.44 ± 0.25	-0.09	$7.1^{+0.8}_{-1.1}$
NGC 5845	S0	no	25.2	$2.6^{+0.4}_{-1.5}$	$-22.96^{+0.88}_{-0.66}$	-23.10 ± 0.25	-0.12	$1.4^{+1.2}_{-0.8}$
NGC 5846	E	yes	24.2	11^{+1}_{-1}	$-25.81^{+0.66}_{-0.58}$	-25.81 ± 0.25	-0.10	22^{+16}_{-10}
NGC 6251	E	yes?	104.6	5^{+2}_{-2}	$-26.75^{+0.18}_{-0.11}$	-26.75 ± 0.25	-0.12	46^{+5}_{-7}
NGC 7052	E	yes	66.4	$3.7^{+2.6}_{-1.5}$	$-26.32^{+0.18}_{-0.11}$	-26.32 ± 0.25	-0.11	33^{+4}_{-5}
NGC 7619	E	yes	51.5	25^{+8}_{-3}	$-26.35^{+0.66}_{-0.58}$	-26.41 ± 0.25	-0.11	33^{+23}_{-15}
NGC 7768	E	yes	112.8	13^{+5}_{-4}	$-26.90^{+0.66}_{-0.58}$	-26.90 ± 0.25	-0.11	57^{+40}_{-26}
UGC 03789	Sp (bar)	no?	48.4	$0.108^{+0.005}_{-0.005}$	$-22.77^{+0.88}_{-0.66}$	-24.20 ± 0.25	-0.07	$1.9^{+1.6}_{-1.0}$

Note. Column (1): Galaxy name. Column (2): morphological type (E = elliptical, S0 = lenticular, Sp = spiral, merger). The morphological classification of four galaxies is uncertain (E/S0 or S0/Sp). The presence of a bar is indicated. Column (3): presence of a partially depleted core. The question mark is used when the classification has come from the velocity dispersion criteria mentioned in Section 2. Column (4): distance. Column (5): black hole mass. Column (6): absolute 3.6 μm bulge magnitude. Bulge magnitudes come from our state-of-the-art multicomponent galaxy decompositions (Paper I), which include bulges, disks, bars, spiral arms, rings, halos, extended or unresolved nuclear sources, and partially depleted cores, and that—for the first time—were checked to be consistent with the galaxy kinematics. The uncertainties were estimated with a method that takes into account systematic errors, which are typically not considered by popular 2D fitting codes. Column (7): absolute 3.6 μm galaxy magnitude. Four galaxies had their magnitudes overestimated, which are given here as upper limits. Column (8): [3.6]–[4.5] color. Column (9): bulge stellar mass.

underestimated¹¹, which are given here as lower limits. Following GS13, we assumed a fixed uncertainty (0.25 mag) for the absolute galaxy magnitude MAG_{gal} .

The morphological classification (E = elliptical; E/S0 = elliptical/lenticular; S0 = lenticular; S0/Sp = lenticular/spiral; Sp = spiral; and “merger”) follows from the galaxy models presented in Paper I. Throughout this paper, we will refer to early-type galaxies (E+S0) and late-type galaxies (Sp). Two galaxies classified as E/S0 are obviously included in the early-type bin, whereas two galaxies classified as S0/Sp and another two classified as mergers are included in neither the early- nor the late-type bins.

The Sérsic/core-Sérsic classification presented in this work comes from the compilation of Savorgnan & Graham (2015), who identified partially depleted cores according to the same criteria used by GS13. When no high-resolution image analysis was available from the literature, they inferred the presence of a partially depleted core based on the stellar velocity dispersion: a spheroid is classified as core-Sérsic if $\sigma > 270 \text{ km s}^{-1}$, or as Sérsic if $\sigma < 166 \text{ km s}^{-1}$. All of the galaxies with velocity dispersions between these two limits had high-resolution images available.

3. ANALYSIS

We performed a linear regression analysis of the $M_{\text{BH}}-L_{\text{gal}}$ (see Table 2), $M_{\text{BH}}-L_{\text{sph}}$ (see Table 3), and $M_{\text{BH}}-M_{*,\text{sph}}$ (see Table 4) data, using the BCES code from Akritas & Bershady (1996). We also repeated the analysis using both the FITEXY routine (Press et al. 1992), as modified by Tremaine et al. (2002), and the Bayesian estimator linmix_err (Kelly 2007). All of these three linear regression routines account for the intrinsic scatter, but only the last two allow one to quantify it. We report linear regressions, both symmetrical and non-symmetrical, for Sérsic/core-Sérsic and for early-/late-type galaxies. Symmetrical regressions are meant to be compared

¹¹ These four cases are discussed in Paper I.

with theoretical expectations, whereas non-symmetrical forward ($M_{\text{BH}}|X$) regressions—which minimize the scatter in the $\log(M_{\text{BH}})$ direction—are best used to predict black hole masses.

4. RESULTS AND DISCUSSION

4.1. Black Hole Mass–Galaxy Luminosity

The $M_{\text{BH}}-L_{\text{gal}}$ diagram is shown in Figure 1. Four spiral galaxies had their total luminosities underestimated (see Table 1) and thus are not included in the linear regression analysis (see Table 2).

Läsker et al. (2014b) analyzed a sample of 35 galaxies, among which only four were classified as spiral galaxies, and claimed that the $M_{\text{BH}}-L_{\text{sph}}$ and $M_{\text{BH}}-L_{\text{gal}}$ relations, which they fit with a single power law, have consistent intrinsic scatter. Here, instead, thanks to our galaxy sample that includes 17 spiral galaxies, we show that the claim made by Läsker et al. (2014b) is valid only for early-type galaxies. That is, when considering only early-type galaxies, we find that the $M_{\text{BH}}-L_{\text{sph}}$ and $M_{\text{BH}}-L_{\text{gal}}$ relations have the same level of intrinsic scatter. However, our $M_{\text{BH}}-L_{\text{sph}}$ relation for all 66 galaxies, irrespective of their morphological type, has an intrinsic scatter $\epsilon_{(Y|X)} = 0.51 \pm 0.06 \text{ dex}$ (forward linear regression) and $\epsilon_{(X|Y)} = 0.60 \pm 0.09 \text{ dex}$ (inverse linear regression), whereas our $M_{\text{BH}}-L_{\text{gal}}$ relation for 62 (=66–4) galaxies has $\epsilon_{(Y|X)} = 0.63 \pm 0.07 \text{ dex}$ and $\epsilon_{(X|Y)} = 0.91 \pm 0.17 \text{ dex}$. Because the value of the intrinsic scatter depends on the size of the uncertainties associated with the absolute magnitudes,¹² we tested the robustness of our conclusion by increasing the uncertainties associated with the galaxy absolute magnitudes¹³

¹² The smaller (larger) the uncertainties, the larger (smaller) the intrinsic scatter.

¹³ The value of the intrinsic scatter obviously depends also on the size of the uncertainties associated with the black hole masses. However, black hole masses and their uncertainties have been estimated by various authors using different methods, thus we have limited to no control on their values.

Table 2
Linear Regression Analysis of the $M_{\text{BH}}-L_{\text{gal}}$ Diagram

Subsample (size)	Regression	α	β	$\langle \text{MAG}_{\text{gal}} \rangle$	ϵ	Δ
$\log[M_{\text{BH}}/M_{\odot}] = \alpha + \beta [(\text{MAG}_{\text{gal}} - \langle \text{MAG}_{\text{gal}} \rangle)/\text{mag}]$						
All (62)	BCES ($Y X$)	8.26 ± 0.08	-0.49 ± 0.06	-24.78	...	0.64
	mFITEXY ($Y X$)	$8.26^{+0.08}_{-0.08}$	$-0.49^{+0.06}_{-0.07}$	-24.78	$0.61^{+0.07}_{-0.06}$	0.64
	linmix_err ($Y X$)	8.26 ± 0.09	-0.49 ± 0.07	-24.78	0.63 ± 0.07	0.64
	BCES ($X Y$)	8.26 ± 0.12	-1.01 ± 0.15	-24.78	...	0.92
	mFITEXY ($X Y$)	$8.26^{+0.11}_{-0.12}$	$-1.03^{+0.13}_{-0.16}$	-24.78	$0.88^{+0.10}_{-0.08}$	0.93
	linmix_err ($X Y$)	8.26 ± 0.12	-1.02 ± 0.15	-24.78	0.91 ± 0.17	0.93
	BCES Bisector	8.26 ± 0.09	-0.72 ± 0.07	-24.78	...	0.71
	mFITEXY Bisector	$8.26^{+0.10}_{-0.10}$	$-0.73^{+0.09}_{-0.10}$	-24.78	...	0.71
	linmix_err Bisector	8.26 ± 0.10	-0.72 ± 0.07	-24.78	...	0.71
Early-type (E+S0) (45)	BCES ($Y X$)	8.56 ± 0.07	-0.44 ± 0.05	-24.88	...	0.45
	mFITEXY ($Y X$)	$8.56^{+0.06}_{-0.06}$	$-0.42^{+0.05}_{-0.05}$	-24.88	$0.41^{+0.06}_{-0.05}$	0.45
	linmix_err ($Y X$)	8.56 ± 0.07	-0.42 ± 0.06	-24.88	0.43 ± 0.06	0.45
	BCES ($X Y$)	8.56 ± 0.08	-0.64 ± 0.05	-24.88	...	0.53
	mFITEXY ($X Y$)	$8.56^{+0.08}_{-0.08}$	$-0.66^{+0.07}_{-0.08}$	-24.88	$0.51^{+0.07}_{-0.06}$	0.55
	linmix_err ($X Y$)	8.56 ± 0.09	-0.65 ± 0.08	-24.88	0.53 ± 0.10	0.54
	BCES Bisector	8.56 ± 0.07	-0.53 ± 0.04	-24.88	...	0.47
	mFITEXY Bisector	$8.56^{+0.07}_{-0.07}$	$-0.54^{+0.06}_{-0.06}$	-24.88	...	0.47
	linmix_err Bisector	8.56 ± 0.08	-0.53 ± 0.05	-24.88	...	0.47

Note. For each subsample, we indicate $\langle \text{MAG}_{\text{gal}} \rangle$, its average value of galaxy magnitudes. In the last two columns, we report ϵ , the intrinsic scatter, and Δ , the total rms scatter in the $\log(M_{\text{BH}})$ direction. Four spiral galaxies had their luminosities underestimated and thus are not included in the linear regression analysis (the sample of all galaxies contains $66-4 = 62$ objects). When considering all galaxies, irrespective of their morphological type, the $M_{\text{BH}}-L_{\text{gal}}$ correlation is weaker than the $M_{\text{BH}}-L_{\text{sph}}$ correlation, in terms of intrinsic scatter. However, when considering only early-type galaxies, the $M_{\text{BH}}-L_{\text{gal}}$ and $M_{\text{BH}}-L_{\text{sph}}$ correlations have consistent intrinsic scatter.

(we originally assumed 0.25 mag). The intrinsic scatter of the $M_{\text{BH}}-L_{\text{gal}}$ relation only becomes smaller than that of the $M_{\text{BH}}-L_{\text{sph}}$ relation when assuming an uncertainty larger than 0.7 mag for L_{gal} , which would be significantly larger than the typical value commonly recognized in the literature, and would also oddly exceed the typical uncertainty that we estimated for L_{sph} . Hence, we conclude that our determination of the relative intrinsic scatter is reliable and that M_{BH} correlates equally well with L_{sph} and L_{gal} only for early-type galaxies¹⁴, but not for all (early+late-type) galaxies.

4.2. Black Hole Mass–Spheroid Luminosity

The $M_{\text{BH}}-L_{\text{sph}}$ diagram is shown in Figure 2, and the linear regression analysis is presented in Table 3. Sérsic and core-Sérsic spheroids have slopes consistent with each other (within their 1σ uncertainties), in disagreement with the findings of GS13. The slope that we obtained for core-Sérsic spheroids ($M_{\text{BH}} \propto L_{\text{sph}}^{1.18 \pm 0.20}$) is consistent with the slope reported by GS13 in the K_s -band for the same population ($M_{\text{BH}} \propto L_{\text{sph}}^{1.10 \pm 0.20}$). However, the slope that we determined for Sérsic spheroids ($M_{\text{BH}} \propto L_{\text{sph}}^{1.53 \pm 0.20}$) is notably shallower than that found by GS13 ($M_{\text{BH}} \propto L_{\text{sph}}^{2.73 \pm 0.55}$).

Although the Sérsic/core-Sérsic classification used by GS13 slightly differs¹⁵ from the classification used here, the main cause of the inconsistency is that the bulge-to-total ratios obtained from our galaxy decompositions are different from

those assumed by GS13 to convert galaxy luminosities into bulge luminosities. Our bulge-to-total ratios for low-luminosity Sérsic spheroids ($3.6 \mu\text{m MAG}_{\text{sph}} \gtrsim -22$ mag) are smaller than those used by GS13. The host galaxies of such bulges are late-type, spiral galaxies, which typically present a complex morphology (bars, double bars, embedded disks, nuclear components, etc.). Our galaxy models account for the extra components, while the average bulge-to-total ratios of GS13 were based on less sophisticated Sérsic-bulge/exponential-disk decompositions which overestimated the bulge luminosity. This results in our bulge magnitudes being on average ~ 0.7 mag fainter than in GS13, after accounting for the different wavelength of the data. At the same time, our bulge-to-total ratios for the high-luminosity Sérsic spheroids ($3.6 \mu\text{m MAG}_{\text{sph}} \lesssim -24$ mag) are on average larger than those adopted by GS13. In this regime, the host systems are early-type galaxies that feature intermediate-scale disks.¹⁶ Past bulge/disk decompositions failed to correctly identify the extent of such disks and treated them as large-scale disks, thus underestimating the bulge luminosity. The magnitudes that we obtained for such spheroids are on average ~ 0.5 mag brighter than in GS13. These two effects explain the shallower slope that we obtained for the Sérsic spheroids.

The slope that we obtained for Sérsic spheroids (1.53 ± 0.20) is not consistent with the value of 2.5 expected from $M_{\text{BH}} \propto \sigma^5$ and $L_{\text{sph}} \propto \sigma^2$. In addition, the Sérsic and core-Sérsic spheroids do not appear to define two distinct $M_{\text{BH}}-L_{\text{sph}}$ sequences. This leads us to investigate substructure

¹⁴ The majority of our early-type galaxies are elliptical galaxies, some of which have a bulge-to-total ratio close to 1 ($L_{\text{gal}} \simeq L_{\text{sph}}$). One might wonder whether this constitutes a bias in our analysis. However, we checked that M_{BH} correlates equally well with L_{sph} and L_{gal} not only for early-type (elliptical+lenticular) galaxies, but also for lenticular galaxies only.

¹⁵ The classification has changed for the galaxies NGC 1316, NGC 1332, and NGC 3998.

¹⁶ Intermediate-scale disks are disks of stars fully embedded in the spheroidal component of their galaxy. They are typical of “disky” elliptical galaxies (e.g., NGC 3377), but they can also be found in other types of host galaxies. They can be considered an intermediate class between nuclear disks, with sizes of $\sim 10-100$ pc, and large-scale disks, that encase the bulge and dominate the light at large radii.

Table 3
Linear Regression Analysis of the $M_{\text{BH}}-L_{\text{sph}}$ Diagram

Subsample (size)	Regression	α	β	$\langle \text{MAG}_{\text{sph}} \rangle$	ϵ	Δ
$\log[M_{\text{BH}}/M_{\odot}] = \alpha + \beta[(\text{MAG}_{\text{sph}} - \langle \text{MAG}_{\text{sph}} \rangle)/\text{mag}]$						
All (66)	BCES ($Y X$)	8.16 ± 0.07	-0.44 ± 0.04	-23.86	...	0.56
	mFITEXY ($Y X$)	$8.17^{+0.06}_{-0.07}$	$-0.43^{+0.03}_{-0.04}$	-23.86	$0.49^{+0.06}_{-0.05}$	0.56
	linmix_err ($Y X$)	8.16 ± 0.07	-0.42 ± 0.04	-23.86	0.51 ± 0.06	0.56
	BCES ($X Y$)	8.16 ± 0.08	-0.61 ± 0.05	-23.86	...	0.68
	mFITEXY ($X Y$)	$8.15^{+0.07}_{-0.08}$	$-0.61^{+0.05}_{-0.05}$	-23.86	$0.58^{+0.07}_{-0.06}$	0.68
	linmix_err ($X Y$)	8.16 ± 0.09	-0.60 ± 0.06	-23.86	0.60 ± 0.09	0.67
	BCES Bisector	8.16 ± 0.07	-0.52 ± 0.04	-23.86	...	0.60
	mFITEXY Bisector	$8.16^{+0.07}_{-0.07}$	$-0.51^{+0.04}_{-0.04}$	-23.86	...	0.60
	linmix_err Bisector	8.16 ± 0.08	-0.51 ± 0.03	-23.86	...	0.59
$n > 2$ (43)	BCES ($Y X$)	8.58 ± 0.07	-0.42 ± 0.06	-24.77	...	0.46
	mFITEXY ($Y X$)	$8.57^{+0.07}_{-0.06}$	$-0.41^{+0.04}_{-0.04}$	-24.77	$0.38^{+0.06}_{-0.06}$	0.46
	linmix_err ($Y X$)	8.56 ± 0.07	-0.39 ± 0.05	-24.77	0.40 ± 0.06	0.46
	BCES ($X Y$)	8.58 ± 0.08	-0.58 ± 0.06	-24.77	...	0.56
	mFITEXY ($X Y$)	$8.56^{+0.08}_{-0.08}$	$-0.57^{+0.06}_{-0.07}$	-24.77	$0.44^{+0.08}_{-0.11}$	0.55
	linmix_err ($X Y$)	8.55 ± 0.09	-0.57 ± 0.08	-24.77	0.49 ± 0.10	0.55
	BCES Bisector	8.58 ± 0.07	-0.50 ± 0.05	-24.77	...	0.49
	mFITEXY Bisector	$8.57^{+0.07}_{-0.07}$	$-0.49^{+0.05}_{-0.05}$	-24.77	...	0.49
	linmix_err Bisector	8.56 ± 0.08	-0.48 ± 0.05	-24.77	...	0.49
Core- Sérsic (22)	BCES ($Y X$)	9.06 ± 0.09	-0.32 ± 0.11	-25.73	...	0.42
	mFITEXY ($Y X$)	$9.06^{+0.08}_{-0.09}$	$-0.26^{+0.08}_{-0.07}$	-25.73	$0.36^{+0.09}_{-0.06}$	0.42
	linmix_err ($Y X$)	9.04 ± 0.10	-0.24 ± 0.09	-25.73	0.40 ± 0.08	0.42
	BCES ($X Y$)	9.06 ± 0.12	-0.65 ± 0.12	-25.73	...	0.61
	mFITEXY ($X Y$)	$9.03^{+0.15}_{-0.16}$	$-0.72^{+0.17}_{-0.31}$	-25.73	$0.61^{+0.14}_{-0.09}$	0.68
	linmix_err ($X Y$)	9.03 ± 0.17	-0.69 ± 0.27	-25.73	0.68 ± 0.30	0.64
	BCES Bisector	9.06 ± 0.10	-0.47 ± 0.08	-25.73	...	0.48
	mFITEXY Bisector	$9.05^{+0.12}_{-0.13}$	$-0.47^{+0.12}_{-0.17}$	-25.73	...	0.48
	linmix_err Bisector	9.04 ± 0.14	-0.44 ± 0.12	-25.73	...	0.46
Sérsic (44)	BCES ($Y X$)	7.71 ± 0.09	-0.41 ± 0.08	-22.92	...	0.61
	mFITEXY ($Y X$)	$7.72^{+0.08}_{-0.09}$	$-0.41^{+0.07}_{-0.08}$	-22.92	$0.54^{+0.08}_{-0.07}$	0.61
	linmix_err ($Y X$)	7.73 ± 0.09	-0.41 ± 0.08	-22.92	0.55 ± 0.08	0.61
	BCES ($X Y$)	7.71 ± 0.14	-0.86 ± 0.16	-22.92	...	0.93
	mFITEXY ($X Y$)	$7.72^{+0.14}_{-0.13}$	$-0.86^{+0.13}_{-0.19}$	-22.92	$0.77^{+0.13}_{-0.10}$	0.93
	linmix_err ($X Y$)	7.73 ± 0.14	-0.86 ± 0.17	-22.92	0.79 ± 0.20	0.93
	BCES Bisector	7.71 ± 0.10	-0.61 ± 0.08	-22.92	...	0.71
	mFITEXY Bisector	$7.72^{+0.11}_{-0.11}$	$-0.61^{+0.10}_{-0.12}$	-22.92	...	0.71
	linmix_err Bisector	7.73 ± 0.12	-0.62 ± 0.09	-22.92	...	0.71
Early-type (E+S0) (45)	BCES ($Y X$)	8.56 ± 0.07	-0.33 ± 0.04	-24.47	...	0.46
	mFITEXY ($Y X$)	$8.56^{+0.06}_{-0.06}$	$-0.32^{+0.03}_{-0.04}$	-24.47	$0.40^{+0.06}_{-0.05}$	0.46
	linmix_err ($Y X$)	8.55 ± 0.07	-0.32 ± 0.04	-24.47	0.41 ± 0.06	0.46
	BCES ($X Y$)	8.56 ± 0.08	-0.48 ± 0.05	-24.47	...	0.55
	mFITEXY ($X Y$)	$8.54^{+0.08}_{-0.08}$	$-0.49^{+0.05}_{-0.06}$	-24.47	$0.49^{+0.08}_{-0.06}$	0.57
	linmix_err ($X Y$)	8.55 ± 0.09	-0.48 ± 0.06	-24.47	0.51 ± 0.10	0.56
	BCES Bisector	8.56 ± 0.07	-0.40 ± 0.04	-24.47	...	0.49
	mFITEXY Bisector	$8.55^{+0.07}_{-0.07}$	$-0.41^{+0.04}_{-0.05}$	-24.47	...	0.49
	linmix_err Bisector	8.55 ± 0.08	-0.40 ± 0.04	-24.47	...	0.49
Late-type (Sp) (17)	BCES ($Y X$)	7.18 ± 0.16	-0.79 ± 0.43	-22.33	—	0.70
	mFITEXY ($Y X$)	$7.20^{+0.15}_{-0.15}$	$-0.53^{+0.22}_{-0.24}$	-22.33	$0.55^{+0.15}_{-0.10}$	0.63
	linmix_err ($Y X$)	7.24 ± 0.19	-0.46 ± 0.32	-22.33	0.63 ± 0.16	0.62
	BCES ($X Y$)	7.18 ± 0.29	-1.71 ± 0.71	-22.33	...	1.26
	mFITEXY ($X Y$)	$7.38^{+0.54}_{-0.36}$	$-2.02^{+0.71}_{-2.13}$	-22.33	$1.09^{+0.41}_{-0.24}$	1.50
	linmix_err ($X Y$)	7.34 ± 0.43	-1.93 ± 1.30	-22.33	1.31 ± 0.97	1.43
	BCES Bisector	7.18 ± 0.20	-1.15 ± 0.27	-22.33	...	0.88
	mFITEXY Bisector	$7.26^{+0.40}_{-0.28}$	$-1.03^{+0.33}_{-0.52}$	-22.33	...	0.82
	linmix_err Bisector	7.27 ± 0.33	-0.96 ± 0.37	-22.33	...	0.78

Note. For each subsample, we indicate $\langle \text{MAG}_{\text{sph}} \rangle$, its average value of spheroid magnitudes. In the last two columns, we report ϵ , the intrinsic scatter, and Δ , the total rms scatter in the $\log(M_{\text{BH}})$ direction. Both the early- and late-type subsamples do not contain the two galaxies classified as S0/Sp and the two galaxies classified as mergers (45+17 = 66-2-2). The bold values are the linear regression parameters quoted in the text.

Table 4
Linear Regression Analysis of the $M_{\text{BH}}-M_{*,\text{sph}}$ Diagram

Subsample (size)	Regression	α	β	$\langle \text{MAG}_{\text{sph}} \rangle$	ϵ	Δ
$\log[M_{\text{BH}}/M_{\odot}] = \alpha + \beta \log[(M_{*,\text{sph}}/\langle M_{*,\text{sph}} \rangle)]$						
Core-Sérsic (22)	BCES ($Y X$)	9.06 ± 0.09	0.86 ± 0.28	$10^{11.28}$...	0.42
	mFITEXY ($Y X$)	$9.06^{+0.08}_{-0.08}$	$0.68^{+0.21}_{-0.20}$	$10^{11.28}$	$0.36^{+0.09}_{-0.06}$	0.42
	linmix_err ($Y X$)	9.04 ± 0.10	0.64 ± 0.25	$10^{11.28}$	0.40 ± 0.09	0.42
	BCES ($X Y$)	9.06 ± 0.12	1.70 ± 0.32	$10^{11.28}$...	0.61
	mFITEXY ($X Y$)	$9.03^{+0.15}_{-0.16}$	$1.90^{+0.85}_{-0.46}$	$10^{11.28}$	$0.62^{+0.13}_{-0.10}$	0.68
	linmix_err ($X Y$)	9.03 ± 0.17	1.80 ± 0.70	$10^{11.28}$	0.67 ± 0.30	0.65
	BCES Bisector	9.06 ± 0.10	1.19 ± 0.23	$10^{11.28}$...	0.47
	mFITEXY Bisector	$9.05^{+0.12}_{-0.13}$	$1.12^{+0.35}_{-0.27}$	$10^{11.28}$...	0.46
	linmix_err Bisector	9.04 ± 0.14	1.06 ± 0.26	$10^{11.28}$...	0.45
Sérsic (44)	BCES ($Y X$)	7.71 ± 0.09	0.95 ± 0.21	$10^{10.25}$...	0.64
	mFITEXY ($Y X$)	$7.72^{+0.10}_{-0.09}$	$0.96^{+0.21}_{-0.21}$	$10^{10.25}$	$0.58^{+0.09}_{-0.07}$	0.64
	linmix_err ($Y X$)	7.73 ± 0.10	0.98 ± 0.24	$10^{10.25}$	0.59 ± 0.08	0.65
	BCES ($X Y$)	7.71 ± 0.16	2.52 ± 0.54	$10^{10.25}$...	1.11
	mFITEXY ($X Y$)	$7.72^{+0.16}_{-0.16}$	$2.49^{+0.69}_{-0.45}$	$10^{10.25}$	$0.93^{+0.15}_{-0.13}$	1.10
	linmix_err ($X Y$)	7.73 ± 0.17	2.48 ± 0.59	$10^{10.25}$	0.95 ± 0.27	1.10
	BCES Bisector	7.71 ± 0.11	1.48 ± 0.20	$10^{10.25}$...	0.74
	mFITEXY Bisector	$7.72^{+0.13}_{-0.13}$	$1.49^{+0.33}_{-0.28}$	$10^{10.25}$...	0.74
	linmix_err Bisector	7.73 ± 0.14	1.49 ± 0.24	$10^{10.25}$...	0.74
Early-type (E+S0) (45)	BCES ($Y X$)	8.56 ± 0.07	0.85 ± 0.12	$10^{10.81}$...	0.48
	mFITEXY ($Y X$)	$8.56^{+0.06}_{-0.07}$	$0.83^{+0.11}_{-0.11}$	$10^{10.81}$	$0.42^{+0.07}_{-0.05}$	0.48
	linmix_err ($Y X$)	8.55 ± 0.07	0.82 ± 0.12	$10^{10.81}$	0.43 ± 0.06	0.48
	BCES ($X Y$)	8.56 ± 0.09	1.27 ± 0.13	$10^{10.81}$...	0.59
	mFITEXY ($X Y$)	$8.54^{+0.08}_{-0.09}$	$1.32^{+0.18}_{-0.15}$	$10^{10.81}$	$0.53^{+0.08}_{-0.07}$	0.61
	linmix_err ($X Y$)	8.55 ± 0.09	1.29 ± 0.17	$10^{10.81}$	0.54 ± 0.11	0.59
	BCES Bisector	8.56 ± 0.07	1.04 ± 0.10	$10^{10.81}$...	0.51
	mFITEXY Bisector	$8.55^{+0.07}_{-0.08}$	$1.05^{+0.14}_{-0.12}$	$10^{10.81}$...	0.51
	linmix_err Bisector	8.55 ± 0.08	1.03 ± 0.10	$10^{10.81}$...	0.51
Late-type (Sp) (17)	BCES ($Y X$)	7.18 ± 0.17	1.95 ± 1.52	$10^{10.05}$...	0.74
	mFITEXY ($Y X$)	$7.20^{+0.15}_{-0.16}$	$1.22^{+0.70}_{-0.62}$	$10^{10.05}$	$0.59^{+0.16}_{-0.11}$	0.66
	linmix_err ($Y X$)	7.23 ± 0.19	0.96 ± 0.96	$10^{10.05}$	0.67 ± 0.16	0.65
	BCES ($X Y$)	7.18 ± 0.39	5.89 ± 3.40	$10^{10.05}$...	1.70
	mFITEXY ($X Y$)	$7.44^{+1.45}_{-0.52}$	$7.14^{+26.31}_{-3.01}$	$10^{10.05}$	$1.49^{+0.56}_{-0.36}$	2.08
	linmix_err ($X Y$)	7.42 ± 0.64	6.96 ± 6.73	$10^{10.05}$	1.83 ± 1.86	2.03
	BCES Bisector	7.18 ± 0.21	3.00 ± 1.30	$10^{10.05}$...	0.94
	mFITEXY Bisector	$7.24^{+1.04}_{-0.39}$	$2.28^{+1.67}_{-1.01}$	$10^{10.05}$...	0.79
	linmix_err Bisector	7.26 ± 0.47	1.94 ± 1.24	$10^{10.05}$...	0.74

Note. For each subsample, we indicate $\langle M_{*,\text{sph}} \rangle$, its average value of spheroid stellar masses. In the last two columns, we report ϵ , the intrinsic scatter, and Δ , the total rms scatter in the $\log(M_{\text{BH}})$ direction. The bold values are the linear regression parameters quoted in the text.

in the $M_{\text{BH}}-L_{\text{sph}}$ diagram for early- and late-type galaxies. First, we checked that the elliptical and lenticular galaxies, taken separately, have slopes consistent with each other, and thus, taken together, they define a single *early-type sequence* in the $M_{\text{BH}}-L_{\text{sph}}$ diagram. We then fit the early-type galaxies with a single log-linear regression, and obtained $M_{\text{BH}} \propto L_{\text{sph}}^{1.00 \pm 0.10}$. We did not find any convincing evidence for the change in slope required for consistency with the $M_{\text{BH}}-\sigma$ and bent $L_{\text{sph}}-\sigma$ correlations. Because the change in slope should occur at $M_{\text{BH}} > 10^{8 \pm 1} M_{\odot}$, but all of the early-type galaxies in our sample have $M_{\text{BH}} \gtrsim 10^7 M_{\odot}$, one possible explanation is that we are still not probing enough low black hole masses for this subsample. An additional possibility is that there is no sharp transition going from $L_{\text{sph}} \propto \sigma^2$ at low luminosities to $L_{\text{sph}} \propto \sigma^5$ at high luminosities. Although the knowledge that many “elliptical” galaxies actually contain embedded stellar disks dates back at least three decades (Capaccioli 1987; Carter 1987; Bender 1990; Rix & White 1990, 1992; Scorza &

Bender 1990, 1995; Nieto et al. 1991), it is mainly thanks to large integral-field-spectrograph surveys of early-type galaxies, such as the ATLAS^{3D} Project (Cappellari et al. 2011), that our view has been further advanced and it is now commonly accepted that most “elliptical” galaxies contain disks. Past studies that investigated the $L_{\text{sph}}-\sigma$ diagram might have failed to identify and consequently model the disks in intermediate-luminosity, early-type galaxies, thus overestimating L_{sph} and mistakenly producing a sharp bend in the $L_{\text{sph}}-\sigma$ correlation, rather than a continuously curved relation (with $L_{\text{sph}} \propto \sigma^{3-4}$ at intermediate luminosities).

For the bulges of late-type galaxies, we obtained $M_{\text{BH}} \propto L_{\text{sph}}^{2.88 \pm 0.68}$. From a cursory inspection of Figure 2, one might be tempted to doubt the statistical significance of this “tentative” *late-type sequence*. However, a visual inspection of the plotted data requires one to take into account the error bars when judging-by-eye the strength of a correlation. Similarly, the Pearson’s and Spearman’s correlation coefficients are not applicable because they do not take into account the error bars

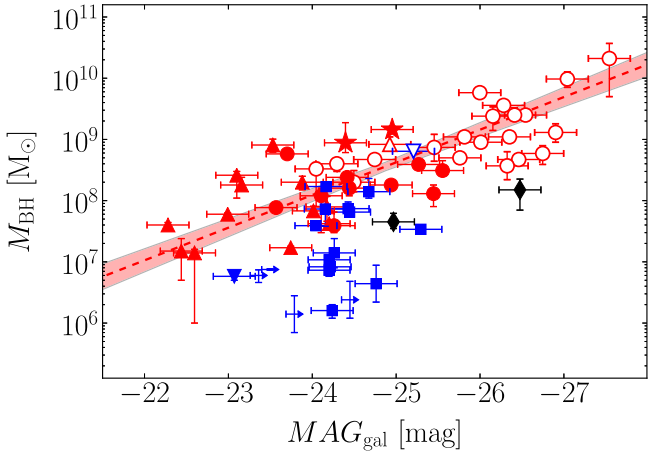


Figure 1. Black hole mass plotted against $3.6 \mu\text{m}$ galaxy absolute magnitude. Symbols are coded according to the galaxy morphological type: red circle = E, red star = E/S0, red upward triangle = S0, blue downward triangle = S0/Sp, blue square = Sp, black diamond = merger. Empty symbols represent core-Sérsic spheroids, whereas filled symbols are used for Sérsic spheroids. Four spiral galaxies had their magnitudes overestimated (luminosities underestimated) and are shown as upper limits. The red dashed line indicates the BCES bisector linear regression for the 45 early-type galaxies (E+S0), with the red shaded area denoting its 1σ uncertainty. M_{BH} correlates equally well with L_{gal} and L_{sph} only for early-type galaxies, but not for all (early+late-type) galaxies.

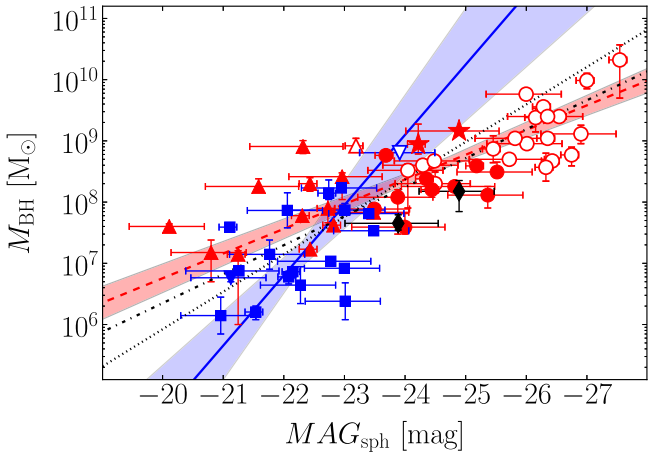


Figure 2. Black hole mass plotted against $3.6 \mu\text{m}$ spheroid absolute magnitude. Symbols have the same meaning as in Figure 1. The red dashed line indicates the BCES bisector linear regression for the spheroidal component of the 45 early-type (E+S0) galaxies, with the red shaded area denoting its 1σ uncertainty. The blue solid line shows the BCES bisector linear regression for the bulges of the 17 late-type (Sp) galaxies, with the blue shaded area denoting its 1σ uncertainty. The black dashed-dotted and dotted lines represent the BCES bisector linear regressions for the core-Sérsic and Sérsic spheroids, respectively.

on our data. We have, therefore, relied on the quantitative regression analysis.

4.2.1. Pseudo- versus Classical Bulges

Current views distinguish between classical bulges (which are considered to be spheroidal, pressure-supported systems, formed through violent processes, such as hierarchical clustering via minor mergers) and pseudo-bulges (thought to be disk-like, rotation-supported systems, built from secular evolution processes, such as instabilities of their surrounding disk or bar). Pseudo-bulges are notoriously hard to identify

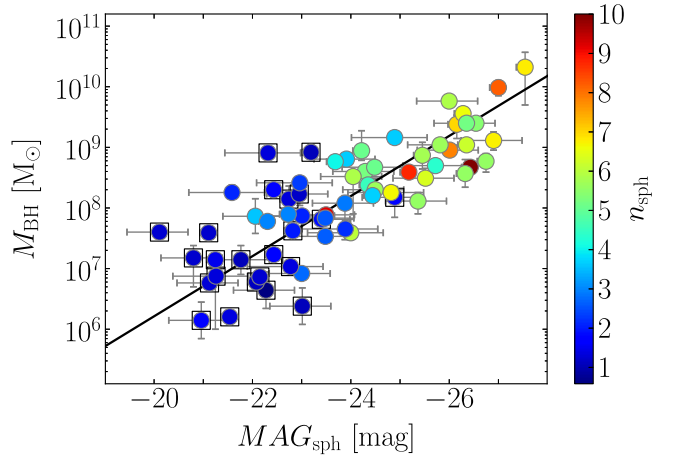


Figure 3. Black hole mass plotted against $3.6 \mu\text{m}$ spheroid absolute magnitude (as in Figure 2). Symbols are color coded according to the spheroid Sérsic index n_{sph} . Bulges with $n_{\text{sph}} < 2$, claimed by some to be pseudo-bulges, are enclosed with a square. The black solid line shows the BCES bisector linear regression for the spheroids that have $n_{\text{sph}} \geq 2$, such that $M_{\text{BH}} \propto L_{\text{sph}}^{1.25 \pm 0.13}$.

(Graham 2013, 2014, 2015, 2016). For example, mergers can create bulges that rotate (e.g., Bekki 2010; Keselman & Nusser 2012), and bars can spin-up classical bulges (e.g., Saha et al. 2012; Saha 2015), thus rotation is not a definitive signature of a pseudo-bulge. Furthermore, many galaxies host both a classical and a pseudo-bulge (e.g., Erwin et al. 2003, 2015; Athanassoula 2005; Gadotti 2009; MacArthur et al. 2009; Erwin 2010; dos Anjos & da Silva 2013; Seidel et al. 2015). In the recent literature, pseudo- and classical bulges have frequently been divided at the Sérsic index $n_{\text{sph}} = 2$ (e.g., Sani et al. 2011; Beifiori et al. 2012), although, from a selection of hundreds of disk galaxies imaged in the K -band, Graham & Worley (2008) observed no bimodality in the bulge Sérsic indices about $n_{\text{sph}} = 2$ or any other value. While pseudo-bulges are expected to have exponential-like surface brightness profiles ($n_{\text{sph}} \simeq 1$), being disk-like components that formed from their surrounding exponential disks (e.g., Bardeen 1975; Hohl 1975; Combes & Sanders 1981; Combes et al. 1990; Pfenniger & Friedli 1991), it has been shown that mergers can create bulges with $n_{\text{sph}} < 2$ (e.g., Eliche-Moral et al. 2011; Scannapieco et al. 2011; Querejeta et al. 2015), just as low-luminosity elliptical galaxies (not built from the secular evolution of a disk) are also well known to have $n_{\text{sph}} < 2$ and even $n_{\text{sph}} < 1$ (e.g., Davies et al. 1988; Young & Currie 1994; Jerjen et al. 2000). The use of the Sérsic index (in addition to rotation) to identify pseudo-bulges is thus a dangerous practice. We therefore do not assume that all bulges with $n_{\text{sph}} < 2$ are built from internal processes in the disk (i.e., are what some authors call pseudo-bulges). Sani et al. (2011) reported that pseudo-bulges—which they labelled as such according to the $n_{\text{sph}} < 2$ criterion—with low black hole masses ($M_{\text{BH}} < 10^7 M_{\odot}$) are significantly displaced from the correlation traced by their (classical) bulges with $n_{\text{sph}} > 2$. In Figure 3, we show the distribution of spheroid Sérsic indices¹⁷ in the $M_{\text{BH}}-L_{\text{sph}}$ diagram. Our aim is to check whether bulges with $n_{\text{sph}} < 2$ are offset to lower black hole masses from the correlation defined by bulges with $n_{\text{sph}} > 2$. To do this, we fit a symmetrical linear regression to the bulges that have $n_{\text{sph}} > 2$

¹⁷ The spheroid Sérsic indices are taken from our galaxy decompositions (Paper I).

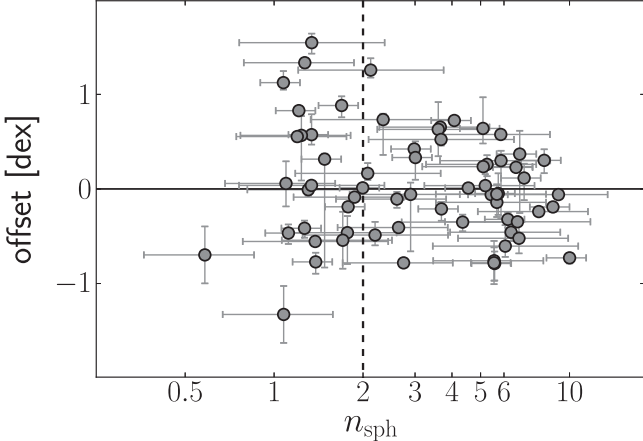


Figure 4. Vertical offset from the $M_{\text{BH}}-L_{\text{sph}}$ correlation defined by spheroids with $n_{\text{sph}} \geq 2$ (see Figure 3), plotted against n_{sph} . The vertical dashed line corresponds to $n_{\text{sph}} = 2$. The horizontal solid line is equivalent to a zero vertical offset. Among the bulges with $n_{\text{sph}} < 2$, 12 have a positive vertical offset and 11 have a negative vertical offset. Hence, bulges with $n_{\text{sph}} < 2$ are not randomly offset to lower black hole masses from the correlation traced by bulges with $n_{\text{sph}} \geq 2$.

and we then compute the vertical offset of all bulges from this regression. In Figure 4, we plot the vertical offset against n_{sph} . Among the 23 bulges with $n_{\text{sph}} < 2$, 12 have a positive vertical offset and 11 have a negative vertical offset. Kormendy (2015) provides a list of many pseudo-bulge classification criteria, including the divide at $n_{\text{sph}} = 2$, and cautions that each individual criterion has a failure rate of 0%–25%. If this is true, we should find that no less than 75% of bulges with $n_{\text{sph}} < 2$ display a negative vertical offset.¹⁸ What we observe, instead, is that there are the same number of bulges with $n_{\text{sph}} < 2$ lying above and below the correlation defined by bulges with $n_{\text{sph}} > 2$, and that the amplitude of their offset is the same ($\lesssim 1.5$ dex). That is, within the current data set, bulges with $n_{\text{sph}} < 2$ do not appear to be offset from the correlation traced by bulges with $n_{\text{sph}} > 2$.

4.3. Black Hole Mass–Spheroid Stellar Mass

Finally, we present the $M_{\text{BH}}-M_{*,\text{sph}}$ diagram in Figure 5, and its linear regression analysis in Table 4. The bulges of the early-type galaxies follow $M_{\text{BH}} \propto M_{*,\text{sph}}^{1.04 \pm 0.10}$, consistent with a dry-merging formation scenario¹⁹, and define a tight *early-type sequence* with intrinsic scatter $\epsilon_{(Y|X)} = 0.43 \pm 0.06$ dex. Graham (2012) reported that the $M_{\text{BH}}/M_{\text{dyn},\text{sph}}$ ratio for core-Sérsic galaxies was 0.36% ($M_{\text{dyn},\text{sph}}$ is the spheroid dynamical mass) and discussed the many implications of this. Using a larger data sample, Graham & Scott (2013) reported that the $M_{\text{BH}}/M_{*,\text{sph}}$ ratio was 0.49% for core-Sérsic galaxies. Here we find a median $M_{\text{BH}}/M_{*,\text{sph}}$ ratio of $0.50 \pm 0.04\%$ for the 22 core-Sérsic galaxies and $0.68 \pm 0.04\%$ for the 45 early-type galaxies. Among other things, this higher value (previously reported to be 0.1%–0.2% for all galaxy types, e.g., Marconi &

¹⁸ One reaches the same conclusion when using the vertical offset from the correlation defined by bulges with $n_{\text{sph}} > 3$ or even $n_{\text{sph}} > 4$. There are 13 and 10 bulges with $n_{\text{sph}} < 2$ that lie above and below, respectively, the correlation traced by bulges with $n_{\text{sph}} > 3$. Similarly, there are 15 and 8 bulges with $n_{\text{sph}} < 2$ that lie above and below, respectively, the correlation traced by bulges with $n_{\text{sph}} > 4$.

¹⁹ In dry mergers, the black hole and the bulge grow at the same pace, increasing their mass in lock step.

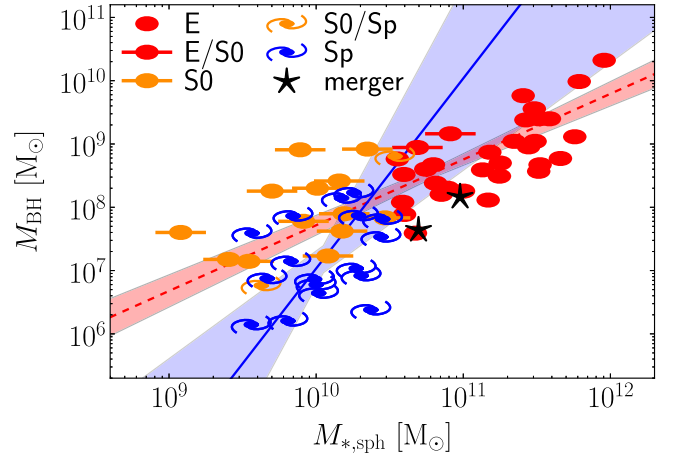


Figure 5. Black hole mass plotted against spheroid stellar mass. Symbols are coded according to the galaxy morphological type (see the legend). The red dashed line indicates the BCES bisector linear regression for the bulges of the 45 early-type galaxies (E+S0), with the red shaded area denoting its 1σ uncertainty. The bulges of early-type galaxies follow $M_{\text{BH}} \propto M_{*,\text{sph}}^{1.04 \pm 0.10}$, a near-linear relation consistent with a dry-merging formation scenario. The steeper blue solid line shows the BCES bisector linear regression for the bulges of the 17 late-type (Sp) galaxies, with the blue shaded area denoting its 1σ uncertainty. The bulges of late-type galaxies follow $M_{\text{BH}} \propto M_{*,\text{sph}}^{2-3}$, indicating that gas-rich processes feed the black hole more efficiently (“quadratically” or “cubically”) than the host bulge grows in stellar mass. We note that AGNs with $10^5 \lesssim M_{\text{BH}}/M_{\odot} \lesssim 2 \times 10^6$ (Jiang et al. 2011) appear to follow the blue line (see A. W. Graham et al. 2015, in preparation).

Hunt 2003), boosts estimates of the black hole mass function and mass density based on galaxy/spheroid luminosity functions.

The bulges of the spiral galaxies trace a steeper *late-type sequence*, whose slope is less well constrained due to the smaller size of the subsample and, more importantly, to the smaller range in $M_{*,\text{sph}}$ that the subsample spans. For the bulges of spiral galaxies, the BCES code returns a log–linear relation with a slope $= 3.00 \pm 1.30$, while the modified FITEXY routine finds a shallower (but still consistent within the 1σ uncertainty) slope $= 2.28^{+1.67}_{-1.01}$. More data would be welcome to better constrain the slope of this *late-type sequence*, though we note that direct measurements of black hole masses below $10^6 M_{\odot}$ are extremely challenging to obtain with the current technological resources. In this regard, using a sample of ~ 140 low-redshift ($z \leq 0.35$, with a median redshift $\langle z \rangle = 0.085$) bulges hosting active galactic nuclei (AGNs) with virial black hole masses $10^5 \lesssim M_{\text{BH}}/M_{\odot} \lesssim 2 \times 10^6$ (Jiang et al. 2011), Graham & Scott (2015) showed that they roughly follow the quadratic $M_{\text{BH}}-M_{*,\text{sph}}$ relation defined by their Sérsic bulges. The majority of our spiral galaxies host an AGN²⁰ and we anticipate here that the correlation traced by our spiral galaxy bulges may track the location of these lower mass AGNs in the $M_{\text{BH}}-M_{*,\text{sph}}$ diagram. That is, the AGNs appear to be the low-mass continuations of our tentative *late-type sequence* shown in Figure 5 and this will be explored with more rigour in a forthcoming paper.

As a final remark, we comment on the work by Reines & Volonteri (2015), who investigated the relationship between black hole mass and total galaxy stellar mass, $M_{*,\text{gal}}$. Their

²⁰ According to the nuclear classification reported on NED (NASA Extragalactic Database), among our 17 spiral galaxies, at least 12 host a Seyfert AGN and one hosts a LINER AGN.

Figure 8 presents the $M_{\text{BH}} - M_{*,\text{gal}}$ distribution for a sample of ≈ 260 local AGNs with virial black hole masses and for ≈ 80 galaxies with dynamical black hole masses. They concluded that the AGN sample and the early-type galaxies with quiescent black holes define two distinct sequences in their $M_{\text{BH}} - M_{*,\text{gal}}$ diagram; these two sequences have similar slopes, but have normalization factors that are different by more than one order of magnitude. Since we noted that the Jiang et al. (2011) AGN sample follows the steeper $M_{\text{BH}} - M_{*,\text{sph}}$ correlation traced by our spiral galaxy bulges (the majority of which host an AGN), it would be interesting to recover the $M_{\text{BH}} - M_{*,\text{sph}}$ distribution also for the AGN sample of Reines & Volonteri (2015). However, we do note that there is emerging evidence (e.g., Busch et al. 2015; Subramanian et al. 2016) for a population of bulges with black hole masses residing below (or to the right of) the red and blue $M_{\text{BH}} - M_{*,\text{sph}}$ sequences constructed here using samples with directly measured black hole masses, as speculated by Batcheldor (2010).

5. CONCLUSIONS

Using $3.6 \mu\text{m}$ *Spitzer* images, we have performed accurate multicomponent decompositions (i.e., bulge, disks, bars, spiral arms, rings, halo, nucleus, depleted core, etc.), which were checked to be consistent with the two-dimensional galaxy kinematics, for 66 nearby galaxies with a dynamical measurement of their black hole mass. We have derived galaxy luminosities, spheroid luminosities, and spheroid stellar masses. Our galaxy sample, besides being to date the largest sample with reliable bulge masses used to investigate black hole mass scaling relations, contains 17 spiral galaxies, half of which have $M_{\text{BH}} < 10^7 M_{\odot}$. This constitutes a significant improvement over past studies whose samples were biased toward high-mass, early-type galaxies.

Using our state-of-the-art data set, we have investigated substructure in the $M_{\text{BH}} - L_{\text{gal}}$, $M_{\text{BH}} - L_{\text{sph}}$ and $M_{\text{BH}} - M_{*,\text{sph}}$ diagrams. Our principal conclusions are as follows.

1. The logarithmic $M_{\text{BH}} - M_{*,\text{sph}}$ relation for the spheroidal components of early-type (elliptical + lenticular) galaxies has a slope of 1.04 ± 0.10 and intrinsic scatter of $\epsilon_{(Y|X)} = 0.43 \pm 0.06$ dex. We call this tight correlation an *early-type sequence*. The $M_{\text{BH}} - M_{*,\text{sph}}$ log-relation for the bulges of late-type (spiral) galaxies has a slope of 2–3, which is less well constrained due to the smaller size of the subsample and, more importantly, the smaller range in spheroid stellar mass ($3 \times 10^9 \lesssim M_{*,\text{sph}}/M_{\odot} \lesssim 3 \times 10^{10}$) that the subsample spans. We refer to this correlation as a *late-type sequence*. In (gas-poor) early-type galaxies, the black hole and the stellar content of the spheroidal component grow at the same pace, following a linear $M_{\text{BH}} - M_{*,\text{sph}}$ relation. In (gas-rich) spiral galaxies, the black hole grows faster than its host bulge, following a quadratic/cubic $M_{\text{BH}} - M_{*,\text{sph}}$ relation. Unsurprisingly, in a color–magnitude diagram²¹, our early- and late-type galaxies occupy the two distinct regions of the red sequence and the blue cloud, respectively. Analogous with this, we refer to our *early-type sequence* as a *red sequence* and to our *late-type sequence* as a *blue sequence*.

²¹ Total $B - V$ colors, corrected for inclination, Galactic extinction and K -correction, were taken from the HyperLEDA online database (Makarov et al. 2014).

2. The median $M_{\text{BH}}/M_{*,\text{sph}}$ ratio for the early-type galaxies is $0.68 \pm 0.04\%$. This value is dramatically larger than what was previously reported (0.1%–0.2% for all galaxy types, e.g., Marconi & Hunt 2003), but in close agreement with the value of 0.49% reported by Graham & Scott (2013) for core-Sérsic spheroids.
3. The logarithmic $M_{\text{BH}} - M_{*,\text{sph}}$ relations for the core-Sérsic and Sérsic spheroids have slopes with overlapping uncertainties (1.19 ± 0.23 and 1.48 ± 0.20 , respectively). The Sérsic relation is less steep than, but also has overlapping uncertainties with, the slope of 2.22 ± 0.58 reported by Scott et al. (2013) for Sérsic spheroids. The distinction between core-Sérsic and Sérsic spheroids found by Scott et al. (2013) is thus less pronounced here.
4. In the $M_{\text{BH}} - L_{\text{sph}}$ (or $M_{\text{BH}} - M_{*,\text{sph}}$) diagram, for early-type galaxies, we did not observe the change in slope required for consistency with the log–linear $M_{\text{BH}} - \sigma$ and bent $L_{\text{sph}} - \sigma$ correlations. This issue of inconsistency, therefore, remains an open question. It might be that we are still not probing enough low-mass black holes ($M_{\text{BH}} < 10^7 M_{\odot}$) for the subsample of early-type galaxies, or that the transition from $L_{\text{sph}} \propto \sigma^2$ at low luminosities to $L_{\text{sph}} \propto \sigma^{(5–6)}$ at high luminosities is less sharp than previously thought. We intend to investigate this point in our future work.
5. It has been argued that pseudo-bulges (disk-like, rotation-supported systems, built from secular processes) do not follow the $M_{\text{BH}} - L_{\text{sph}}$ correlation defined by classical bulges (spheroidal, pressure-supported systems, formed through violent processes). The recent literature (e.g., Sani et al. 2011; Beifiori et al. 2012) has distinguished between pseudo- and classical bulges according to their Sérsic index, n_{sph} . Although we do not consider the Sérsic index a good indicator of the nature of a bulge (e.g., Graham & Worley 2008), we investigated this point and found that, within the current data set, spheroids with $n_{\text{sph}} < 2$ are not offset to lower M_{BH} from the $M_{\text{BH}} - L_{\text{sph}}$ correlation defined by spheroids with $n_{\text{sph}} > 2$.
6. The $M_{\text{BH}} - L_{\text{gal}}$ and $M_{\text{BH}} - L_{\text{sph}}$ correlations have the same level of intrinsic scatter when considering early-type galaxies only. Once reasonable numbers of spiral galaxies are included, M_{BH} correlates better with L_{sph} than with L_{gal} (see also Beifiori et al. 2012; Erwin & Gadotti 2012).

Finally, we note that some of the literature-sourced black hole mass measurements used by Kormendy & Ho (2013) are different from those used here. While these differences are smaller than 18% for 78% of the galaxies, in three cases (NGC 0821, NGC 4291, and NGC 3393) they are larger than a factor of 2.3. We repeated our entire analysis using only the 58 galaxies that are in common between our sample and the sample of Kormendy & Ho (2013), assuming for these galaxies the black hole mass measurements published by Kormendy & Ho (2013). In doing so, we found that none of our conclusions changed.

G.S. warmly thanks Luca Cortese, Elisabete Lima Da Cunha, Duncan Forbes, and Gonzalo Diaz for useful discussion. We also thank the anonymous referee for useful comments and suggestions. This research was supported by Australian Research Council funding through grants DP110103509 and FT110100263. This work is based on observations made with the IRAC instrument (Fazio

et al. 2004) on board the *Spitzer Space Telescope*, which is operated by the Jet Propulsion Laboratory, California Institute of Technology under a contract with NASA. This research has made use of the GOLDMine database (Gavazzi et al. 2003) and the NASA/IPAC Extragalactic Database (NED) which is operated by the Jet Propulsion Laboratory, California Institute of Technology, under contract with the National Aeronautics and Space Administration. We acknowledge the usage of the HyperLeda database (<http://leda.univ-lyon1.fr>). The BCES routine (Akritas & Bershady 1996) was run via the python module written by Rodrigo Nemmen (Nemmen et al. 2012), which is available at <https://github.com/rsnemmen/BCES>.

REFERENCES

- Akritas, M. G., & Bershady, M. A. 1996, *ApJ*, **470**, 706
 Arnold, J. A., Romanowsky, A. J., Brodie, J. P., et al. 2014, *ApJ*, **791**, 80
 Athanassoula, E. 2005, *MNRAS*, **358**, 1477
 Balcells, M., Graham, A. W., & Peletier, R. F. 2007, *ApJ*, **665**, 1104
 Bardeen, J. M. 1975, in IAU Symp. 69, Dynamics of the Solar Systems, ed. A. Hayli, 297
 Batcheldor, D. 2010, *ApJL*, **711**, L108
 Beifiori, A., Courteau, S., Corsini, E. M., & Zhu, Y. 2012, *MNRAS*, **419**, 2497
 Bekki, K. 2010, *MNRAS*, **401**, L58
 Bender, R. 1990, *A&A*, **229**, 441
 Busch, G., Fazeli, N., Eckart, A., et al. 2015, arXiv:1511.00904
 Capaccioli, M. 1987, IAU Symp. 127, Structure and Dynamics of Elliptical Galaxies, ed. P. T. de Zeeuw, 47
 Cappellari, M., Emsellem, E., Krajnović, D., et al. 2011, *MNRAS*, **413**, 813
 Carter, D. 1987, *ApJ*, **312**, 514
 Chilingarian, I. V., Cayatte, V., Durret, F., et al. 2008, *A&A*, **486**, 85
 Cody, A. M., Carter, D., Bridges, T. J., Mobasher, B., & Poggianti, B. M. 2009, *MNRAS*, **396**, 1647
 Combes, F., Debbasch, F., Friedli, D., & Pfenniger, D. 1990, *A&A*, **233**, 82
 Combes, F., & Sanders, R. H. 1981, *A&A*, **96**, 164
 Davies, J. I., Phillipps, S., Cawson, M. G. M., Disney, M. J., & Kibblewhite, E. J. 1988, *MNRAS*, **232**, 239
 Davies, R. L., Efstathiou, G., Fall, S. M., Illingworth, G., & Schechter, P. L. 1983, *ApJ*, **266**, 41
 de Rijcke, S., Michielson, D., Dejonghe, H., Zeilinger, W. W., & Hau, G. K. T. 2005, *A&A*, **438**, 491
 dos Anjos, S., & da Silva, M. B. 2013, *MSAIS*, **25**, 33
 Dressler, A. 1989, in IAU Symp. 134, Active Galactic Nuclei, ed. D. E. Osterbrock & J. S. Miller, 217
 Eliche-Moral, M. C., González-García, A. C., Balcells, M., et al. 2011, *A&A*, **533**, A104
 Emsellem, E., Cappellari, M., Krajnović, D., et al. 2011, *MNRAS*, **414**, 888
 Erwin, P. 2010, arXiv:1002.1445
 Erwin, P., Beltrán, J. C. V., Graham, A. W., & Beckman, J. E. 2003, *ApJ*, **597**, 929
 Erwin, P., & Gadotti, D. A. 2012, *AdAst*, **2012**, 4
 Erwin, P., Saglia, R., Thomas, J., et al. 2015, in IAU Symp. 309, Using 3D Spectroscopy to Probe the Orbital Structure of Composite Bulges, ed. B. L. Ziegler et al., 359
 Fazio, G. G., Hora, J. L., Allen, L. E., et al. 2004, *ApJS*, **154**, 10
 Ferrarese, L., & Ford, H. 2005, *SSRv*, **116**, 523
 Ferrarese, L., & Merritt, D. 2000, *ApJL*, **539**, L9
 Forbes, D. A., Lasky, P., Graham, A. W., & Spitler, L. 2008, *MNRAS*, **389**, 1924
 Gadotti, D. A. 2009, *MNRAS*, **393**, 1531
 Gavazzi, G., Boselli, A., Donati, A., Franzetti, P., & Scoglio, M. 2003, *A&A*, **400**, 451
 Gebhardt, K., Bender, R., Bower, G., et al. 2000, *ApJL*, **539**, L13
 Graham, A. 2015, *H&A*, **16**, 360
 Graham, A. W. 2007, *MNRAS*, **379**, 711
 Graham, A. W. 2012, *ApJ*, **746**, 113
 Graham, A. W. 2013, in Elliptical and Disk Galaxy Structure and Modern Scaling, ed. T. D. Oswalt, & W. C. Keel, 91
 Graham, A. W. 2014, in ASP Conf. Ser. 480, Structure and Dynamics of Disk Galaxies, ed. M. S. Seigar & P. Treuthardt (San Francisco, CA: ASP), 185
 Graham, A. W. 2016, *Galactic Bulges*, **418**, 263
 Graham, A. W., Erwin, P., Trujillo, I., & Asensio Ramos, A. 2003, *AJ*, **125**, 2951
 Graham, A. W., Onken, C. A., Athanassoula, E., & Combes, F. 2011, *MNRAS*, **412**, 2211
 Graham, A. W., & Scott, N. 2013, *ApJ*, **764**, 151
 Graham, A. W., & Scott, N. 2015, *ApJ*, **798**, 54
 Graham, A. W., & Worley, C. C. 2008, *MNRAS*, **388**, 1708
 Gültekin, K., Richstone, D. O., Gebhardt, K., et al. 2009, *ApJ*, **698**, 198
 Häring, N., & Rix, H.-W. 2004, *ApJL*, **604**, L89
 Held, E. V., de Zeeuw, T., Mould, J., & Picard, A. 1992, in IAU Symp. 149, The Stellar Populations of Galaxies, ed. B. Barbuy & A. Renzini, **429**
 Hohl, F. 1975, in IAU Symp. 69, Dynamics of the Solar Systems ed. A. Hayli, 349
 Jerjen, H., Binggeli, B., & Freeman, K. C. 2000, *AJ*, **119**, 593
 Jiang, Y.-F., Greene, J. E., & Ho, L. C. 2011, *ApJL*, **737**, L45
 Kelly, B. C. 2007, *ApJ*, **665**, 1489
 Keselman, J. A., & Nusser, A. 2012, *MNRAS*, **424**, 1232
 Kormendy, J. 2015, arXiv:1504.03330
 Kormendy, J., & Ho, L. C. 2013, *ARA&A*, **51**, 511
 Kormendy, J., & Richstone, D. 1995, *ARA&A*, **33**, 581
 Kourkchi, E., Khosroshahi, H. G., Carter, D., et al. 2012, *MNRAS*, **420**, 2819
 Laor, A. 1998, *ApJL*, **505**, L83
 Laor, A. 2001, *ApJ*, **553**, 677
 Läsker, R., Ferrarese, L., & van de Ven, G. 2014a, *ApJ*, **780**, 69
 Läsker, R., Ferrarese, L., van de Ven, G., & Shankar, F. 2014b, *ApJ*, **780**, 70
 Lauer, T. R., Faber, S. M., Richstone, D., et al. 2007a, *ApJ*, **662**, 808
 Lauer, T. R., Faber, S. M., Richstone, D., et al. 2007b, *ApJ*, **662**, 808
 Liu, F. S., Xia, X. Y., Mao, S., Wu, H., & Deng, Z. G. 2008, *MNRAS*, **385**, 23
 MacArthur, L. A., González, J. J., & Courteau, S. 2009, *MNRAS*, **395**, 28
 Magorrian, J., Tremaine, S., Richstone, D., et al. 1998, *AJ*, **115**, 2285
 Makarov, D., Prugniel, P., Terekhova, N., Courtois, H., & Vauglin, I. 2014, *A&A*, **570**, A13
 Malumuth, E. M., & Kirshner, R. P. 1981, *ApJ*, **251**, 508
 Marconi, A., & Hunt, L. K. 2003, *ApJL*, **589**, L21
 Matković, A., & Guzmán, R. 2005, *MNRAS*, **362**, 289
 McConnell, N. J., & Ma, C.-P. 2013, *ApJ*, **764**, 184
 McConnell, N. J., Ma, C.-P., Gebhardt, K., et al. 2011, *Natur*, **480**, 215
 Meidt, S. E., Schinnerer, E., van de Ven, G., et al. 2014, *ApJ*, **788**, 144
 Montero-Dorta, A. D., Shu, Y., Bolton, A. S., Brownstein, J. R., & Weiner, B. J. 2015, arXiv:1505.03866
 Nemmen, R. S., Georganopoulos, M., Guiric, S., et al. 2012, *Sci*, **338**, 1445
 Nieto, J.-L., Bender, R., Arnaud, J., & Surma, P. 1991, *A&A*, **244**, L25
 Peletier, R. F., Kutdemir, E., van der Wolk, G., et al. 2012, *MNRAS*, **419**, 2031
 Pfenniger, D., & Friedli, D. 1991, *A&A*, **252**, 75
 Press, W. H., Teukolsky, S. A., Vetterling, W. T., & Flannery, B. P. 1992, Numerical Recipes in FORTRAN. The Art of Scientific Computing (2nd ed.; Cambridge: Cambridge Univ. Press)
 Querejeta, M., Eliche-Moral, M. C., Tapia, T., et al. 2015, *A&A*, **573**, A78
 Reines, A. E., & Volonteri, M. 2015, *ApJ*, **813**, 82
 Rix, H.-W., & White, S. D. M. 1990, *ApJ*, **362**, 52
 Rix, H.-W., & White, S. D. M. 1992, *MNRAS*, **254**, 389
 Rusli, S. P., Thomas, J., Saglia, R. P., et al. 2013, *AJ*, **146**, 45
 Ryan, C. J., De Robertis, M. M., Virani, S., Laor, A., & Dawson, P. C. 2007, *ApJ*, **654**, 799
 Saha, K. 2015, *ApJL*, **806**, L29
 Saha, K., Martinez-Valpuesta, I., & Gerhard, O. 2012, *MNRAS*, **421**, 333
 Sani, E., Marconi, A., Hunt, L. K., & Risaliti, G. 2011, *MNRAS*, **413**, 1479
 Savorgnan, G. A. D., & Graham, A. W. 2015, *MNRAS*, **446**, 2330
 Scannapieco, C., White, S. D. M., Springel, V., & Tissera, P. B. 2011, *MNRAS*, **417**, 154
 Schechter, P. L. 1980, *AJ*, **85**, 801
 Scorza, C., & Bender, R. 1990, *A&A*, **235**, 49
 Scorza, C., & Bender, R. 1995, *A&A*, **293**, 20
 Scott, N., Davies, R. L., Houghton, R. C. W., et al. 2014, *MNRAS*, **441**, 274
 Scott, N., Graham, A. W., & Schombert, J. 2013, *ApJ*, **768**, 76
 Seidel, M. K., Cacho, R., Ruiz-Lara, T., et al. 2015, *MNRAS*, **446**, 2837
 Sheth, K., Regan, M., Hinz, J. L., et al. 2010, *PASP*, **122**, 1397
 Subramanian, S., Ramya, S., Das, M., et al. 2016, *MNRAS*, **455**, 3148
 Tortora, C., Napolitano, N. R., Romanowsky, A. J., Capaccioli, M., & Covone, G. 2009, *MNRAS*, **396**, 1132
 Tremaine, S., Gebhardt, K., Bender, R., et al. 2002, *ApJ*, **574**, 740
 Trujillo, I., Erwin, P., Asensio Ramos, A., & Graham, A. W. 2004, *AJ*, **127**, 1917
 van den Bosch, R. C. E., Gebhardt, K., Gültekin, K., et al. 2012, *Natur*, **491**, 729

- Vika, M., Driver, S. P., Cameron, E., Kelvin, L., & Robotham, A. 2012,
[MNRAS](#), **419**, 2264
- von der Linden, A., Best, P. N., Kauffmann, G., & White, S. D. M. 2007,
[MNRAS](#), **379**, 867
- Wandel, A. 1999, [ApJL](#), **519**, L39
- Yee, H. K. C. 1992, in ASP Conf. Ser. 31, Relationships Between Active
Galactic Nuclei and Starburst Galaxies, ed. A. V. Filippenko (San
Francisco, CA: ASP), [417](#)
- Young, C. K., & Currie, M. J. 1994, [MNRAS](#), **268**, L11

$$M_{\text{BH}} - n_{\text{sph}}$$

While the previous Chapter was dedicated to the study of the relations between black hole mass and galaxy or spheroid luminosity, in this Chapter we perform an analogous analysis to explore the relation between black hole mass and spheroid Sérsic index ($M_{\text{BH}} - n_{\text{sph}}$). To address the issue of consistency between galaxy scaling relations that was outlined in Chapter 1, it is mandatory to include also an analysis of the relation between spheroid luminosity and spheroid Sérsic index ($L_{\text{sph}} - n_{\text{sph}}$). The reliability of the uncertainties associated with the Sérsic index measurements obtained from our 1D decompositions ensures a robust estimate of the intrinsic scatter in the $M_{\text{BH}} - n_{\text{sph}}$ diagram, which can be compared with that in the $M_{\text{BH}} - L_{\text{sph}}$ diagram.

From a physical point of view, the $M_{\text{BH}} - n_{\text{sph}}$ correlation is interesting because the Sérsic index is a measure of the central radial concentration of stars, which dictates the radial distribution of mass within a galaxy's spheroid and therefore determines the dynamical response of stars as measured through the observable σ_* (Graham & Driver, 2007a).

The remainder of this Chapter comprises the peer-reviewed version of the paper “Supermassive Black Holes and Their Host Spheroids. III. The $M_{\text{BH}} - n_{\text{sph}}$ correlation” by G. A. D. Sa-vorgnan, accepted for publication in the *The Astrophysical Journal*.

SUPERMASSIVE BLACK HOLES AND THEIR HOST SPHEROIDS III. THE $M_{\text{BH}} - n_{\text{sph}}$ CORRELATION

GILIA A. D. SAVORGNA¹

Centre for Astrophysics and Supercomputing, Swinburne University of Technology, Hawthorn, Victoria 3122, Australia.

Draft version March 9, 2016

ABSTRACT

The Sérsic $R^{1/n}$ model is the best approximation known to date for describing the light distribution of stellar spheroidal and disk components, with the Sérsic index n providing a direct measure of the central radial concentration of stars. The Sérsic index of a galaxy's spheroidal component, n_{sph} , has been shown to tightly correlate with the mass of the central supermassive black hole, M_{BH} . The $M_{\text{BH}} - n_{\text{sph}}$ correlation is also expected from other two well known scaling relations involving the spheroid luminosity, L_{sph} : the $L_{\text{sph}} - n_{\text{sph}}$ and the $M_{\text{BH}} - L_{\text{sph}}$. Obtaining an accurate estimate of the spheroid Sérsic index requires a careful modelling of a galaxy's light distribution and some studies have failed to recover a statistically significant $M_{\text{BH}} - n_{\text{sph}}$ correlation. With the aim of re-investigating the $M_{\text{BH}} - n_{\text{sph}}$ and other black hole mass scaling relations, we performed a detailed (i.e. bulge, disks, bars, spiral arms, rings, halo, nucleus, etc.) decomposition of 66 galaxies, with directly measured black hole masses, that had been imaged at 3.6 μm with *Spitzer*. In this paper, the third of this series, we present an analysis of the $L_{\text{sph}} - n_{\text{sph}}$ and $M_{\text{BH}} - n_{\text{sph}}$ diagrams. While early-type (elliptical+lenticular) and late-type (spiral) galaxies split into two separate relations in the $L_{\text{sph}} - n_{\text{sph}}$ and $M_{\text{BH}} - L_{\text{sph}}$ diagrams, they reunite into a single $M_{\text{BH}} \propto n_{\text{sph}}^{3.39 \pm 0.15}$ sequence with relatively small intrinsic scatter ($\epsilon \simeq 0.25$ dex). The black hole mass appears to be closely related to the spheroid central concentration of stars, which mirrors the inner gradient of the spheroid gravitational potential.

Subject headings: black hole physics; galaxies: bulges; galaxies: elliptical and lenticular, cD; galaxies: evolution; galaxies: structure

1. INTRODUCTION

The empirical Sérsic (1963, 1968) $R^{1/n}$ model has been demonstrated to provide adequate description of the light distribution of the stellar spheroidal¹ and disk components of galaxies (e.g. Caon et al. 1993; Andredakis et al. 1995; Iodice et al. 1997, 1999; Seigar & James 1998; Khosroshahi et al. 2000), yet its physical origin has remained unexplained for decades. The Sérsic model parameterizes the intensity of light I as a function of the projected galactic radius R such that

$$I(R; I_e, R_e, n) = I_e \exp \left\{ -b_n \left[\left(\frac{R}{R_e} \right)^{1/n} - 1 \right] \right\},$$

where I_e indicates the intensity at the effective radius R_e that encloses half of the total light from the model, the Sérsic index n is the parameter that regulates the curvature of the radial light profile, and b_n is a constant defined in terms of the Sérsic index (see Graham & Driver 2005, and references therein). A large Sérsic index corresponds to a steep inner profile and a shallow outer profile, whereas a small Sérsic index corresponds to a shallow inner profile and a steep outer profile. This means that, for a stellar spheroidal system whose light distribution is well approximated by the Sérsic model, the larger the

Sérsic index is, the more centrally concentrated the stars are and the more extended the outer envelope is.

A compelling physical interpretation for the Sérsic profile family was recently theorized by Cen (2014) and later confirmed by Nipoti (2015) by means of N -body simulations. Cen (2014) conjectured that, when structures form within a standard cold dark matter model seeded by random Gaussian fluctuations, any centrally concentrated stellar structure always possesses an extended stellar envelope, and vice versa. Nipoti (2015) quantitatively explored Cen's hypothesis and showed that systems originated from several mergers have a large Sérsic index ($n \gtrsim 4$), whereas systems with a Sérsic index as small as $n \simeq 2$ can be produced by coherent dissipationless collapse, and exponential profiles ($n = 1$) can only be obtained through dissipative processes. This scenario sets the theoretical framework for the well known correlation between the spheroid luminosity, L_{sph} , and the spheroid Sérsic index, n_{sph} , (e.g. Young & Currie 1994; Jerjen et al. 2000; Graham & Guzmán 2003), although the numerical results of Nipoti (2015) seem to lack of spheroidal systems with Sérsic indices as large as 7–10, which are commonly observed in the local Universe.

Given the existence of the $L_{\text{sph}} - n_{\text{sph}}$ correlation and the relation between the central black hole mass, M_{BH} , and the spheroid luminosity (e.g. Kormendy & Richstone 1995; Magorrian et al. 1998; Marconi & Hunt 2003; Häring & Rix 2004), an $M_{\text{BH}} - n_{\text{sph}}$ relation must exist. After Graham (2001) showed that the black hole mass is tightly linked to the stellar light concentration of spheroids (measured through a parameter different from,

gsavorgn@astro.swin.edu.au

¹ Throughout the text, we use the term “spheroid” to indicate either a disk-less elliptical galaxy or the bulge component of a disk galaxy; we do not attempt at distinguishing between classical bulges and disk-like pseudo-bulges (see Graham 2015b or Graham 2015a).

but closely related to the Sérsic index), Graham & Driver (2007) presented for the first time the $M_{\text{BH}} - n_{\text{sph}}$ correlation using a sample of 27 elliptical and disk galaxies. Graham & Driver (2007) fit their data with a log-quadratic regression, finding that the $M_{\text{BH}} - n_{\text{sph}}$ log-relation is steeper for spheroids with small Sérsic indices and shallower for spheroids with large Sérsic indices, and measured a relatively small level of scatter². A few years later, Sani et al. (2011), Vika et al. (2012) and Beifiori et al. (2012) performed multi-component decompositions for samples of galaxies similar to that used by Graham & Driver (2007), but they failed to recover a strong $M_{\text{BH}} - n_{\text{sph}}$ relation. This issue was tackled by Savorgnan et al. (2013), who collected the Sérsic index measurements published by Graham & Driver (2007), Sani et al. (2011), Vika et al. (2012) and Beifiori et al. (2012) for a sample of 54 galaxies, and showed that, by rejecting the most discrepant measurements and averaging the remaining ones, a strong $M_{\text{BH}} - n_{\text{sph}}$ relation was retrieved. Remarkably, Savorgnan et al. (2013) repeated their analysis upon excluding the Sérsic index measurements of Graham & Driver (2007) and still regained a significant $M_{\text{BH}} - n_{\text{sph}}$ correlation. This was suggesting that the individual galaxy decompositions of Sani et al. (2011), Vika et al. (2012) and Beifiori et al. (2012) were not accurate, i.e. each individual study obtained “noisy” Sérsic index measurements which prevented the recovery of a strong $M_{\text{BH}} - n_{\text{sph}}$ relation.

Motivated by the need for more accurate galaxy decompositions to refine and re-investigate scaling relations between the black hole mass and several host spheroid structural parameters, we performed state-of-the-art modelling for the largest sample of galaxies to date (Savorgnan & Graham 2015b, hereafter *Paper I*) for which a dynamical measurement of the black hole mass was available. In doing so, we used 3.6 μm *Spitzer* satellite imagery, given its superb capability to trace the stellar mass (Sheth et al. 2010, and references therein). In Savorgnan et al. (2015, hereafter *Paper II*) we examined the correlations between the black hole mass and the total galaxy luminosity, the spheroid luminosity and the spheroid stellar mass. Here we focus on the $M_{\text{BH}} - n_{\text{sph}}$ relation.

2. DATA

We populated the $L_{\text{sph}} - n_{\text{sph}}$ and $M_{\text{BH}} - n_{\text{sph}}$ diagrams with the same galaxy sample used in *Paper II* (and presented here in Table 1), i.e. 66 galaxies for which a dynamical measurement of the black hole mass has been reported in the literature (by Graham & Scott 2013 or Rusli et al. 2013) and for which we were able to successfully model the light distribution and measure the spheroid structural parameters using 3.6 μm *Spitzer* satellite images. Our galaxy decompositions take into account bulge, disks, spiral arms, bars, rings, halo, extended or unresolved nuclear source and partially depleted core, and – for the first time – they were checked to be consistent with the galaxy kinematics (Emsellem et al. 2011; Scott et al. 2014; Arnold et al. 2014). Kinematical information was used to confirm the presence

² At the time, the $M_{\text{BH}} - \sigma$ relation (Ferrarese & Merritt 2000; Gebhardt et al. 2000) was reported to have the same level of scatter as the $M_{\text{BH}} - n_{\text{sph}}$ relation ($\simeq 0.3$ dex).

of disk components in the majority of early-type (elliptical + lenticular) galaxies and, more importantly, to establish the radial extent of these disks, which in most cases is not obvious from a visual inspection of the galaxy images. This enabled us to distinguish between intermediate-scale disks, that are fully embedded in the spheroid, and large-scale disks, that encase the bulge and dominate the light at large radii. Savorgnan & Graham (2015a) demonstrate that when an intermediate-scale disk is misclassified and modeled as a large-scale disk, the luminosity of the spheroid is underestimated, hence the galaxy incorrectly appears as a positive outlier (an “over-massive” black hole) in the $M_{\text{BH}} - L_{\text{sph}}$ diagram. A detailed description of the dataset used here, the data reduction process and the galaxy modelling technique that we developed can be found in *Paper I*, along with a discussion of how we estimated the uncertainties on the spheroid Sérsic indices³. For the present analysis, we elected to use the spheroid Sérsic indices obtained from the decomposition of the one-dimensional major-axis surface brightness profiles of our galaxies. The morphological classification (E = elliptical; E/S0 = elliptical/lenticular; S0 = lenticular; S0/Sp = lenticular/spiral; Sp = spiral; and “merger”) follows from the galaxy decompositions illustrated in *Paper I*. As in *Paper II*, we will refer to early-type galaxies (E+S0) and late-type galaxies (Sp). The early-type bin includes the two galaxies classified as E/S0, whereas the two galaxies classified as S0/Sp and the two galaxies classified as “mergers” are included in neither the early- nor the late-type bin.

3. ANALYSIS AND RESULTS

As in *Paper II*, a linear regression analysis of the $L_{\text{sph}} - n_{\text{sph}}$ (Table 3 and Figure 1) and $M_{\text{BH}} - n_{\text{sph}}$ (Table 4 and Figure 2) diagrams was performed using three different routines: the BCES code from Akritas & Bershady (1996), the FITEXY routine (Press et al. 1992), as modified by Tremaine et al. (2002), and the Bayesian estimator `linmix_err` (Kelly 2007). All of these three routines take into account the intrinsic scatter, but only the FITEXY and the `linmix_err` codes allow one to quantify it. Tremaine et al. (2002) cautioned that the BCES estimator becomes ineffective when the dataset contains at least one low-precision measurement – regardless of how many high-precision measurements are in the sample – and tends to be biased in case of low number statistics, or if the mean square of the uncertainties associated to the independent variable is comparable to the variance of the distribution of the independent variable. According to the results from the Monte Carlo Markov Chain simulations of Tremaine et al. (2002) and Novak et al. (2006), these problems can be overcome with the use of the modified FITEXY routine. Park et al. (2012) also concluded that the modified FITEXY routine performs better and returns less biased results than the BCES estimator, and noted that the the modified FITEXY routine is computationally less intensive than the Bayesian

³ The uncertainties associated with the spheroid Sérsic indices were estimated with a method that takes into account systematic errors. This method consists in comparing, for each of our galaxies, the measurements of the spheroid Sérsic index obtained by other studies with that obtained by us. Systematic errors are typically not considered by popular 2D fitting codes, which report only the statistical errors associated with their fitted parameters. Readers should refer to *Paper I* for a more detailed discussion on this topic.

TABLE 1
 GALAXY SAMPLE.

Galaxy	Type	Distance	M_{BH}	MAG_{sph}	$n_{\text{sph}}^{\text{maj}}$
(1)	(2)	[Mpc]	[$10^8 M_{\odot}$]	[mag]	(6)
IC 1459	E	28.4	24^{+10}_{-10}	$-26.15^{+0.18}_{-0.11}$	$6.6^{+0.9}_{-0.8}$
IC 2560	Sp (bar)	40.7	$0.044^{+0.044}_{-0.022}$	$-22.27^{+0.66}_{-0.58}$	$0.8^{+0.4}_{-0.3}$
IC 4296	E	40.7	11^{+2}_{-2}	$-26.35^{+0.18}_{-0.11}$	$5.8^{+0.8}_{-0.7}$
M31	Sp (bar)	0.7	$1.4^{+0.9}_{-0.3}$	$-22.74^{+0.18}_{-0.11}$	$2.2^{+0.3}_{-0.3}$
M49	E	17.1	25^{+3}_{-1}	$-26.54^{+0.18}_{-0.11}$	$6.6^{+0.9}_{-0.8}$
M59	E	17.8	$3.9^{+0.4}_{-0.4}$	$-25.18^{+0.18}_{-0.11}$	$5.5^{+0.8}_{-0.7}$
M64	Sp	7.3	$0.016^{+0.004}_{-0.004}$	$-21.54^{+0.18}_{-0.11}$	$0.8^{+0.1}_{-0.1}$
M81	Sp (bar)	3.8	$0.74^{+0.21}_{-0.11}$	$-23.01^{+0.88}_{-0.66}$	$1.7^{+1.3}_{-0.7}$
M84	E	17.9	$9.0^{+0.9}_{-0.8}$	$-26.01^{+0.66}_{-0.58}$	$7.8^{+3.6}_{-2.5}$
M87	E	15.6	$58.0^{+3.5}_{-3.5}$	$-26.00^{+0.66}_{-0.58}$	$10.0^{+4.7}_{-3.2}$
M89	E	14.9	$4.7^{+0.5}_{-0.5}$	$-24.48^{+0.66}_{-0.58}$	$4.6^{+2.2}_{-1.5}$
M94	Sp (bar)	4.4	$0.060^{+0.014}_{-0.014}$	$-22.08^{+0.18}_{-0.11}$	$0.9^{+0.1}_{-0.1}$
M96	Sp (bar)	10.1	$0.073^{+0.015}_{-0.015}$	$-22.15^{+0.18}_{-0.11}$	$1.5^{+0.2}_{-0.2}$
M104	S0/Sp	9.5	$6.4^{+0.4}_{-0.4}$	$-23.91^{+0.66}_{-0.58}$	$5.8^{+2.7}_{-1.8}$
M105	E	10.3	4^{+1}_{-1}	$-24.29^{+0.66}_{-0.58}$	$5.2^{+2.4}_{-1.6}$
M106	Sp (bar)	7.2	$0.39^{+0.01}_{-0.01}$	$-21.11^{+0.18}_{-0.11}$	$2.0^{+0.3}_{-0.2}$
NGC 0524	S0	23.3	$8.3^{+2.7}_{-1.3}$	$-23.19^{+0.18}_{-0.11}$	$1.1^{+0.2}_{-0.1}$
NGC 0821	E	23.4	$0.39^{+0.26}_{-0.09}$	$-24.00^{+0.88}_{-0.66}$	$5.3^{+4.1}_{-2.3}$
NGC 1023	S0 (bar)	11.1	$0.42^{+0.04}_{-0.04}$	$-22.82^{+0.18}_{-0.11}$	$2.1^{+0.3}_{-0.3}$
NGC 1300	Sp (bar)	20.7	$0.73^{+0.69}_{-0.35}$	$-22.06^{+0.66}_{-0.58}$	$3.8^{+1.8}_{-1.2}$
NGC 1316	merger	18.6	$1.50^{+0.75}_{-0.80}$	$-24.89^{+0.66}_{-0.58}$	$2.0^{+1.0}_{-0.7}$
NGC 1332	E/S0	22.3	14^{+2}_{-2}	$-24.89^{+0.88}_{-0.66}$	$5.1^{+3.9}_{-2.2}$
NGC 1374	E	19.2	$5.8^{+0.5}_{-0.5}$	$-23.68^{+0.18}_{-0.11}$	$3.7^{+0.5}_{-0.5}$
NGC 1399	E	19.4	$4.7^{+0.6}_{-0.6}$	$-26.43^{+0.18}_{-0.11}$	$10.0^{+1.4}_{-1.2}$
NGC 2273	Sp (bar)	28.5	$0.083^{+0.004}_{-0.004}$	$-23.00^{+0.66}_{-0.58}$	$2.1^{+1.0}_{-0.7}$
NGC 2549	S0 (bar)	12.3	$0.14^{+0.02}_{-0.13}$	$-21.25^{+0.18}_{-0.11}$	$2.3^{+0.3}_{-0.3}$
NGC 2778	S0 (bar)	22.3	$0.15^{+0.09}_{-0.10}$	$-20.80^{+0.66}_{-0.58}$	$1.3^{+0.6}_{-0.4}$
NGC 2787	S0 (bar)	7.3	$0.40^{+0.04}_{-0.05}$	$-20.11^{+0.66}_{-0.58}$	$1.1^{+0.5}_{-0.4}$
NGC 2974	Sp (bar)	20.9	$1.7^{+0.2}_{-0.2}$	$-22.95^{+0.66}_{-0.58}$	$1.4^{+0.7}_{-0.5}$
NGC 3079	Sp (bar)	20.7	$0.024^{+0.024}_{-0.012}$	$-23.01^{+0.66}_{-0.58}$	$1.3^{+0.6}_{-0.4}$
NGC 3091	E	51.2	36^{+1}_{-2}	$-26.28^{+0.18}_{-0.11}$	$7.6^{+1.0}_{-0.9}$
NGC 3115	E/S0	9.4	$8.8^{+10.0}_{-2.7}$	$-24.22^{+0.18}_{-0.11}$	$4.4^{+0.6}_{-0.5}$
NGC 3227	Sp (bar)	20.3	$0.14^{+0.10}_{-0.06}$	$-21.76^{+0.66}_{-0.58}$	$1.7^{+0.8}_{-0.5}$
NGC 3245	S0 (bar)	20.3	$2.0^{+0.5}_{-0.5}$	$-22.43^{+0.18}_{-0.11}$	$2.9^{+0.4}_{-0.3}$
NGC 3377	E	10.9	$0.77^{+0.04}_{-0.06}$	$-23.49^{+0.66}_{-0.58}$	$7.7^{+3.6}_{-2.5}$
NGC 3384	S0 (bar)	11.3	$0.17^{+0.01}_{-0.02}$	$-22.43^{+0.18}_{-0.11}$	$1.6^{+0.2}_{-0.2}$
NGC 3393	Sp (bar)	55.2	$0.34^{+0.02}_{-0.02}$	$-23.48^{+0.66}_{-0.58}$	$3.4^{+1.6}_{-1.1}$
NGC 3414	E	24.5	$2.4^{+0.3}_{-0.3}$	$-24.35^{+0.18}_{-0.11}$	$4.8^{+0.7}_{-0.6}$
NGC 3489	S0/Sp (bar)	11.7	$0.058^{+0.008}_{-0.008}$	$-21.13^{+0.66}_{-0.58}$	$1.5^{+0.7}_{-0.5}$
NGC 3585	E	19.5	$3.1^{+1.4}_{-0.6}$	$-25.52^{+0.66}_{-0.58}$	$5.2^{+2.4}_{-1.7}$
NGC 3607	E	22.2	$1.3^{+0.5}_{-0.5}$	$-25.36^{+0.66}_{-0.58}$	$5.5^{+2.6}_{-1.7}$
NGC 3608	E	22.3	$2.0^{+1.1}_{-0.6}$	$-24.50^{+0.66}_{-0.58}$	$5.2^{+2.4}_{-1.7}$
NGC 3842	E	98.4	97^{+30}_{-26}	$-27.00^{+0.18}_{-0.11}$	$8.1^{+1.1}_{-1.0}$
NGC 3998	S0 (bar)	13.7	$8.1^{+2.0}_{-1.9}$	$-22.32^{+0.88}_{-0.66}$	$1.2^{+0.9}_{-0.5}$
NGC 4026	S0 (bar)	13.2	$1.8^{+0.6}_{-0.6}$	$-21.58^{+0.88}_{-0.66}$	$2.4^{+1.8}_{-1.0}$
NGC 4151	Sp (bar)	20.0	$0.65^{+0.07}_{-0.07}$	$-23.40^{+0.66}_{-0.58}$	$1.4^{+0.6}_{-0.4}$
NGC 4261	E	30.8	5^{+1}_{-1}	$-25.72^{+0.66}_{-0.58}$	$4.7^{+2.2}_{-1.5}$
NGC 4291	E	25.5	$3.3^{+0.9}_{-2.5}$	$-24.05^{+0.66}_{-0.58}$	$4.2^{+2.0}_{-1.4}$
NGC 4388	Sp (bar)	17.0	$0.075^{+0.002}_{-0.002}$	$-21.26^{+0.88}_{-0.66}$	$0.6^{+0.5}_{-0.3}$
NGC 4459	S0	15.7	$0.68^{+0.13}_{-0.13}$	$-23.48^{+0.66}_{-0.58}$	$3.1^{+1.5}_{-1.0}$
NGC 4473	E	15.3	$1.2^{+0.4}_{-0.9}$	$-23.88^{+0.66}_{-0.58}$	$2.3^{+1.1}_{-0.7}$
NGC 4564	S0	14.6	$0.60^{+0.03}_{-0.09}$	$-22.30^{+0.18}_{-0.11}$	$2.6^{+0.4}_{-0.3}$
NGC 4596	S0 (bar)	17.0	$0.79^{+0.38}_{-0.33}$	$-22.73^{+0.18}_{-0.11}$	$2.7^{+0.4}_{-0.3}$

Galaxy	Type	Distance	M_{BH}	MAG_{sph}	$n_{\text{sph}}^{\text{maj}}$
(1)	(2)	[Mpc]	[$10^8 M_{\odot}$]	[mag]	(6)
(3)	(4)	(5)			
NGC 4697	E	11.4	$1.8^{+0.2}_{-0.1}$	$-24.82^{+0.88}_{-0.66}$	$7.2^{+5.5}_{-3.1}$
NGC 4889	E	103.2	210^{+160}_{-160}	$-27.54^{+0.18}_{-0.11}$	$8.1^{+1.1}_{-1.0}$
NGC 4945	Sp (bar)	3.8	$0.014^{+0.014}_{-0.007}$	$-20.96^{+0.66}_{-0.58}$	$1.4^{+0.7}_{-0.5}$
NGC 5077	E	41.2	$7.4^{+4.7}_{-3.0}$	$-25.45^{+0.18}_{-0.11}$	$4.2^{+0.6}_{-0.5}$
NGC 5128	merger	3.8	$0.45^{+0.17}_{-0.10}$	$-23.89^{+0.88}_{-0.66}$	$1.2^{+0.9}_{-0.5}$
NGC 5576	E	24.8	$1.6^{+0.3}_{-0.4}$	$-24.44^{+0.18}_{-0.11}$	$3.3^{+0.5}_{-0.4}$
NGC 5845	S0	25.2	$2.6^{+0.4}_{-1.5}$	$-22.96^{+0.88}_{-0.66}$	$2.5^{+1.9}_{-1.1}$
NGC 5846	E	24.2	11^{+1}_{-1}	$-25.81^{+0.66}_{-0.58}$	$6.4^{+3.0}_{-2.1}$
NGC 6251	E	104.6	5^{+2}_{-2}	$-26.75^{+0.18}_{-0.11}$	$6.8^{+0.9}_{-0.8}$
NGC 7052	E	66.4	$3.7^{+2.6}_{-1.5}$	$-26.32^{+0.18}_{-0.11}$	$4.2^{+0.6}_{-0.5}$
NGC 7619	E	51.5	25^{+8}_{-3}	$-26.35^{+0.66}_{-0.58}$	$5.3^{+2.5}_{-1.7}$
NGC 7768	E	112.8	13^{+5}_{-4}	$-26.90^{+0.66}_{-0.58}$	$8.4^{+3.9}_{-2.7}$
UGC 03789	Sp (bar)	48.4	$0.108^{+0.005}_{-0.005}$	$-22.77^{+0.88}_{-0.66}$	$1.9^{+1.4}_{-0.8}$

NOTE. — *Column (1):* Galaxy name. *Column (2):* Morphological type (E=elliptical, S0=lenticular, Sp=spiral, merger). The morphological classification of four galaxies is uncertain (E/S0 or S0/Sp). The presence of a bar is indicated. *Column (3):* Distance. *Column (4):* Black hole mass. *Column (5):* Absolute 3.6 μm spheroid magnitude. *Column (6):* Spheroid major-axis Sérsic index. Spheroid magnitudes and Sérsic indices come from our state-of-the-art multicomponent galaxy decompositions (*Paper I*), which include bulge, disks, bars, spiral arms, rings, halo, extended or unresolved nuclear source and partially depleted core, and that – for the first time – were checked to be consistent with the galaxy kinematics. The uncertainties were estimated with a method that takes into account systematic errors, which are typically not considered by popular 2D fitting codes.

technique `linmix_err`. Given that at least one of our subsamples (the lenticular galaxies) has a small size and that the uncertainties associated to n_{sph} are relatively large compared to the range spanned by the n_{sph} values for most of our subsamples, we put more trust in the results obtained with the modified FITEXY routine and throughout the text we quote only those.

We report both symmetrical and nonsymmetrical linear regressions. Symmetrical regressions are meant to be compared with theoretical expectations, whereas nonsymmetrical forward ($Y|X$) regressions – which minimize the scatter in the Y direction – allow one to predict the value of the observable Y with the best possible precision.

We searched for extreme outliers in both the $L_{\text{sph}} - n_{\text{sph}}$ and $M_{\text{BH}} - n_{\text{sph}}$ diagrams, and found that in our $L_{\text{sph}} - n_{\text{sph}}$ plot there are no 3σ outliers, whereas in our $M_{\text{BH}} - n_{\text{sph}}$ plot the lenticular galaxies NGC 0524 and NGC 3998 reside more than 3σ from the bisector linear regression for all galaxies. These two galaxies have therefore been excluded from the rest of the analysis.

3.1. $L_{\text{sph}} - n_{\text{sph}}$

Following Graham (2001), who showed that the $L_{\text{sph}} - n_{\text{sph}}$ relation is different for elliptical galaxies and the bulges of disk galaxies (S0+Sp), Savorgnan et al. (2013) re-analyzed the data from Graham & Guzmán (2003) and Graham & Worley (2008) and obtained two separate $L_{\text{sph}} - n_{\text{sph}}$ linear regressions for elliptical galaxies and the bulges of disk galaxies (in the B- and K-band, respectively). At the time, the $L_{\text{sph}} - n_{\text{sph}}$ datasets from Graham & Guzmán (2003) and Graham & Worley (2008) were of the best quality available to investigate the $L_{\text{sph}} - n_{\text{sph}}$ relation for different galaxy morphological types. However, these datasets were not obtained from a homogeneous analysis, but they were a collection of results taken from various past bulge/disk decomposition studies. Here we re-investigate the $L_{\text{sph}} - n_{\text{sph}}$ diagram (Figure 1) using only our high-quality dataset. Our spheroid luminosities and Sérsic indices were obtained from accurate multicomponent decompositions, performed in a consistent manner using the $3.6 \mu\text{m}$ band, which is less affected by dust extinction than the K-band. Graham & Worley (2008) presented a single $L_{\text{sph}} - n_{\text{sph}}$ correlation for the bulges of disk galaxies (S0+Sp). However, using our dataset, we fit the $L_{\text{sph}} - n_{\text{sph}}$ relation for elliptical, lenticular and spiral galaxies separately, and found that the values of the slope and intercept for the lenticular galaxies are not consistent within the errors with those for the spiral galaxies, but are consistent within the errors with those for the elliptical galaxies. Given this, we conclude that in the $L_{\text{sph}} - n_{\text{sph}}$ diagram elliptical and lenticular galaxies form together a single (*early-type*) sequence, whereas the combination of lenticular and spiral galaxies do not. According to the modified FITEXY routine, early-type galaxies⁴ fol-

⁴ Using the BCES estimator, Savorgnan et al. (2013) re-analyzed the dataset from Graham & Guzmán (2003) and obtained $L_{\text{sph}} \propto n_{\text{sph}}^{3.60 \pm 0.19}$ for the elliptical galaxies only. This result is in excellent agreement with the BCES linear regression obtained here for the early-type galaxies ($L_{\text{sph}} \propto n_{\text{sph}}^{3.89 \pm 0.42}$) and, remarkably, it is exactly the same proportionality obtained here for the early-type galaxies with the modified FITEXY routine.

low $L_{\text{sph}} \propto n_{\text{sph}}^{3.60 \pm 0.19}$, whereas late-type galaxies follow a shallower $L_{\text{sph}} \propto n_{\text{sph}}^{1.44 \pm 0.52}$ sequence.

Because the log-slopes of the correlations for early- and late-type galaxies are not consistent with each other within their 1σ uncertainties, our quantitative linear regression analysis suggests that the $L_{\text{sph}} - n_{\text{sph}}$ diagram is better described with a four-parameter model (two separate power-laws) rather than with a two-parameter model (single power-law). In addition, the relative quality of these two statistical models can be independently assessed using the Akaike Information Criterion (*AIC*, Akaike 1974). *AIC* is a trade-off between the statistical significance of a fit and the complexity of the model used. It benefits from the goodness of a fit, but at the same time is also penalized by the number of parameters of the model, hence it discourages overfitting. The *AICc* is a variation of the *AIC* that takes into account a correction for finite sample sizes:

$$AICc = 2k - 2 \ln(\mathcal{L}) + \frac{2k(k+1)}{n-k-1}, \quad (1)$$

where k is the number of parameter of the model, n is the sample size, and \mathcal{L} is the maximum value of the likelihood function for the model. Within a set of candidate models for a given dataset, the best model has the smallest *AICc* value. Using our $L_{\text{sph}} - n_{\text{sph}}$ dataset, the *AICc* value for a double power-law model is a factor of $3/4$ smaller than the *AICc* value for a single power-law model.

3.2. $M_{\text{BH}} - n_{\text{sph}}$

Graham & Scott (2013) presented two different $M_{\text{BH}} - L_{\text{sph}}$ relations for Sérsic and core-Sérsic spheroids⁵ (Graham et al. 2003; Trujillo et al. 2004). However, in *Paper II* we found that the slopes of the $M_{\text{BH}} - L_{\text{sph}}$ correlations for Sérsic and core-Sérsic spheroids are consistent with each other within their 1σ uncertainties, which prevented us from considering them as two separate sequences. On the other hand, our analysis showed that early- and late-type galaxies follow two different $M_{\text{BH}} - L_{\text{sph}}$ relations. Given that early- and late-type galaxies define two separate sequences in both the $L_{\text{sph}} - n_{\text{sph}}$ and $M_{\text{BH}} - L_{\text{sph}}$ diagrams, we investigate substructure in the $M_{\text{BH}} - n_{\text{sph}}$ diagram. Using the results from the modified FITEXY routine, we know that the early-type galaxies follow $M_{\text{BH}} \propto L_{\text{sph}}^{1.03 \pm 0.11}$ and $L_{\text{sph}} \propto n_{\text{sph}}^{3.60 \pm 0.19}$, therefore we expect to find $M_{\text{BH}} \propto n_{\text{sph}}^{3.69 \pm 0.44}$; this prediction is in excellent agreement with the observed log-slope of 3.58 ± 0.27 obtained here. On the other hand, late-type galaxies follow $M_{\text{BH}} \propto L_{\text{sph}}^{2.58 \pm 1.06}$ and $L_{\text{sph}} \propto n_{\text{sph}}^{1.44 \pm 0.52}$, from which one can predict $M_{\text{BH}} \propto n_{\text{sph}}^{3.72 \pm 2.03}$; this is consistent with the observed log-slope of 4.55 ± 0.66 . The Bayesian estimator `linmix_err` returns consistent results: a log-slope of 3.44 ± 0.33 for the early-type galaxies and a log-slope of 4.12 ± 1.07 for the late-type galaxies. Regardless of the linear regression routine used, the values of the slope and intercept for the early- and late-type galaxies are consistent with each other within their 1σ uncertainties⁶. Our

⁵ Core-Sérsic spheroids have partially depleted cores relative to their outer Sérsic light profile, whereas Sérsic spheroids have no central deficit of stars.

⁶ In effect, considering the results of the modified FITEXY routine, the slopes of the relations for early- and late-type galaxies are

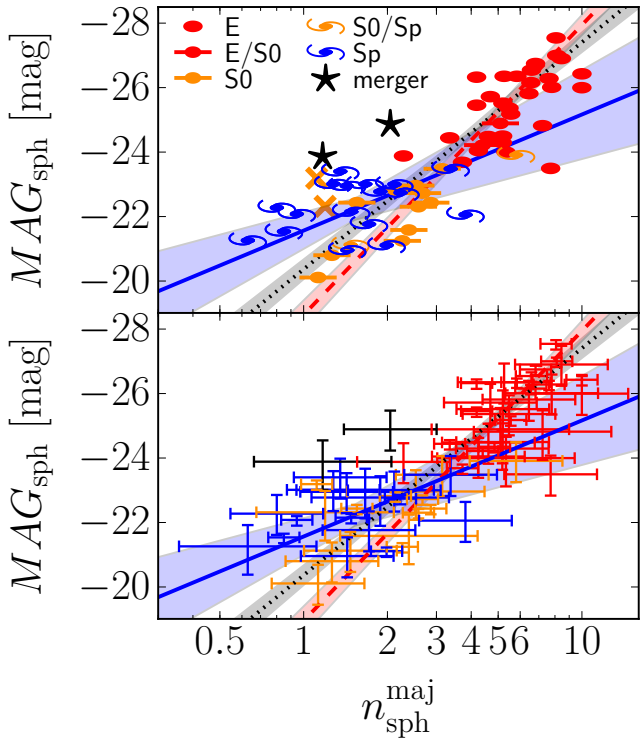


FIG. 1.— Spheroid absolute magnitude (at 3.6 μm) plotted against spheroid Sérsic index measured along the galaxy major-axis. The top and bottom panels show the data points and their error bars, respectively. Symbols are coded according to the galaxy morphological type (see legend in the top panel). The orange crosses denote two lenticular galaxies (NGC 0524 and NGC 3998) which were excluded from the linear regression analysis (see Section 3). The black dotted line is the FITEXY bisector linear regression for all (64) galaxies, with the gray shaded area denoting its 1σ uncertainty. The red dashed line is the FITEXY bisector linear regression for the $45 - 2 = 43$ early-type galaxies (E+S0), with the red shaded area denoting its 1σ uncertainty. The shallower blue solid line is the FITEXY bisector linear regression for the bulges of the 17 late-type (Sp) galaxies, with the blue shaded area denoting its 1σ uncertainty. The error bars in the bottom panel have the same color coding as the symbols in the top panel.

analysis shows that the early- and late-type galaxies do not follow two separate trends in the $M_{\text{BH}} - n_{\text{sph}}$ diagram, i.e. we do not identify any significant substructure based on the galaxy morphological type. The $AICc$ value for a single power-law model is a factor of 2/3 smaller than the $AICc$ value for a double power-law model. The symmetrical linear regression for all galaxies obtained with the modified FITEXY routine is:

$$\log\left(\frac{M_{\text{BH}}}{M_{\odot}}\right) = (8.15 \pm 0.06) + (3.37 \pm 0.15)(\log n_{\text{sph}} - 0.50).$$

We have seen that the early- and late-type galaxies in the $M_{\text{BH}} - n_{\text{sph}}$ diagram can be fit (together) with a

only marginally consistent with each other within their 1σ uncertainties. However, the same slopes obtained with Bayesian estimator `linmix_err` are fully consistent with each other within their 1σ uncertainties.

single power-law, whereas they follow two different correlations in the $M_{\text{BH}} - L_{\text{sph}}$ diagram (*Paper II*). We now want to compare the amount of intrinsic scatter in these two plots. In Table 5 we report the values of the intrinsic scatter in the $M_{\text{BH}} - n_{\text{sph}}$ and $M_{\text{BH}} - L_{\text{sph}}$ diagrams for all, early- and late-type galaxies, obtained with the modified FITEXY routine and the Bayesian estimator `linmix_err`. When considering all galaxies, irrespective of their morphological type, the intrinsic scatter of the $M_{\text{BH}} - n_{\text{sph}}$ relation is smaller than that of the $M_{\text{BH}} - L_{\text{sph}}$ relation. However, this is obviously not a fair comparison, because of the different nature of the $M_{\text{BH}} - n_{\text{sph}}$ and $M_{\text{BH}} - L_{\text{sph}}$ correlations (single and double power-law, respectively). One can obtain more informative results by considering early- and late-type galaxies separately. For the early-type galaxies, the intrinsic scatter of the $M_{\text{BH}} - n_{\text{sph}}$ relation is consistent⁷ with that of the $M_{\text{BH}} - L_{\text{sph}}$ relation (within their 1σ uncertainties). For the late-type galaxies, the intrinsic scatter of the $M_{\text{BH}} - n_{\text{sph}}$ relation is consistent with that of the $M_{\text{BH}} - L_{\text{sph}}$ relation, except for the inverse ($X|Y$) regression obtained with the modified FITEXY routine. In passing, we note that the values of the intrinsic scatter of the $M_{\text{BH}} - n_{\text{sph}}$ relation are systematically smaller – although consistent within the errors – than the corresponding values of the intrinsic scatter of the $M_{\text{BH}} - L_{\text{sph}}$ relation. In addition, the values of the intrinsic scatter returned by the modified FITEXY routine are systematically smaller than those output by the Bayesian estimator `linmix_err`.

4. CONCLUSIONS

The Sérsic index of a galaxy’s spheroidal component, n_{sph} , constitutes a direct measure of its central radial concentration of stars. After Graham (2001) proved that the central black hole mass, M_{BH} , correlates with the stellar light concentration of a galaxy’s spheroidal component, Graham & Driver (2007) presented and analyzed for the first time a tight $M_{\text{BH}} - n_{\text{sph}}$ correlation using a sample of 27 elliptical and disk galaxies for which they had performed photometric bulge/disk decomposition. The $M_{\text{BH}} - n_{\text{sph}}$ correlation can be predicted from the combination of two well known scaling relations involving the spheroid luminosity, L_{sph} : the $M_{\text{BH}} - L_{\text{sph}}$ (e.g. Kormendy & Richstone 1995; Magorrian et al. 1998; Marconi & Hunt 2003; Häring & Rix 2004) and the $L_{\text{sph}} - n_{\text{sph}}$ (e.g. Young & Currie 1994; Jerjen et al. 2000; Graham & Guzmán 2003). However, upon independently attempting photometric multicomponent decompositions for galaxy samples that were similar to that used by Graham & Driver (2007), three subsequent studies (Sani et al. 2011; Vika et al. 2012; Beifiori et al. 2012) failed to recover a statistically significant $M_{\text{BH}} - n_{\text{sph}}$ relation. Savorgnan et al. (2013) collected and compared the Sérsic index measurements obtained by Graham & Driver (2007), Sani et al. (2011), Vika et al. (2012) and Beifiori et al. (2012), and argued that the discrepancies were due to inaccurate galaxy decompositions.

Moved by a urgent need to re-investigate and refine

⁷ Looking at the results obtained with the modified FITEXY routine, the values of the intrinsic scatter are only marginally consistent with each other, but looking at the results obtained with the Bayesian estimator `linmix_err`, the values of the intrinsic scatter are fully consistent with each other.

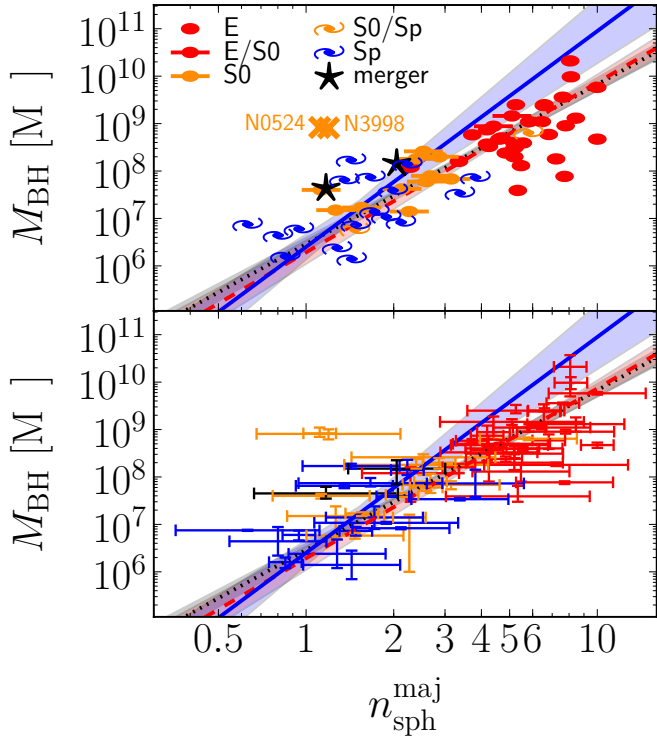


FIG. 2.— Black hole mass plotted against spheroid Sérsic index measured along the galaxy major-axis. The top and bottom panels show the data points and their error bars, respectively. Symbols are coded according to the galaxy morphological type (see legend). The orange crosses denote two lenticular galaxies (NGC 0524 and NGC 3998) which were excluded from the linear regression analysis (see Section 3). The black dotted line is the FITEXY bisector linear regression for all (64) galaxies, with the gray shaded area denoting its 1σ uncertainty. The red dashed line is the FITEXY bisector linear regression for the $45 - 2 = 43$ early-type galaxies (E+S0), with the red shaded area denoting its 1σ uncertainty. The blue solid line is the FITEXY bisector linear regression for the bulges of the 17 late-type (Sp) galaxies, with the blue shaded area denoting its 1σ uncertainty. The linear regressions for early- and late-type galaxies are consistent with each other within their 1σ uncertainties. The error bars in the bottom panel have the same color coding as the symbols in the top panel.

several black hole mass scaling relations, we performed state-of-the-art photometric multicomponent decompositions (i.e. bulge, disks, bars, spiral arms, rings, halo, nucleus, depleted core, etc.) for 66 galaxies with a dynamical measurement of their black hole mass (*Paper I*).

We carefully measured the Sérsic index of each galaxy’s spheroidal component and estimated its associated uncertainty with a method that takes into account statistical and systematic errors. Our analysis shows that early-(elliptical + lenticular) and late-type (spiral) galaxies define two different correlations in the $L_{\text{sph}} - n_{\text{sph}}$ diagram, whereas they reunite in a single sequence in the $M_{\text{BH}} - n_{\text{sph}}$ diagram. With the current dataset, we measured an amount of intrinsic scatter in the $M_{\text{BH}} - n_{\text{sph}}$ diagram systematically smaller, but still consistent within the errors, with that observed in the $M_{\text{BH}} - L_{\text{sph}}$ diagram (*Paper II*).

Our results suggest that the black hole mass is intimately connected to the spheroid central concentration of stars, which reflects the inner gradient of the spheroid gravitational potential. Besides conferring the spheroid Sérsic index a predictive power to infer the black hole mass from a galaxy’s image only (even photometrically uncalibrated), the $M_{\text{BH}} - n_{\text{sph}}$ correlation should become a fundamental ingredient in semi-analytic models and simulations of galaxy formation.

GS warmly thanks Chris Blake, Alister Graham and Carlo Nipoti for useful discussion. We also thank the anonymous referee for useful comments and suggestions. This research was supported by Australian Research Council funding through grants DP110103509 and FT110100263. This work is based on observations made with the IRAC instrument (Fazio et al. 2004) on-board the Spitzer Space Telescope, which is operated by the Jet Propulsion Laboratory, California Institute of Technology under a contract with NASA. This research has made use of the GOLDMine database (Gavazzi et al. 2003) and the NASA/IPAC Extragalactic Database (NED) which is operated by the Jet Propulsion Laboratory, California Institute of Technology, under contract with the National Aeronautics and Space Administration. We acknowledge the usage of the HyperLeda database (<http://leda.univ-lyon1.fr>). The BCES routine (Akritas & Bershady 1996) was run via the python module written by Rodrigo Nemmen (Nemmen et al. 2012), which is available at <https://github.com/rsnemmen/BCES>. The modified FITEXY linear regressions were performed using the IDL routine MPFITEXY (Williams et al. 2010), which is available at <http://purl.org/mike/mpfitexy>. The MPFITEXY routine depends on the MPFIT package (Markwardt 2009).

REFERENCES

- Akaike, H. 1974, Automatic Control, IEEE Transactions, 19, 716
 Akritas, M. G., & Bershady, M. A. 1996, ApJ, 470, 706
 Andredakis, Y. C., Peletier, R. F., & Balcells, M. 1995, MNRAS, 275, 874
 Arnold, J. A., Romanowsky, A. J., Brodie, J. P., et al. 2014, ApJ, 791, 80
 Beifiori, A., Courteau, S., Corsini, E. M., & Zhu, Y. 2012, MNRAS, 419, 2497
 Caon, N., Capaccioli, M., & D’Onofrio, M. 1993, MNRAS, 265, 1013
 Cen, R. 2014, ApJ, 790, L24
 Emsellem, E., Cappellari, M., Krajnović, D., et al. 2011, MNRAS, 414, 888
 Fazio, G. G., Hora, J. L., Allen, L. E., et al. 2004, ApJS, 154, 10
 Ferrarese, L., & Merritt, D. 2000, ApJ, 539, L9
 Gavazzi, G., Boselli, A., Donati, A., Franzetti, P., & Scodéglio, M. 2003, A&A, 400, 451
 Gebhardt, K., Bender, R., Bower, G., et al. 2000, ApJ, 539, L13
 Graham, A. 2015a, Highlights of Astronomy, 16, 360
 Graham, A. W. 2001, AJ, 121, 820
 —. 2015b, ArXiv e-prints, arXiv:1501.02937
 Graham, A. W., & Driver, S. P. 2005, PASA, 22, 118
 —. 2007, ApJ, 655, 77
 Graham, A. W., Erwin, P., Trujillo, I., & Asensio Ramos, A. 2003, AJ, 125, 2951
 Graham, A. W., & Guzmán, R. 2003, AJ, 125, 2936
 Graham, A. W., & Scott, N. 2013, ApJ, 764, 151
 Graham, A. W., & Worley, C. C. 2008, MNRAS, 388, 1708

TABLE 2
LINEAR REGRESSION ANALYSIS OF THE $L_{\text{sph}} - n_{\text{sph}}$ DIAGRAM.

Subsample (size)	Regression	α	β	$\langle \log n_{\text{sph}}^{\text{maj}} \rangle$	ϵ	Δ
$MAG_{\text{sph}}/[\text{mag}] = \alpha + \beta(\log n_{\text{sph}}^{\text{maj}} - \langle \log n_{\text{sph}}^{\text{maj}} \rangle)$						
All (64)	BCES ($Y X$)	-23.89 ± 0.15	-6.90 ± 0.74	0.50	—	1.22
	mFITEXY ($Y X$)	-23.91 ± 0.13	-6.63 ± 0.45	0.50	$0.59^{+0.16}_{-0.11}$	1.01
	linmix_err ($Y X$)	-23.89 ± 0.14	-6.34 ± 0.57	0.50	0.74 ± 0.13	1.14
	BCES ($X Y$)	-23.89 ± 0.15	-6.75 ± 0.52	0.50	—	1.20
	mFITEXY ($X Y$)	-23.89 ± 0.14	-7.49 ± 0.53	0.50	$0.62^{+0.18}_{-0.12}$	1.32
	linmix_err ($X Y$)	-23.90 ± 0.16	-7.49 ± 0.62	0.50	0.80 ± 0.16	1.32
	BCES Bisector	-23.89 ± 0.15	-6.83 ± 0.58	0.50	—	1.21
	mFITEXY Bisector	-23.90 ± 0.13	-7.04 ± 0.35	0.50	—	1.24
	linmix_err Bisector	-23.89 ± 0.15	-6.87 ± 0.42	0.50	—	1.21
Elliptical (E) (30)	BCES ($Y X$)	-25.46 ± 1.12	38.47 ± 114.45	0.76	—	6.37
	mFITEXY ($Y X$)	-25.74 ± 0.18	-9.74 ± 1.59	0.76	$0.24^{+0.32}_{-0.24}$	0.94
	linmix_err ($Y X$)	-25.65 ± 0.21	-7.87 ± 2.15	0.76	0.61 ± 0.22	1.06
	BCES ($X Y$)	-25.46 ± 0.23	-10.73 ± 3.21	0.76	—	1.29
	mFITEXY ($X Y$)	-25.74 ± 0.20	-10.42 ± 1.79	0.76	$0.22^{+0.38}_{-0.22}$	1.29
	linmix_err ($X Y$)	-25.72 ± 0.28	-10.92 ± 2.70	0.76	0.73 ± 0.34	1.33
	BCES Bisector	-25.46 ± 0.20	0.03 ± 0.05	0.76	—	1.14
	mFITEXY Bisector	-25.74 ± 0.19	-10.07 ± 1.19	0.76	—	1.26
	linmix_err Bisector	-25.68 ± 0.25	-9.15 ± 1.74	0.76	—	1.16
Lenticular (S0) (11)	BCES ($Y X$)	-22.08 ± 1.66	33.52 ± 98.87	0.33	—	6.09
	mFITEXY ($Y X$)	-22.11 ± 0.24	-6.31 ± 2.45	0.33	$0.42^{+0.28}_{-0.17}$	0.71
	linmix_err ($Y X$)			0.33		
	BCES ($X Y$)	-22.08 ± 0.19	-6.83 ± 1.16	0.33	—	0.71
	mFITEXY ($X Y$)	-21.94 ± 0.44	-13.16 ± 7.91	0.33	$0.61^{+0.60}_{-0.56}$	1.39
	linmix_err ($X Y$)			0.33		
	BCES Bisector	-22.08 ± 0.30	0.06 ± 0.05	0.33	—	1.09
	mFITEXY Bisector	-22.05 ± 0.35	-8.55 ± 2.79	0.33	—	0.84
	linmix_err Bisector			0.33		
Spiral (Sp) (17)	BCES ($Y X$)	-22.33 ± 0.26	-5.31 ± 5.83	0.18	—	1.15
	mFITEXY ($Y X$)	-22.22 ± 0.19	-2.17 ± 0.98	0.18	$0.53^{+0.24}_{-0.13}$	0.72
	linmix_err ($Y X$)	-22.26 ± 0.24	-1.53 ± 1.88	0.18	0.71 ± 0.22	0.78
	BCES ($X Y$)	-22.33 ± 0.26	-5.19 ± 3.77	0.18	—	1.13
	mFITEXY ($X Y$)	-22.28 ± 0.44	-9.08 ± 5.31	0.51	$1.12^{+0.54}_{-0.31}$	1.83
	linmix_err ($X Y$)	-22.24 ± 0.71	-11.12 ± 13.59	0.18	1.95 ± 2.47	2.24
	BCES Bisector	-22.33 ± 0.26	-5.25 ± 3.38	0.18	—	1.14
	mFITEXY Bisector	-22.23 ± 0.33	-3.60 ± 1.29	0.18	—	0.92
	linmix_err Bisector	-22.25 ± 0.53	-2.88 ± 2.66	0.18	—	0.84

- Häring, N., & Rix, H.-W. 2004, ApJ, 604, L89
- Iodice, E., D'Onofrio, M., & Capaccioli, M. 1997, in Astronomical Society of the Pacific Conference Series, Vol. 116, The Nature of Elliptical Galaxies; 2nd Stromlo Symposium, ed. M. Arnaboldi, G. S. Da Costa, & P. Saha, 84
- Iodice, E., D'Onofrio, M., & Capaccioli, M. 1999, in Astronomical Society of the Pacific Conference Series, Vol. 176, Observational Cosmology: The Development of Galaxy Systems, ed. G. Giuricin, M. Mezzetti, & P. Salucci, 402
- Jerjen, H., Binggeli, B., & Freeman, K. C. 2000, AJ, 119, 593
- Kelly, B. C. 2007, ApJ, 665, 1489
- Khosroshahi, H. G., Wadadekar, Y., & Kembhavi, A. 2000, ApJ, 533, 162
- Kormendy, J., & Richstone, D. 1995, ARA&A, 33, 581
- Magorrian, J., Tremaine, S., Richstone, D., et al. 1998, AJ, 115, 2285
- Marconi, A., & Hunt, L. K. 2003, ApJ, 589, L21
- Markwardt, C. B. 2009, in Astronomical Society of the Pacific Conference Series, Vol. 411, Astronomical Data Analysis Software and Systems XVIII, ed. D. A. Bohlander, D. Durand, & P. Dowler, 251
- Nemmen, R. S., Georgopoulos, M., Guiriec, S., et al. 2012, Science, 338, 1445
- Nipoti, C. 2015, ApJ, 805, L16
- Novak, G. S., Faber, S. M., & Dekel, A. 2006, ApJ, 637, 96
- Park, D., Kelly, B. C., Woo, J.-H., & Treu, T. 2012, ApJS, 203, 6
- Press, W. H., Teukolsky, S. A., Vetterling, W. T., & Flannery, B. P. 1992, Numerical recipes in FORTRAN. The art of scientific computing
- Rusli, S. P., Erwin, P., Saglia, R. P., et al. 2013, AJ, 146, 160
- Sani, E., Marconi, A., Hunt, L. K., & Risaliti, G. 2011, MNRAS, 413, 1479
- Savorgnan, G., Graham, A. W., Marconi, A., et al. 2013, MNRAS, 434, 387
- Savorgnan, G. A. D., & Graham, A. W. 2015a, ArXiv e-prints, arXiv:1511.05654
- . 2015b, ArXiv e-prints, arXiv:1511.07446
- Savorgnan, G. A. D., Graham, A. W., Marconi, A., & Sani, E. 2015, ArXiv e-prints, arXiv:1511.07437
- Scott, N., Davies, R. L., Houghton, R. C. W., et al. 2014, MNRAS, 441, 274
- Seigar, M. S., & James, P. A. 1998, MNRAS, 299, 672
- Sérsic, J. L. 1963, Boletín de la Asociación Argentina de Astronomía La Plata Argentina, 6, 41
- . 1968, Atlas de galaxias australes
- Sheth, K., Regan, M., Hinz, J. L., et al. 2010, PASP, 122, 1397
- Tremaine, S., Gebhardt, K., Bender, R., et al. 2002, ApJ, 574, 740
- Trujillo, I., Erwin, P., Asensio Ramos, A., & Graham, A. W. 2004, AJ, 127, 1917

TABLE 3
LINEAR REGRESSION ANALYSIS OF THE $L_{\text{sph}} - n_{\text{sph}}$ DIAGRAM.

Subsample (size)	Regression	α	β	$\langle \log n_{\text{sph}}^{\text{maj}} \rangle$	ϵ	Δ
Early-type (E+S0) (43)	BCES ($Y X$)	-24.55 ± 0.22	-11.84 ± 2.29	0.64	—	1.50
	mFITEXY ($Y X$)	-24.74 ± 0.14	-8.86 ± 0.66	0.51	$0.27^{+0.20}_{-0.27}$	0.87
	linmix_err ($Y X$)	-24.70 ± 0.17	-8.28 ± 0.87	0.64	0.58 ± 0.17	0.98
	BCES ($X Y$)	-24.55 ± 0.14	-8.25 ± 0.63	0.64	—	0.96
	mFITEXY ($X Y$)	-24.74 ± 0.14	-9.13 ± 0.68	0.64	$0.23^{+0.25}_{-0.23}$	1.08
	linmix_err ($X Y$)	-24.73 ± 0.18	-9.08 ± 0.87	0.64	0.60 ± 0.21	1.07
	BCES Bisector	-24.55 ± 0.17	-9.73 ± 1.05	0.64	—	1.14
	mFITEXY Bisector	-24.74 ± 0.14	-8.99 ± 0.48	0.64	—	1.06
	linmix_err Bisector	-24.72 ± 0.17	-8.66 ± 0.63	0.64	—	1.02
	BCES ($Y X$)	-22.25 ± 0.20	-5.88 ± 3.06	0.26	—	1.16
	mFITEXY ($Y X$)	-22.19 ± 0.14	-2.99 ± 0.73	0.26	$0.52^{+0.18}_{-0.10}$	0.75
	linmix_err ($Y X$)	-22.20 ± 0.17	-2.48 ± 1.21	0.26	0.67 ± 0.15	0.83
Bulge (S0+Sp) (30)	BCES ($X Y$)	-22.25 ± 0.20	-5.85 ± 1.83	0.26	—	1.15
	mFITEXY ($X Y$)	-22.17 ± 0.25	-7.65 ± 2.43	0.26	$0.87^{+0.30}_{-0.18}$	1.46
	linmix_err ($X Y$)	-22.16 ± 0.31	-7.80 ± 3.89	0.26	1.18 ± 0.65	1.48
	BCES Bisector	-22.25 ± 0.20	-5.87 ± 2.06	0.26	—	1.16
	mFITEXY Bisector	-22.18 ± 0.20	-4.34 ± 0.84	0.26	—	0.96
	linmix_err Bisector	-22.19 ± 0.25	-3.83 ± 1.39	0.26	—	0.91

NOTE. — For each subsample, we indicate $\langle \log n_{\text{sph}} \rangle$, its average value of spheroid Sérsic index. In the last two columns, we report ϵ , the intrinsic scatter, and Δ , the total rms scatter in the L_{sph} direction. The lenticular galaxies NGC 0524 and NGC 3998 were excluded from the linear regression analysis (see Section 3). Both the early- and late-type subsamples do not contain the two galaxies classified as S0/Sp and the two galaxies classified as mergers (45+17=66-2-2).

Vika, M., Driver, S. P., Cameron, E., Kelvin, L., & Robotham, A. 2012, MNRAS, 419, 2264

Williams, M. J., Bureau, M., & Cappellari, M. 2010, MNRAS, 409, 1330

Young, C. K., & Currie, M. J. 1994, MNRAS, 268, L11

TABLE 4
LINEAR REGRESSION ANALYSIS OF THE $M_{\text{BH}} - n_{\text{sph}}$ DIAGRAM.

Subsample (size)	Regression	α	β	$\langle \log n_{\text{sph}}^{\text{maj}} \rangle$	ϵ	Δ
$\log(M_{\text{BH}}/\text{M}_{\odot}) = \alpha + \beta(\log n_{\text{sph}}^{\text{maj}} - \langle \log n_{\text{sph}}^{\text{maj}} \rangle)$						
All (64)	BCES ($Y X$)	8.14 ± 0.07	3.49 ± 0.36	0.50	—	0.61
	mFITEXY ($Y X$)	8.15 ± 0.06	3.26 ± 0.21	0.50	$0.22^{+0.10}_{-0.07}$	0.46
	linmix_err ($Y X$)	8.15 ± 0.06	3.17 ± 0.24	0.50	0.28 ± 0.07	0.56
	BCES ($X Y$)	8.14 ± 0.08	3.52 ± 0.25	0.50	—	0.61
	mFITEXY ($X Y$)	8.15 ± 0.06	3.49 ± 0.23	0.50	$0.23^{+0.10}_{-0.07}$	0.61
	linmix_err ($X Y$)	8.15 ± 0.07	3.49 ± 0.26	0.50	0.29 ± 0.08	0.61
	BCES Bisector	8.14 ± 0.07	3.51 ± 0.28	0.50	—	0.61
	mFITEXY Bisector	8.15 ± 0.06	3.37 ± 0.15	0.50	—	0.59
	linmix_err Bisector	8.15 ± 0.07	3.32 ± 0.18	0.50	—	0.58
Early-type (E+S0) (43)	BCES ($Y X$)	8.54 ± 0.10	4.07 ± 0.87	0.64	—	0.65
	mFITEXY ($Y X$)	8.58 ± 0.07	3.32 ± 0.34	0.64	$0.24^{+0.10}_{-0.07}$	0.45
	linmix_err ($Y X$)	8.57 ± 0.08	3.12 ± 0.43	0.64	0.32 ± 0.08	0.53
	BCES ($X Y$)	8.54 ± 0.09	3.95 ± 0.55	0.64	—	0.63
	mFITEXY ($X Y$)	8.59 ± 0.08	3.88 ± 0.43	0.64	$0.26^{+0.11}_{-0.08}$	0.62
	linmix_err ($X Y$)	8.59 ± 0.09	3.82 ± 0.50	0.64	0.35 ± 0.10	0.61
	BCES Bisector	8.54 ± 0.10	4.01 ± 0.63	0.64	—	0.64
	mFITEXY Bisector	8.59 ± 0.07	3.58 ± 0.27	0.64	—	0.58
	linmix_err Bisector	8.58 ± 0.08	3.44 ± 0.33	0.64	—	0.56
Spiral (Sp) (17)	BCES ($Y X$)	7.18 ± 0.28	6.78 ± 6.62	0.18	—	1.23
	mFITEXY ($Y X$)	7.24 ± 0.13	4.48 ± 0.90	0.18	$0.13^{+0.42}_{-0.13}$	0.52
	linmix_err ($Y X$)	7.22 ± 0.16	3.57 ± 1.36	0.18	0.39 ± 0.19	0.70
	BCES ($X Y$)	7.18 ± 0.23	5.48 ± 1.93	0.18	—	0.99
	mFITEXY ($X Y$)	7.24 ± 0.14	4.62 ± 0.96	0.18	$0.13^{+0.43}_{-0.13}$	0.85
	linmix_err ($X Y$)	7.21 ± 0.21	4.86 ± 1.64	0.18	0.45 ± 0.31	0.89
	BCES Bisector	7.18 ± 0.25	6.06 ± 3.66	0.18	—	1.10
	mFITEXY Bisector	7.24 ± 0.14	4.55 ± 0.66	0.18	—	0.84
	linmix_err Bisector	7.22 ± 0.19	4.12 ± 1.07	0.18	—	0.77

NOTE. — For each subsample, we indicate $\langle \log n_{\text{sph}} \rangle$, its average value of spheroid Sérsic index. In the last two columns, we report ϵ , the intrinsic scatter, and Δ , the total rms scatter in the M_{BH} direction. The lenticular galaxies NGC 0524 and NGC 3998 were excluded from the linear regression analysis (see Section 3). Both the early- and late-type subsamples do not contain the two galaxies classified as S0/Sp and the two galaxies classified as mergers (45+17=66-2-2).

TABLE 5
INTRINSIC SCATTER ϵ OF THE $M_{\text{BH}} - n_{\text{sph}}$ AND $M_{\text{BH}} - L_{\text{sph}}$ RELATIONS.

Subsample	Regression	ϵ for $M_{\text{BH}} - n_{\text{sph}}$	ϵ for $M_{\text{BH}} - L_{\text{sph}}$
All	mFITEXY ($Y X$)	$0.22^{+0.10}_{-0.07}$	$0.49^{+0.06}_{-0.05}$
	linmix_err ($Y X$)	0.29 ± 0.07	0.51 ± 0.06
	mFITEXY ($X Y$)	$0.23^{+0.10}_{-0.07}$	$0.58^{+0.07}_{-0.06}$
	linmix_err ($X Y$)	0.30 ± 0.07	0.60 ± 0.09
Early-type	mFITEXY ($Y X$)	$0.24^{+0.10}_{-0.07}$	$0.40^{+0.06}_{-0.05}$
	linmix_err ($Y X$)	0.32 ± 0.08	0.41 ± 0.06
	mFITEXY ($X Y$)	$0.26^{+0.11}_{-0.08}$	$0.49^{+0.08}_{-0.06}$
	linmix_err ($X Y$)	0.35 ± 0.10	0.51 ± 0.10
Late-type	mFITEXY ($Y X$)	$0.13^{+0.42}_{-0.13}$	$0.55^{+0.15}_{-0.10}$
	linmix_err ($Y X$)	0.39 ± 0.19	0.63 ± 0.16
	mFITEXY ($X Y$)	$0.13^{+0.43}_{-0.13}$	$1.09^{+0.41}_{-0.24}$
	linmix_err ($X Y$)	0.45 ± 0.31	1.31 ± 0.97

6

Monster Black Holes in Massive Galaxies

A precise measurement of the log-slope of the $M_{\text{BH}} - \sigma_*$ correlation is important to constrain theoretical models of AGN feedback. For example, energy driven outflows are expected to produce a scaling of $M_{\text{BH}} \propto \sigma_*^5$, whereas momentum driven outflows should result into a shallower $M_{\text{BH}} \propto \sigma_*^4$ relation (Silk & Rees, 1998; Fabian, 1999). Since the $M_{\text{BH}} - \sigma_*$ correlation was presented for the first time by Ferrarese & Merritt (2000) and Gebhardt et al. (2000), there has been an ongoing, lively debate about its log-slope, whose estimates differed by up to a few standard deviations depending on the choice of galaxy sample, the method used to measure the velocity dispersion, the assumed uncertainty associated with the velocity dispersion, and the linear regression algorithm (e.g. Tremaine et al. 2002).

Recent measurements of SMBH masses in Central Cluster Galaxies (CCGs) have added new data points at the high-mass end of the $M_{\text{BH}} - \sigma_*$ diagram (McConnell et al., 2011, 2012), which appear to be outlying (“over-massive”) with respect to the observed correlation. Volonteri & Ciotti (2013) explained the presence of over-massive black holes in CCGs (they included in this definition either central dominant galaxies or brightest cluster galaxies) as a natural consequence of the fact that these galaxies have experienced more dry mergers than any other early-type galaxy (see also Kormendy & Ho 2013). Their semi-analytical models are based on the idea that parabolic dissipationless dry mergers increase a galaxy’s mass, luminosity and effective radius, but do not significantly change its velocity dispersion (e.g. Ciotti et al. 2007). Let an elliptical galaxy be a non rotating, isotropic and virialized spheroidal system with stellar mass M_* and gas mass $M_g = \alpha M_*$. The total energy E of this galaxy is the sum of its total kinetic energy K and its total gravitational energy W . The total kinetic energy is given by the sum of the stellar

kinetic energy K_* and the gas internal energy K_g , therefore the total energy can be expressed as:

$$E = K_* + K_g + W . \quad (6.1)$$

The stellar kinetic energy is

$$K_* = \frac{3}{2} M_* \sigma_*^2 , \quad (6.2)$$

where σ_* is the stellar velocity dispersion.

The gas internal energy is defined as

$$K_g = \frac{3 k_B}{2 \bar{m}} \int_{\mathcal{V}} \rho_g T d\mathcal{V} , \quad (6.3)$$

where k_B is the Boltzmann constant, \bar{m} is the gas mean molecular mass, and ρ_g and T are the density spatial distribution and the temperature of the gas, respectively, within the galaxy's volume \mathcal{V} .

The total gravitational energy is defined as

$$W = \frac{1}{2} \int_{\mathcal{V}} (\rho_* + \rho_g)(\phi_* + \phi_g) d\mathcal{V} , \quad (6.4)$$

where ρ_* is the density spatial distribution of stars, and ϕ_* and ϕ_g indicate the gravitational potential of stars and gas, respectively.

Under the assumption of gas in equilibrium in the total gravitational field, from the Jeans and hydrostatic equations one has that $T = \bar{m}\sigma_*^2/k_B$ and thus

$$K_g = \alpha K_* . \quad (6.5)$$

Assuming also that the spatial distribution of gas is proportional to that of stars (i.e. $\rho_g = \alpha\rho_*$ and $\phi_g = \alpha\phi_*$), the total gravitational energy can be written as

$$W = \frac{1}{2}(1 + \alpha)^2 \int_{\mathcal{V}} \rho_* \phi_* d\mathcal{V} = (1 + \alpha)^2 W_* , \quad (6.6)$$

where W_* is the gravitational energy of the stellar component only.

From the virial theorem (i.e. $E = K + W = W/2 = -2K$), the galaxy's total energy can be expressed as

$$E = \frac{1}{2}(1 + \alpha)^2 W_* = -(1 + \alpha) K_* . \quad (6.7)$$

We now consider the parabolic dissipationless merger of two galaxies (with stellar masses M_{*1} and M_{*2} , and total energies E_1 and E_2), i.e. a merger where both the total energy and the total

mass are conserved, and no gas is converted into stars.

The gas fraction α of the merger remnant is by definition

$$\alpha = \frac{M_g}{M_*} = \frac{M_{g1} + M_{g2}}{M_{*1} + M_{*2}} , \quad (6.8)$$

where the nomenclature is self-explicative.

By imposing the conservation of total energy, we get

$$\begin{aligned} E &= E_1 + E_2 \\ -(1+\alpha)\frac{3}{2}M_*\sigma_*^2 &= -(1+\alpha_1)\frac{3}{2}M_{*1}\sigma_{*1}^2 - (1+\alpha_2)\frac{3}{2}M_{*2}\sigma_{*2}^2 \\ [(1+\alpha_1)M_{*1} + (1+\alpha_2)M_{*2}]\sigma_*^2 &= (1+\alpha_1)M_{*1}\sigma_{*1}^2 + (1+\alpha_2)M_{*2}\sigma_{*2}^2 \\ \sigma_*^2 &= \frac{(1+\alpha_1)M_{*1}\sigma_{*1}^2 + (1+\alpha_2)M_{*2}\sigma_{*2}^2}{[(1+\alpha_1)M_{*1} + (1+\alpha_2)M_{*2}]} . \end{aligned} \quad (6.9)$$

By defining $c_1 = (1+\alpha_1)M_{*1}/[(1+\alpha_1)M_{*1} + (1+\alpha_2)M_{*2}]$ and $c_2 = (1+\alpha_2)M_{*2}/[(1+\alpha_1)M_{*1} + (1+\alpha_2)M_{*2}]$, Equation 6.9 can be simplified as

$$\sigma_*^2 = c_1\sigma_{*1}^2 + c_2\sigma_{*2}^2 . \quad (6.10)$$

Finally, since $c_1 + c_2 = 1$, we have that

$$\min(\sigma_{*1}^2, \sigma_{*2}^2) \leq \sigma_*^2 \leq \max(\sigma_{*1}^2, \sigma_{*2}^2) , \quad (6.11)$$

that is, the velocity dispersion of the merger remnant cannot be larger than the maximum velocity dispersion of the progenitor galaxies. This conclusion is not true in case of a wet merger or non-parabolic (i.e. bound) orbits of the progenitors.

Whether or not considering the over-massive black holes as an “exception to the rule”, or in other words legitimately excluding them from the linear regression analysis of the $M_{\text{BH}} - \sigma_*$ diagram, obviously has an impact on the estimate of the log-slope of the correlation. Therefore, it is important to test the scenario proposed by Volonteri & Ciotti (2013) with empirical data.

The remainder of this Chapter comprises the published version of the paper “Overmassive black holes in the $M_{\text{BH}} - \sigma$ diagram do not belong to over (dry) merged galaxies” by G. A. D. Savorgnan & A. W. Graham, as it appears in Volume 446 of *Monthly Notices of the Royal Astronomical Society*.



Overmassive black holes in the $M_{\text{BH}}-\sigma$ diagram do not belong to over (dry) merged galaxies

Giulia A. D. Savorgnan[★] and Alister W. Graham

Centre for Astrophysics and Supercomputing, Swinburne University of Technology, Hawthorn, VIC 3122, Australia

Accepted 2014 October 27. Received 2014 October 21; in original form 2014 July 9

ABSTRACT

Semi-analytical models in a Λ cold dark matter cosmology have predicted the presence of outlying, ‘overmassive’ black holes at the high-mass end of the (black hole mass–galaxy velocity dispersion) $M_{\text{BH}}-\sigma$ diagram (which we update here with a sample of 89 galaxies). They are a consequence of having experienced more dry mergers – thought not to increase a galaxy’s velocity dispersion – than the ‘main-sequence’ population. Wet mergers and gas-rich processes, on the other hand, preserve the main correlation. Due to the scouring action of binary supermassive black holes, the extent of these dry mergers (since the last significant wet merger) can be traced by the ratio between the central stellar mass deficit and the black hole mass ($M_{\text{def},*}/M_{\text{BH}}$). However, in a sample of 23 galaxies with partially depleted cores, including central cluster galaxies, we show that the ‘overmassive’ black holes are actually hosted by galaxies that appear to have undergone the lowest degree of such merging. In addition, the rotational kinematics of 37 galaxies in the $M_{\text{BH}}-\sigma$ diagram reveals that fast and slow rotators are not significantly offset from each other, also contrary to what is expected if these two populations were the product of wet and dry mergers, respectively. The observations are thus not in accordance with model predictions and further investigation is required.

Key words: black hole physics – galaxies: elliptical and lenticular, cD – galaxies: evolution – galaxies: formation.

1 INTRODUCTION

Our growing awareness of substructures and the actual relations within various black hole mass (M_{BH}) scaling diagrams is important because it provides us with clues into the joint evolution of black hole and host spheroid. For example, Graham (2012), Graham & Scott (2013) and Scott, Graham & Schombert (2013) have shown that the bent $M_{\text{BH}}-M_{\text{sph,dyn}}$ (spheroid dynamical mass), $M_{\text{BH}}-L_{\text{sph}}$ (spheroid luminosity) and $M_{\text{BH}}-M_{\text{sph,*}}$ (spheroid stellar mass) relations reveal that black holes grow roughly quadratically with their host spheroid until the onset of dry merging, as signalled by the presence of partially depleted galaxy cores and a linear scaling at the high-mass end of these diagrams. The clever many-merger model of Peng (2007), Hirschmann et al. (2010) and Jahnke & Macciò (2011) was therefore ruled out because it required convergence along a distribution in the $M_{\text{BH}}-M_{\text{sph,*}}$ diagram with a slope of unity, rather than the observed buildup (to higher masses) along the quadratic relation.

In addition, the demographics in the $M_{\text{BH}}-\sigma$ (stellar velocity dispersion) diagram (Ferrarese & Merritt 2000; Gebhardt et al. 2000) have disclosed a tendency for barred galaxies to be offset,

to higher velocity dispersions, than non-barred galaxies (Graham 2007, 2008a,b; Hu 2008; Graham & Li 2009). This may well be due to the elevated kinematics associated with bars (e.g. Graham et al. 2011; Brown et al. 2013; Hartmann et al. 2014). Speculation as to the role played by secular evolution and the possibility of ‘anaemic’ black holes in pseudo-bulges (e.g. Graham 2008b; Hu 2008) does however still remain an intriguing possibility (Kormendy, Bender & Cornell 2011), although their current lack of an offset about the bent $M_{\text{BH}}-M_{\text{sph,*}}$ relation (Graham & Scott 2013) argues against this.

An interesting suggestion for the presence of additional substructure in the $M_{\text{BH}}-\sigma$ diagram has recently been offered by Volonteri & Ciotti (2013), who investigated why central cluster galaxies tend to be outliers, hosting black holes that appear to be ‘overmassive’ compared to expectations from their velocity dispersion. On theoretical grounds it is well known that – as a consequence of the virial theorem and the conservation of the total energy – the mass, luminosity and size of a spheroidal galaxy increases more readily than its velocity dispersion when a galaxy undergoes (parabolic)¹

[★]E-mail: gsavorgn@astro.swin.edu.au

¹ In a parabolic dissipationless merger between two spheroidal galaxies, the virial velocity dispersion of the merger product cannot be larger than the maximum velocity dispersion of the progenitors. Therefore, when we say

dissipationless mergers with other spheroidal galaxies (e.g. Ciotti & van Albada 2001; Nipoti, Londrillo & Ciotti 2003; Ciotti, Lanzoni & Volonteri 2007; Naab, Johansson & Ostriker 2009). In this scenario, the supermassive black hole grows through black hole binary merger events, while the galaxy velocity dispersion remains unaffected, moving the black hole/galaxy pair upwards in the $M_{\text{BH}}-\sigma$ diagram. Using a combination of analytical and semi-analytical models, Volonteri & Ciotti (2013) show that central cluster galaxies can naturally become outliers in the $M_{\text{BH}}-\sigma$ diagram because they experience more mergers with spheroidal systems than any other galaxy and because these mergers are preferentially gas-poor.

Here we test this interesting idea with the latest observational data. In so doing, we update the $M_{\text{BH}}-\sigma$ diagram to include 89 galaxies now reported to have directly measured black hole masses.

2 RATIONALE

The high-mass end of the $M_{\text{BH}}-\sigma$ diagram, where a few ‘overmassive’ outliers have now been reported to exist, is mainly populated by core-Sérsic galaxies (Graham et al. 2003; Trujillo et al. 2004), i.e. galaxies (or bulges) with partially depleted cores relative to their outer Sérsic light profile. While these galaxies are also ‘core galaxies’, as given by the Nuker definition (Lauer et al. 2007), it should be noted that ~ 20 per cent of ‘core galaxies’ are not core-Sérsic galaxies (Dullo & Graham 2014, their appendix A.2), i.e. do not have depleted cores. Such Sérsic galaxies have no central deficit of stars. It has long been hypothesized that the presence of a partially depleted core indicates that the host galaxy has experienced one or more ‘dry’ major mergers (Begelman, Blandford & Rees 1980). During such dissipationless mergers, the progenitor supermassive black holes are expected to sink towards the centre of the remnant, form a bound pair and release their binding energy to the surrounding stars (Milosavljević & Merritt 2001; Merritt 2013b and references therein). Indeed, the latest high-resolution observations (e.g. Sillanpää et al. 1988; Komossa et al. 2003; Maness et al. 2004; Rodriguez et al. 2006; Dotti et al. 2009; Burke-Spolaor 2011; Fabbiano et al. 2011; Ju et al. 2013; U et al. 2013; Liu et al. 2014) are providing us with compelling evidence of tight black hole binary systems. The evacuation of stars takes place within the so-called loss-cone of the black hole binary and has the effect of lowering the galaxy’s central stellar density (e.g. Merritt 2006a, his fig. 5; Dotti, Sesana & Decarli 2012; Colpi 2014). Upon analysing the central stellar kinematics of a sample of core galaxies, Thomas et al. (2014) concluded that the homology of the distribution of the orbits matches the predictions from black hole binary theoretical models, and argued that the small values of central rotation velocities favour a sequence of several minor mergers rather than a few equal-mass mergers. Subsequent to the dry merging events, AGN feedback likely prevents further star formation in the spheroids of the core-Sérsic galaxies (e.g. Ciotti, Ostriker & Proga 2010, and references therein). High-accuracy N -body simulations (Merritt 2006b) have shown that, after \mathcal{N} (equivalent) major mergers, the magnitude of the stellar mass deficit $M_{\text{def},*}$ scales as \mathcal{N} times the final mass of the relic black hole ($M_{\text{def},*} \approx 0.5\mathcal{N} M_{\text{BH}}$). This result has been used to make inferences about the galaxy merger history (e.g. Graham 2004; Ferrarese et al. 2006; Hyde et al. 2008; Dullo & Graham 2014).

that, after such a merger, a galaxy experiences a growth of its black hole mass at a fixed velocity dispersion, we are referring to the progenitor galaxy with the highest velocity dispersion.

If one assumes that the ‘overmassive’ black holes belong to galaxies that have undergone a larger number of dry mergers compared to galaxies that obey the observed $M_{\text{BH}}-\sigma$ correlation (Graham & Scott 2013; McConnell & Ma 2013), it is a natural expectation that these $M_{\text{BH}}-\sigma$ outliers may also display a higher $M_{\text{def},*}/M_{\text{BH}}$ ratio when compared to the ‘main-sequence’ population. This argument motivates our first test.

A second test can be built by looking at the kinematics of the objects that populate the $M_{\text{BH}}-\sigma$ diagram. A galaxy’s velocity dispersion remains unaffected only in the case of a dissipationless merger (with another spheroidal galaxy), whereas it accordingly increases after a dissipational (gas-rich) merger, preserving the $M_{\text{BH}}-\sigma$ correlation (Volonteri & Ciotti 2013). Wet and dry mergers may produce remnants with different kinematical structures, classified as fast (disc) and slow rotators, respectively (e.g. Emsellem et al. 2008 and references therein). Therefore, an instinctive question is whether the populations of slow and fast rotators are significantly offset from each other in the $M_{\text{BH}}-\sigma$ diagram. This will be our second test.

3 DATA

Our galaxy sample (see Table 1) consists of 89 objects for which a dynamical detection of the black hole mass and a measure of the stellar velocity dispersion have been reported in the literature. We include in our sample all the 78 objects presented in the catalogue of Graham & Scott (2013), plus 10 objects taken from Rusli et al. (2013a) and 1 object from Greenhill et al. (2003). Partially depleted cores have been identified according to the same criteria used by Graham & Scott (2013). When no high-resolution image analysis was available from the literature, we inferred the presence of a partially depleted core based on the stellar velocity dispersion, σ : a galaxy is classified as core-Sérsic if $\sigma > 270 \text{ km s}^{-1}$, or as Sérsic if $\sigma \leq 166 \text{ km s}^{-1}$. This resulted in us assigning cores to just six galaxies, none of which were used in the following mass deficit analysis. We employ a 5 per cent uncertainty on σ in our regression analysis.

A kinematical classification (slow/fast rotator) is available for 34 of our 89 galaxies from the ATLAS^{3D} survey (Emsellem et al. 2011) and for 3 additional galaxies² from Scott et al. (2014). It is however beyond the scope of this paper to derive slow/fast rotator classifications for the remaining galaxies.

All galaxies are categorized as barred/unbarred objects according to the classification reported by Graham & Scott (2013), with the following updates. An isophotal analysis and unsharp masking of *Spitzer*/IRAC 3.6 μm images (Savorgnan et al., in preparation) has revealed the presence of a bar in the galaxies NGC 0224 (in agreement with Athanassoula & Beaton 2006; Beaton et al. 2007; Morrison et al. 2011), NGC 2974 (confirming the suggestion of Jeong et al. 2007), NGC 3031 (see also Elmegreen, Chromeley & Johnson 1995; Gutiérrez et al. 2011; Erwin & Debattista 2013), NGC 3245 (see also Laurikainen et al. 2010; Gutiérrez et al. 2011), NGC 3998 (as already noted by Gutiérrez et al. 2011), NGC 4026, NGC 4388 and NGC 4736 (see also Moellenhoff, Matthias & Gerhard 1995).

Although the fast rotator galaxy NGC 1316 has been frequently classified in the literature as an elliptical merger remnant, Graham & Scott (2013) identified this object as a barred lenticular galaxy. D’Onofrio (2001) found that a single-component model

² NGC 1316, NGC 1374 and NGC 1399.

Table 1. Galaxy sample. Column (1): galaxy names; for the 18 galaxies marked with a *, the black hole masses were estimated including in the modelling the effects of dark matter. Column (2): distances. Column (3): black hole masses; for the 10 measurements taken from Rusli et al. (2013a), we report in parenthesis also the measurements obtained without including in the modelling the effects of dark matter. Column (4): stellar velocity dispersions. Column (5): references of black hole mass and velocity dispersion measurements reported here (G+03 = Greenhill et al. 2003, R+13 = Rusli et al. 2013a, GS13 = Graham & Scott 2013). Column (6): presence of a partially depleted core. The question mark is used when the classification has come from the velocity dispersion criteria mentioned in Section 3. Column (7): presence of a bar. Column (8): central stellar mass deficits as measured by Rusli et al. (2013b). For seven galaxies we reconstructed the ‘no-dark-matter’ values (see Section 3.1), which are reported in parenthesis. Column (9): central stellar mass deficits as measured by Dullo & Graham (2014). Column (10): kinematical classification (fast/slow rotator).

Galaxy (1)	Dist Mpc (2)	M_{BH} $(10^8 M_{\odot})$ (3)	σ (km s^{-1}) (4)	Ref. (5)	Core (6)	Bar (7)	$M_{\text{def},*}^{R+13}$ $(10^8 M_{\odot})$ (8)	$M_{\text{def},*}^{\text{DG13}}$ $(10^8 M_{\odot})$ (9)	Kinematics (10)
A1836-BCG	158.0	39_{-5}^{+4}	309_{-15}^{+15}	GS13	yes?	no	–	–	–
A3565-BCG	40.7	11_{-2}^{+2}	335_{-17}^{+17}	GS13	yes?	no	–	–	–
Circinus	4.0	$0.017_{-0.003}^{+0.004}$	158_{-8}^{+8}	G+03	no?	no	–	–	–
CygnusA	232.0	25_{-7}^{+7}	270_{-13}^{+13}	GS13	yes?	no	–	–	–
IC 1459	28.4	24_{-10}^{+10}	306_{-15}^{+15}	GS13	yes	no	-16_{-7}^{+7}	–	–

Note. The full table is made available online in the electronic version.

cannot provide a good description of the light profile of this galaxy and de Souza, Gadotti & dos Anjos (2004) fitted NGC 1316 with a bulge + exponential disc model. Sani et al. (2011) adopted a three-component model, featuring a bulge, an exponential disc and a central Gaussian (attributed to non-stellar nuclear emission). Upon an analysis of the two-dimensional velocity field obtained from the kinematics of planetary nebulae, McNeil-Moylan et al. (2012) claimed that NGC 1316 represents a transition phase from a major-merger event to a bulge-dominated galaxy like the Sombrero galaxy (M104). We find evidence for the presence of a bar in NGC 1316 from an isophotal analysis and unsharp masking of its *Spitzer*/IRAC 3.6 μm image (Savorgnan et al., in preparation), but we exclude it for now to avoid any controversy.

Central stellar mass deficits (with individual uncertainties) have been estimated for 23 core-Sérsic galaxies – with directly measured black hole masses – by Rusli et al. (2013b). Briefly, they fit the surface brightness profiles of these galaxies with a core-Sérsic model and computed the light deficit as the difference between the luminosity of the Sérsic component of the best-fitting core-Sérsic model and the luminosity of the core-Sérsic model itself. Light deficits were then converted into stellar mass deficits through dynamically-determined, individual stellar mass-to-light ratios. Rusli et al. (2013b) used galaxy distances slightly different from those adopted in this work (see Table 1); therefore, we adjusted their stellar mass deficits (and uncertainties) accordingly.³ Among the 23 core-Sérsic galaxies whose stellar mass deficits have been computed by Rusli et al. (2013b), 10 were also analysed by Dullo & Graham (2014). Dullo & Graham (2014) measured light deficits with a method similar to that employed by Rusli et al. (2013b), but they converted light deficits into stellar mass deficits using stellar mass-to-light ratios derived from $V - I$ colours together with the colour-age-metallicity diagram (Graham & Spitler 2009). Their stellar mass deficits are accurate to 60 per cent (Dullo, private communication) and were rescaled according to the galaxy distances

³ Mass deficits and their uncertainties from Rusli et al. (2013b) were corrected by a factor of (D/D_{prev}) . Mass deficits from Dullo & Graham (2014) were corrected by a factor of $(D/D_{\text{prev}})^2$. Here, D are the galaxy distances adopted in this work and D_{prev} are the galaxy distances used in the original works.

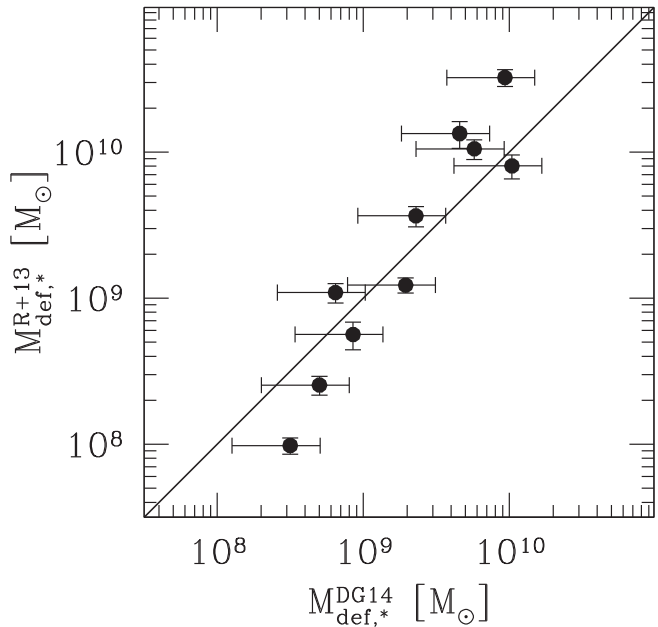


Figure 1. Comparison between the central stellar mass deficits estimated by Rusli et al. (2013b, R+13) and Dullo & Graham (2014, DG14) for 10 galaxies in common. The black solid line shows the 1:1 relation. As noted in the text, the small ‘apparent’ systematic difference is actually due to random causes.

adopted here. In Fig. 1, we compare these 10 common mass deficit estimates. The agreement is remarkably good, although a slight deviation from the 1:1 line can be noticed for the galaxies with the lowest or highest mass deficits, for which $M_{\text{def},*}$ reported by Dullo & Graham (2014) is larger or smaller than Rusli et al. (2013b), respectively. We checked and found that this effect actually depends in a random, i.e. non-systematic, way on the different choices to estimate the stellar mass-to-light ratios and/or their different galaxy data and modelling. We return to this point in the next section. For these individual 10 galaxies, we compute a weighted arithmetic mean of their two available stellar mass deficits.

3.1 Dark matter

The 10 black hole masses from Rusli et al. (2013a) – not to be confused with the different 10 galaxies with central mass deficits from Rusli et al. (2013b) that are in common with Dullo & Graham (2014) – were computed by taking into account the effects of dark matter. For these 10 galaxies, Rusli et al. (2013a) also published black hole masses estimated without the inclusion of dark matter haloes. Among the 78 black hole masses reported by Graham & Scott (2013), only 8 had dark matter included in their derivation, and no dark matter halo was included by Greenhill et al. (2003) in their black hole mass estimate.

The majority⁴ of the 23 stellar mass deficits from Rusli et al. (2013b) were derived from their analysis which incorporated dark matter to obtain the central mass-to-light ratios. However, Rusli et al. (2013b) did not publish the corresponding stellar mass deficits for the no-dark-matter case. Therefore, the sample of 89 galaxies that we use in our analysis contains 18 black hole masses estimated with the inclusion of a dark matter halo and the 23 stellar mass deficits published by Rusli et al. (2013b).

We have already shown in Section 3 that the stellar mass deficits measured by Dullo & Graham (2014), without accounting for dark matter, are in good agreement with the Rusli et al. (2013b) estimates which accounted for dark matter. The slight disagreement observed for the lowest and highest mass deficits (see Fig. 1) does not significantly affect the conclusions of our analysis. However, one could wonder whether our results change when using exclusively black hole masses and stellar mass deficits derived without the inclusion of dark matter. To address this question, we derived the no-dark-matter stellar mass deficits⁵ for 7 of the 10 galaxies whose black hole masses were measured by Rusli et al. (2013a). We repeated the analysis by (i) employing for these seven galaxies the no-dark-matter black hole masses (published by Rusli et al. 2013a) and the no-dark-matter stellar mass deficits (derived by us), and (ii) excluding the remaining black hole masses estimated with the inclusion of dark matter. We found that none of our conclusions was affected by this change.

4 RESULTS

In Fig. 2, we show the updated $M_{\text{BH}}-\sigma$ diagram for the 89 galaxies listed in Table 1. Core-Sérsic galaxies are colour coded according to their $M_{\text{def},*}/M_{\text{BH}}$ ratio (or, if no $M_{\text{def},*}$ estimate is available, they appear as empty symbols⁶). It is immediately evident that the ‘overmassive’ black holes are not hosted by galaxies with a high $M_{\text{def},*}/M_{\text{BH}}$ value.

NGC 4889, NGC 3842 and NGC 1407 are the three objects with the largest positive vertical offset from the $M_{\text{BH}}-\sigma$ correlation. Contrary to expectations, these three galaxies have a small

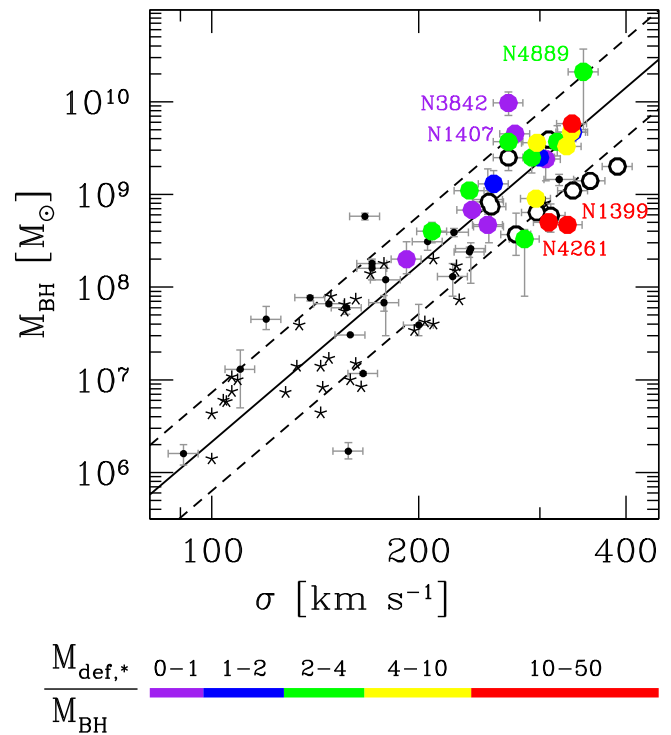


Figure 2. $M_{\text{BH}}-\sigma$ diagram for the 89 galaxies presented in Table 1. Core-Sérsic galaxies are colour coded according to their $M_{\text{def},*}/M_{\text{BH}}$ ratio. If no $M_{\text{def},*}$ estimate is available, they appear as open circles. Unbarred Sérsic galaxies are represented with (small) black dots and barred Sérsic galaxies with starred symbols. Error bars are reported only for unbarred galaxies used to derive equation (1). The black solid line shows the OLS($\sigma|M_{\text{BH}}$) linear regression for all non-barred galaxies and the black dashed lines mark the associated total rms scatter ($\Delta = 0.53$) in the log(M_{BH}) direction.

$M_{\text{def},*}/M_{\text{BH}}$ ratio, consistent with $\sim 1-2$ major dry merger events (Merritt 2006b).

Remarkably, NGC 4261 and NGC 1399 – the central galaxy in the Fornax cluster – which are two of the three galaxies with $M_{\text{def},*}/M_{\text{BH}} > 10$ (red symbols in Fig. 2), display a negative vertical offset from the correlation.⁷ While the offset of NGC 1399 and NGC 4261 is at odds with predictions from semi-analytical models (see Section 1), their large stellar deficits might be due to the effects of a recoiling black hole (see also Dullo & Graham 2014; Lena et al. 2014). A recoiling black hole is the final product of a coalesced black hole binary after the anisotropic emission of gravitational waves, which imparts a net impulse – a kick – to the remnant black hole (Bekenstein 1973; Fitchett & Detweiler 1984; Favata, Hughes & Holz 2004; Holley-Bockelmann et al. 2008; Batcheldor et al. 2010). The kicked black hole oscillates about the centre of the newly merged galaxy with decreasing amplitude, transferring kinetic energy to the stars and thus further lowering the core density (Redmount & Rees 1989; Merritt et al. 2004; Boylan-Kolchin, Ma & Quataert 2004). Kick-induced partially depleted cores can be as large as $M_{\text{def},*} \sim (4-5)M_{\text{BH}}$ (Gualandris & Merritt 2008) and could complicate the use of central mass deficits as a tracer of dry galaxy mergers. However, they do not explain the low $M_{\text{def},*}/M_{\text{BH}}$ ratios observed in the ‘overmassive’ black hole sample.

⁴ Stellar mass deficits for IC 1459, NGC 3379, NGC 4374 and NGC 4261 were estimated by Rusli et al. (2013b) with single-component dynamical modelling, i.e. without dark matter.

⁵ The no-dark-matter stellar mass deficits were calculated as $M_{\text{def},*}^{\text{noDM}} = M_{\text{def},*}^{\text{DM}} \cdot [(M/L)^{\text{DM}}]^{-1} \cdot (M/L)^{\text{noDM}}$, where $M_{\text{def},*}^{\text{DM}}$ are the mass deficits from Rusli et al. (2013b), which had dark matter incorporated in their derivation, and $(M/L)^{\text{DM}}$ and $(M/L)^{\text{noDM}}$ are the mass-to-light ratios from Rusli et al. (2013a) estimated with and without accounting for dark matter, respectively.

⁶ The 10 empty symbols refer to 6 suspected, plus 4 apparent core-Sérsic galaxies.

⁷ Although we have used the black hole mass for NGC 1399 from Gebhardt et al. (2007), we note that Houghton et al. (2006) had reported a value twice as large ($\sim 10^9 M_{\odot}$). Nevertheless, this is still too low to yield a positive offset for this galaxy in Fig. 2.

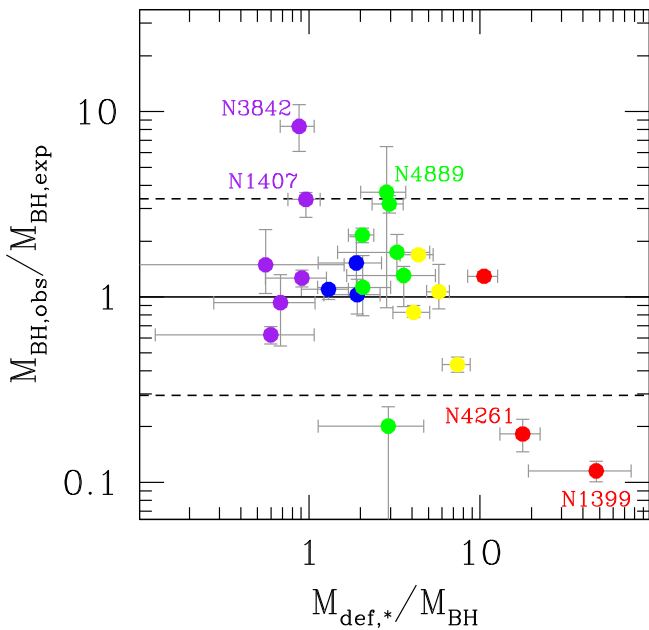


Figure 3. Vertical offset from the $M_{\text{BH}}-\sigma$ relation versus the $M_{\text{def},*}/M_{\text{BH}}$ ratio. Symbols are colour coded according to Fig. 2. The vertical error bars represent the uncertainty on M_{BH} . The horizontal solid line is equivalent to a zero vertical offset from the expected mass ($M_{\text{BH,obs}}/M_{\text{BH,exp}} = 1$) and the horizontal dashed lines show the total rms scatter ($\Delta = 0.53$) of the OLS($\sigma|M_{\text{BH}}$) linear regression in the log(M_{BH}) direction.

In Fig. 3, we plot the vertical offset from the $M_{\text{BH}}-\sigma$ relation versus the $M_{\text{def},*}/M_{\text{BH}}$ ratio. The vertical offset is defined as $\log(M_{\text{BH,obs}}/M_{\text{BH,exp}})$, where $M_{\text{BH,obs}}$ is the *observed* black hole mass and $M_{\text{BH,exp}}$ is the black hole mass *expected* from the galaxy velocity dispersion using an OLS($\sigma|M_{\text{BH}}$) linear regression⁸ for all non-barred⁹ galaxies:

$$\log \left(\frac{M_{\text{BH,exp}}}{M_{\odot}} \right) = (8.24 \pm 0.10) + (6.34 \pm 0.80) \times \log \left(\frac{\sigma}{200 \text{ km s}^{-1}} \right). \quad (1)$$

Clearly, there is no positive trend in Fig. 3. The significance of a correlation is rejected by a Spearman's test (Spearman's correlation coefficient $r_s = -0.33$, likelihood of the correlation occurring by chance $P > 5$ per cent). We conclude that no positive correlation is observed between the vertical offset from the $M_{\text{BH}}-\sigma$ relation and the $M_{\text{def},*}/M_{\text{BH}}$ ratio.

Repeating the analysis using only the Rusli et al. (2013b) mass deficits, i.e. without computing 10 weighted arithmetic means for the galaxies in common with Dullo & Graham (2014), gives the same conclusion. Similarly, the same conclusion is reached when using only the 10 Dullo & Graham (2014) derived mass deficits.

⁸ See Graham & Scott (2013, their section 3.1) for a discussion on the choice of an ordinary least-squares (OLS) regression of the abscissa on the ordinate. Their OLS($\sigma|M_{\text{BH}}$) linear regression for unbarred galaxies ($\log(M_{\text{BH,exp}}/M_{\odot}) = (8.22 \pm 0.05) + (5.53 \pm 0.34) \times \log(\sigma/200 \text{ km s}^{-1})$) is consistent within the overlapping 1σ uncertainties. It is however beyond the scope of this paper to repeat the same detailed analysis presented by Graham & Scott (2013).

⁹ As noted in Section 1, barred galaxies tend to be offset from non-barred galaxies in the $M_{\text{BH}}-\sigma$ diagram.

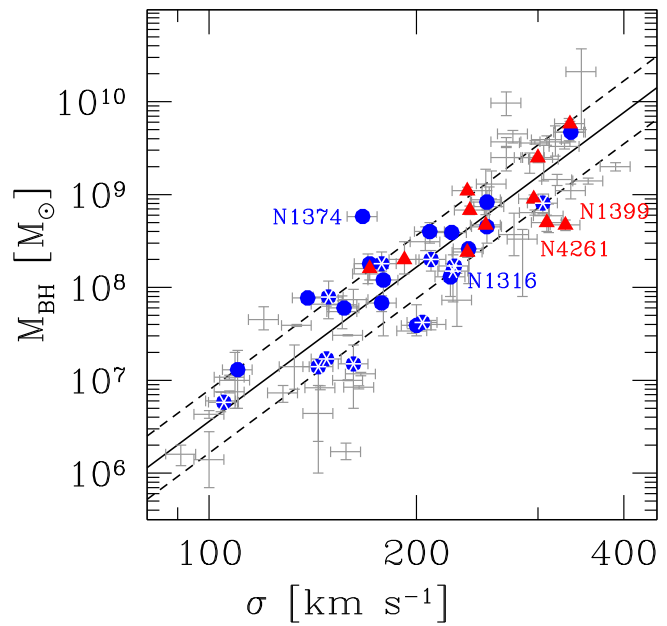


Figure 4. Fast (blue circles) and slow (red triangles) rotators in the $M_{\text{BH}}-\sigma$ diagram. Starred symbols mark barred galaxies. The black solid and dashed lines are the same as in Fig. 2.

In Fig. 4, we show the distribution of fast and slow rotators in the $M_{\text{BH}}-\sigma$ diagram. Our aim is to check whether the two populations are vertically offset from each other, in the sense that wet mergers can create fast rotating discs, while dry mergers can increase the black hole mass but not the velocity dispersion. Since the work of Graham (2008a,b), see also Hu (2008), we know that barred galaxies tend to be offset rightwards from the $M_{\text{BH}}-\sigma$ correlation defined by non-barred galaxies. It is therefore crucial to exclude the barred galaxies from the following analysis, to avoid biasing the results. We follow Graham & Scott (2013) in using the BCES code from Akritas & Bershady (1996) to obtain four different linear regressions for both the (unbarred) fast and slow rotators. The results are shown in the first part of Table 2. Regardless of the linear regression method used, the best-fitting slopes and intercepts of fast and slow rotators are consistent with each other within the 1σ uncertainty. To test the robustness of our results, we repeated the linear regression analysis excluding the most deviating data points: one fast rotator with a positive vertical offset (NGC 1374) and two slow rotators with a negative vertical offset (NGC 1399 and NGC 4261). The second

Table 2. Linear regression analysis for the populations of unbarred fast and slow rotators.

Regression	Slow rot.		Fast rot.	
	β	α	β	α
OLS($M_{\text{BH}} \sigma$)	3.7 ± 1.1	8.40 ± 0.08	4.4 ± 0.6	8.33 ± 0.09
OLS(σM_{BH})	6.8 ± 1.7	8.1 ± 0.3	5.9 ± 1.0	8.3 ± 0.1
Bisector	4.8 ± 1.0	8.3 ± 0.1	5.1 ± 0.5	8.33 ± 0.09
Orthogonal	6.7 ± 1.6	8.1 ± 0.3	5.8 ± 1.0	8.3 ± 0.1
<i>Excluding NGC 1374, NGC 1399 and NGC 4261.</i>				
OLS($M_{\text{BH}} \sigma$)	5.3 ± 0.8	8.36 ± 0.09	4.7 ± 0.6	8.27 ± 0.08
OLS(σM_{BH})	6.2 ± 0.9	8.3 ± 0.1	5.4 ± 0.8	8.28 ± 0.08
Bisector	5.7 ± 0.8	8.3 ± 0.1	5.0 ± 0.6	8.27 ± 0.08
Orthogonal	6.1 ± 0.9	8.3 ± 0.1	5.4 ± 0.8	8.28 ± 0.08

part of Table 2 reports the new values of the best-fitting slopes and intercepts, which remain consistent with each other.

5 DISCUSSION AND CONCLUSIONS

The presence of a central, supermassive black hole, coupled with the scarcity of binary supermassive black hole systems, suggests that the progenitor black holes have coalesced in most merged galaxies. They can do this by transferring their orbital angular momentum to the stars near the centre of their host galaxy and thereby evacuating the core. If a galaxy's $M_{\text{def},*}/M_{\text{BH}}$ ratio is a proxy for its equivalent number of major dry merger events since its last wet merger (e.g. Merritt 2006b), then our analysis (see Figs 2 and 3) reveals that the apparent ‘overmassive’ outliers at the high-mass end of the $M_{\text{BH}}-\sigma$ diagram are galaxies that have undergone the lowest degree of such recent dry merging. Although a final major wet merger may contribute to their low $M_{\text{def},*}/M_{\text{BH}}$ ratio, these galaxies are among the most massive early-type galaxies in the local Universe and they reside in the central regions of galaxy clusters, where wet major mergers are unlikely to occur (e.g. Fraser-McKelvie, Brown & Pimbblet 2014) due to prior ram pressure stripping of gas from infalling galaxies (Boselli & Gavazzi 2006; Haines et al. 2013; Boselli et al. 2014a,b). That is, the ‘overmassive’ black holes in central cluster galaxies cannot be explained by a large number of dissipationless mergers growing the black hole mass at a fixed galaxy velocity dispersion.

In addition to this, no significant offset is observed between the (unbarred) populations of fast and slow rotators in the $M_{\text{BH}}-\sigma$ diagram (see Table 2), contrary to what is expected if fast and slow rotators are, in general, the products of wet and dry mergers, respectively. This is because dry mergers will increase the black hole mass, but are said not to increase the velocity dispersion. This result is also in broad agreement with the observation that the (unbarred) Sérsic and core-Sérsic galaxies follow the same $M_{\text{BH}}-\sigma$ relation (Graham & Scott 2013). Our results appear consistent with studies of luminous elliptical galaxies which have shown that the galaxy luminosity scales with the velocity dispersion (Schechter 1980; Malumuth & Kirshner 1981; Bernardi et al. 2007; Lauer et al. 2007; von der Linden et al. 2007; Liu et al. 2008), i.e. the velocity dispersion appears not to completely saturate but rather still increases with increasing galaxy luminosity, contrary to what one would predict if these galaxies were built only by dry mergers on parabolic orbits.

An alternative possibility for the central cluster galaxies may be that they experience minor dry merger events that do not bring in a massive black hole but rather stars, and nuclear star clusters, which may partly or fully refill a depleted galaxy core. However, simulations are needed to verify whether, in a Λ cold dark matter cosmology, the extent of minor dry mergers experienced by a central cluster galaxy in late cosmic times can supply enough stellar mass ($\sim 10^9$ – $10^{10} M_{\odot}$) to replenish the galaxy's core.

Eventually, one should also consider the possibility that some of the overmassive black holes might have had their masses overestimated. Past studies have demonstrated the importance of resolving the black hole sphere-of-influence¹⁰ when measuring a black hole mass, to avoid systematic errors or even spurious detections (e.g. Ferrarese & Merritt 2000; Merritt & Ferrarese 2001a,b; Valluri, Merritt & Emsellem 2004; Ferrarese & Ford 2005). Merritt (2013a)

cautions against the use of black hole mass measurements obtained from stellar-dynamical data sets. His fig. 2.5 points out that no more than three galaxies – all belonging to the Local Group – have been observed with enough spatial resolution to exhibit a *prima facie* convincing Keplerian rise in their central stellar velocities. At the same time, gas kinematics can have motions not solely due to the gravitational potential of the black hole. For example, Mazzalay et al. (2014) showed that the gas dynamics in the innermost parsecs of spiral galaxies is typically far from simple circular motion. One possible example of such an overestimated black hole may be that reported by van den Bosch et al. (2012) for the galaxy NGC 1277 ($M_{\text{BH}} = 1.7 \times 10^{10} M_{\odot}$). In fact, upon re-analysing the same data, Emsellem (2013) showed that a model with a 2 times smaller black hole mass provides an equally good fit to the observed kinematics, and emphasized the need for higher spatial resolution spectroscopic data.

ACKNOWLEDGEMENTS

GS would like to acknowledge the valuable feedback provided by David Merritt and Luca Ciotti on an early version of the manuscript. GS thanks Gonzalo Díaz and Bililign Dullo for useful discussions. This research was supported by Australian Research Council funding through grants DP110103509 and FT110100263. This research has made use of the GOLDMine website (Gavazzi et al. 2003) and the NASA/IPAC Extragalactic Database (NED) which is operated by the Jet Propulsion Laboratory, California Institute of Technology, under contract with the National Aeronautics and Space Administration. We wish to thank an anonymous referee whose criticism helped improving the manuscript.

REFERENCES

- Akritas M. G., Bershady M. A., 1996, ApJ, 470, 706
- Athanassoula E., Beaton R. L., 2006, MNRAS, 370, 1499
- Batcheldor D., Robinson A., Axon D. J., Perlman E. S., Merritt D., 2010, ApJ, 717, L6
- Beaton R. L. et al., 2007, ApJ, 658, L91
- Begelman M. C., Blandford R. D., Rees M. J., 1980, Nature, 287, 307
- Bekenstein J. D., 1973, ApJ, 183, 657
- Bernardi M., Hyde J. B., Sheth R. K., Miller C. J., Nichol R. C., 2007, AJ, 133, 1741
- Boselli A., Gavazzi G., 2006, PASP, 118, 517
- Boselli A., Cortese L., Boquien M., Boissier S., Catinella B., Gavazzi G., Lagos C., Saintonge A., 2014a, A&A, 564, A67
- Boselli A. et al., 2014b, A&A, 570, A69
- Boylan-Kolchin M., Ma C.-P., Quataert E., 2004, ApJ, 613, L37
- Brown J. S., Valluri M., Shen J., Debattista V. P., 2013, ApJ, 778, 151
- Burke-Spolaor S., 2011, MNRAS, 410, 2113
- Ciotti L., van Albada T. S., 2001, ApJ, 552, L13
- Ciotti L., Lanzoni B., Volonteri M., 2007, ApJ, 658, 65
- Ciotti L., Ostriker J. P., Proga D., 2010, ApJ, 717, 708
- Colpi M., 2014, Space Sci. Rev., 183, 189
- D'Onofrio M., 2001, MNRAS, 326, 1517
- de Souza R. E., Gadotti D. A., dos Anjos S., 2004, ApJS, 153, 411
- Dotti M., Montuori C., Decarli R., Volonteri M., Colpi M., Haardt F., 2009, MNRAS, 398, L73
- Dotti M., Sesana A., Decarli R., 2012, Adv. Astron., 2012, 940568
- Dullo B. T., Graham A. W., 2014, MNRAS, 444, 2700
- Elmegreen D. M., Chromey F. R., Johnson C. O., 1995, AJ, 110, 2102
- Emsellem E., 2013, MNRAS, 433, 1862
- Emsellem E. et al., 2008, in Bureau M., Athanassoula E., Barbuy B., eds, Proc. IAU Symp. 245, Formation and Evolution of Galaxy Bulges. Cambridge Univ. Press, Cambridge, p. 11

¹⁰ The sphere-of-influence is the region of space within which the gravitational potential of the black hole dominates over that of the surrounding stars.

- Emsellem E. et al., 2011, MNRAS, 414, 888
 Erwin P., Debattista V. P., 2013, MNRAS, 431, 3060
 Fabbiano G., Wang J., Elvis M., Risaliti G., 2011, Nature, 477, 431
 Favata M., Hughes S. A., Holz D. E., 2004, ApJ, 607, L5
 Ferrarese L., Ford H., 2005, Space Sci. Rev., 116, 523
 Ferrarese L., Merritt D., 2000, ApJ, 539, L9
 Ferrarese L. et al., 2006, ApJS, 164, 334
 Fitchett M. J., Detweiler S., 1984, MNRAS, 211, 933
 Fraser-McKevie A., Brown M. J. I., Pimbblet K. A., 2014, MNRAS, 444, L63
 Gavazzi G., Boselli A., Donati A., Franzetti P., Scodéggi M., 2003, A&A, 400, 451
 Gebhardt K. et al., 2000, ApJ, 539, L13
 Gebhardt K. et al., 2007, ApJ, 671, 1321
 Graham A. W., 2004, ApJ, 613, L33
 Graham A., 2007, BAAS, 39, 759
 Graham A. W., 2008a, PASA, 25, 167
 Graham A. W., 2008b, ApJ, 680, 143
 Graham A. W., 2012, ApJ, 746, 113
 Graham A. W., Li I.-h., 2009, ApJ, 698, 812
 Graham A. W., Scott N., 2013, ApJ, 764, 151
 Graham A. W., Spitler L. R., 2009, MNRAS, 397, 2148
 Graham A. W., Erwin P., Trujillo I., Asensio Ramos A., 2003, AJ, 125, 2951
 Graham A. W., Onken C. A., Athanassoula E., Combes F., 2011, MNRAS, 412, 2211
 Greenhill L. J. et al., 2003, ApJ, 590, 162
 Gualandris A., Merritt D., 2008, ApJ, 678, 780
 Gutiérrez L., Erwin P., Aladro R., Beckman J. E., 2011, AJ, 142, 145
 Haines C. P. et al., 2013, ApJ, 775, 126
 Hartmann M., Debattista V. P., Cole D. R., Valluri M., Widrow L. M., Shen J., 2014, MNRAS, 441, 1243
 Hirschmann M., Khochfar S., Burkert A., Naab T., Genel S., Somerville R. S., 2010, MNRAS, 407, 1016
 Holley-Bockelmann K., Gültekin K., Shoemaker D., Yunes N., 2008, ApJ, 686, 829
 Houghton R. C. W., Magorrian J., Sarzi M., Thatte N., Davies R. L., Krajnović D., 2006, MNRAS, 367, 2
 Hu J., 2008, MNRAS, 386, 2242
 Hyde J. B., Bernardi M., Sheth R. K., Nichol R. C., 2008, MNRAS, 391, 1559
 Jahnke K., Macciò A. V., 2011, ApJ, 734, 92
 Jeong H., Bureau M., Yi S. K., Krajnović D., Davies R. L., 2007, MNRAS, 376, 1021
 Ju W., Greene J. E., Rafikov R. R., Bickerton S. J., Badenes C., 2013, ApJ, 777, 44
 Komossa S., Burwitz V., Hasinger G., Predehl P., Kaastra J. S., Ikebe Y., 2003, ApJ, 582, L15
 Kormendy J., Bender R., Cornell M. E., 2011, Nature, 469, 374
 Lauer T. R. et al., 2007, ApJ, 662, 808
 Laurikainen E., Salo H., Buta R., Knapen J. H., Comerón S., 2010, MNRAS, 405, 1089
 Lena D., Robinson A., Marconi A., Axon D. J., Capetti A., Merritt D., Batcheldor D., 2014, ApJ, 795, 146
 Liu F. S., Xia X. Y., Mao S., Wu H., Deng Z. G., 2008, MNRAS, 385, 23
 Liu X., Shen Y., Bian F., Loeb A., Tremaine S., 2014, ApJ, 789, 140
 McConnell N. J., Ma C.-P., 2013, ApJ, 764, 184
 McNeil-Moylan E. K., Freeman K. C., Arnaboldi M., Gerhard O. E., 2012, A&A, 539, A11
 Malumuth E. M., Kirshner R. P., 1981, ApJ, 251, 508
 Maness H. L., Taylor G. B., Zavala R. T., Peck A. B., Pollack L. K., 2004, ApJ, 602, 123
 Mazzalay X. et al., 2014, MNRAS, 438, 2036
 Merritt D., 2006a, Rep. Prog. Phys., 69, 2513
 Merritt D., 2006b, ApJ, 648, 976
 Merritt D., 2013a, Dynamics and Evolution of Galactic Nuclei. Princeton Univ. Press, Princeton, NJ
 Merritt D., 2013b, Class. Quantum Gravity, 30, 244005
 Merritt D., Ferrarese L., 2001a, in Knapen J. H., Beckman J. E., Shlosman I., Mahoney T. J., eds, ASP Conf. Ser. Vol. 249, The Central Kiloparsec of Starbursts and AGN: The La Palma Connection. Astron. Soc. Pac, San Francisco, p. 335
 Merritt D., Ferrarese L., 2001b, ApJ, 547, 140
 Merritt D., Milosavljević M., Favata M., Hughes S. A., Holz D. E., 2004, ApJ, 607, L9
 Milosavljević M., Merritt D., 2001, ApJ, 563, 34
 Moellenhoff C., Matthias M., Gerhard O. E., 1995, A&A, 301, 359
 Morrison H., Caldwell N., Schiavon R. P., Athanassoula E., Romanowsky A. J., Harding P., 2011, ApJ, 726, L9
 Naab T., Johansson P. H., Ostriker J. P., 2009, ApJ, 699, L178
 Nipoti C., Londrillo P., Ciotti L., 2003, MNRAS, 342, 501
 Peng C. Y., 2007, ApJ, 671, 1098
 Redmount I. H., Rees M. J., 1989, Comments Astrophys., 14, 165
 Rodriguez C., Taylor G. B., Zavala R. T., Peck A. B., Pollack L. K., Romani R. W., 2006, ApJ, 646, 49
 Rusli S. P. et al., 2013a, AJ, 146, 45
 Rusli S. P., Erwin P., Saglia R. P., Thomas J., Fabricius M., Bender R., Nowak N., 2013b, AJ, 146, 160
 Sani E., Marconi A., Hunt L. K., Risaliti G., 2011, MNRAS, 413, 1479
 Schechter P. L., 1980, AJ, 85, 801
 Scott N., Graham A. W., Schombert J., 2013, ApJ, 768, 76
 Scott N., Davies R. L., Houghton R. C. W., Cappellari M., Graham A. W., Pimbblet K. A., 2014, MNRAS, 441, 274
 Sillanpää A., Haarala S., Valtonen M. J., Sundelius B., Byrd G. G., 1988, ApJ, 325, 628
 Thomas J., Saglia R. P., Bender R., Erwin P., Fabricius M., 2014, ApJ, 782, 39
 Trujillo I., Erwin P., Asensio Ramos A., Graham A. W., 2004, AJ, 127, 1917
 U V. et al., 2013, ApJ, 775, 115
 Valluri M., Merritt D., Emsellem E., 2004, ApJ, 602, 66
 van den Bosch R. C. E., Gebhardt K., Gültekin K., van de Ven G., van der Wel A., Walsh J. L., 2012, Nature, 491, 729
 Volonteri M., Ciotti L., 2013, ApJ, 768, 29
 von der Linden A., Best P. N., Kauffmann G., White S. D. M., 2007, MNRAS, 379, 867

SUPPORTING INFORMATION

Additional Supporting Information may be found in the online version of this article:

Table 1. Galaxy sample (<http://mnras.oxfordjournals.org/lookup/suppl/doi:10.1093/mnras/stu2259/-DC1>).

Please note: Oxford University Press are not responsible for the content or functionality of any supporting materials supplied by the authors. Any queries (other than missing material) should be directed to the corresponding author for the paper.

This paper has been typeset from a TeX/LaTeX file prepared by the author.

Monster Black Holes in (Compact) Massive Spheroids with Intermediate-Scale Discs

This Chapter brings together three “hot topics” of today’s astrophysical debate, that is, over-massive black holes in the $M_{\text{BH}} - L_{\text{sph}}$ diagram, the variety of bulge-to-disc ratios in local early-type galaxies, and the evolution of the mass-size relationship from $z = 2$ to $z = 0$. While an overview about the first two topics was given in Sections 1.1.8 and 1.2.1, no mention of the mass-size relation was made in Chapter 1 because it is not immediately related to SMBHs. Therefore, a more extensive introduction of this last point is given here.

It has been claimed that a considerable number of high-redshift passive galaxies are significantly more compact than their local counterparts. Daddi et al. (2005) reported on the observation of seven quiescent early-type galaxies at $z = 1.4 - 2.5$ with stellar masses $\gtrsim 10^{11} M_{\odot}$ and effective radii significantly smaller than those of local counterparts. Trujillo et al. (2006) analysed ten massive $\approx 5 \times 10^{11} M_{\odot}$ galaxies at $z = 1.2 - 1.7$ and measured for them sizes a factor of 4 smaller than $z = 0$ galaxies with similar stellar masses. From this, they concluded that the observed rapid evolution of the structural properties of massive quiescent galaxies over the last ≈ 10 Gyr cannot be reconciled with a monolithic formation scenario. Kriek et al. (2008) and van Dokkum et al. (2008) found that nearly half of $z \approx 2$ massive ($\approx 10^{11} M_{\odot}$) galaxies have old stellar populations, negligible star formation, and sizes a factor of 5 smaller than those of local descendants, and similar conclusions were reached by several other studies (e.g. Toft et al. 2007; Trujillo et al. 2007; Zirm et al. 2007; Buitrago et al. 2008; Damjanov et al. 2009). While some studies have pointed out that “progenitor bias”¹ (e.g. Carollo et al. 2014) might play

¹“Progenitor bias” refers to sample confusion of the local descendants of high-redshift massive quiescent

140 Monster Black Holes in (Compact) Massive Spheroids with Intermediate-Scale Discs

an important role when tracking the evolution of massive quiescent galaxies, minor dry mergers have been commonly advocated to explain the size growth of these galaxies (e.g. Hopkins et al. 2009; Carrasco et al. 2010; Cimatti et al. 2012; Fan et al. 2013; De et al. 2014). However, not enough satellites have been found around massive galaxies to support the minor dry merger scenario (e.g. Khochfar & Burkert 2006; Maller et al. 2006; Hopkins et al. 2009; Naab et al. 2009; McLure et al. 2013). A fascinating solution to the problem was proposed by Graham (2013), who suggested that the high-redshift compact massive spheroids (also dubbed “red nuggets”, Damjanov et al. 2009) have evolved into the bulges of today’s massive early-type disc galaxies (see also Dullo & Graham 2014 and Driver et al. 2013). This view was confirmed by Graham et al. (2015), who used published, reliable bulge/disc decompositions to unveil a large number of previously unnoticed local stellar spheroidal systems with the same structural properties, old stellar populations, and similar number density as the high-redshift compact massive spheroids. Graham et al. (2015) advocated the growth of two-dimensional stellar discs around the compact massive spheroids to explain the evolution of these objects.

Here we focus on five local early-type galaxies (Mrk 1216, NGC 1271, NGC 1277, NGC 1332, and NGC 3115) for which we performed accurate multicomponent decomposition with the aid of photometric and kinematic information. Our analysis shows that these galaxies all share the same morphological structure: a stellar spheroidal component with the same properties (massive, compact, and old) as the high-redshift red nuggets, and an intermediate-scale stellar disc that remains embedded within the spheroid. These five galaxies had their black hole masses estimated with a direct method. Four of them had been previously modelled by other studies (Rusli et al., 2011; van den Bosch et al., 2012; Walsh et al., 2015; Yıldırım et al., 2015), which failed to account for the correct radial extent of the stellar disc and consequently underestimated the spheroid luminosity. This yielded unusually large $M_{\text{BH}}/L_{\text{sph}}$ ratios.

The remainder of this Chapter comprises the published version of the paper “Explaining the reportedly overmassive black holes in early-type galaxies with intermediate-scale discs” by G. A. D. Savorgnan & A. W. Graham, as it appears in Volume 457 of *Monthly Notices of the Royal Astronomical Society*.

galaxies. While some of the $z = 0$ red-sequence galaxies might have had a passive evolution since $z \approx 2$, other $z = 0$ red-sequence galaxies might descend from $z \approx 2$ star-forming galaxies.



Explaining the reportedly overmassive black holes in early-type galaxies with intermediate-scale discs

Giulia A. D. Savorgnan[★] and Alister W. Graham

Centre for Astrophysics and Supercomputing, Swinburne University of Technology, Hawthorn, Victoria 3122, Australia

Accepted 2015 November 17. Received 2015 November 10; in original form 2015 September 22

ABSTRACT

The classification ‘early-type’ galaxy includes both elliptically and lenticular-shaped galaxies. Theoretically, the spheroid-to-disc flux ratio of an early-type galaxy can assume any positive value, but in practice studies often consider only spheroid/disc decompositions in which the disc neatly dominates over the spheroid at large galaxy radii, creating an inner ‘bulge’ as observed in most spiral galaxies. Here we show that decompositions in which the disc remains embedded within the spheroid, labelled by some as ‘unphysical’, correctly reproduce both the photometric and kinematic properties of early-type galaxies with intermediate-scale discs. Intermediate-scale discs have often been confused with large-scale discs and incorrectly modelled as such; when this happens, the spheroid luminosity is considerably underestimated. This has recently led to some surprising conclusions, such as the claim that a number of galaxies with intermediate-scale discs (Mrk 1216, NGC 1277, NGC 1271, and NGC 1332) host a central black hole whose mass is abnormally large compared to expectations from the (underestimated) spheroid luminosity. We show that when these galaxies are correctly modelled, they no longer appear as extreme outliers in the (black hole mass)–(spheroid mass) diagram. This not only nullifies the need for invoking different evolutionary scenarios for these galaxies but it strengthens the significance of the observed (black hole mass)–(spheroid mass) correlation and confirms its importance as a fundamental ingredient for theoretical and semi-analytic models used to describe the coevolution of spheroids and their central supermassive black holes.

Key words: black hole physics – galaxies: bulges – galaxies: elliptical and lenticular, cD – galaxies: evolution – galaxies: individual: Mrk 1216, NGC 1271, NGC 1277, NGC 1332, NGC 4291 – galaxies: structure.

1 INTRODUCTION

The awareness that *many* early-type galaxies contain previously overlooked stellar discs dates back half a century (Liller 1966; Strom & Strom 1978; Michard 1984; Djorgovski 1985; Bender & Moellenhoff 1987; Jedrzejewski 1987a; Capaccioli 1987; Carter 1987; Capaccioli, Piotto & Rampazzo 1988). It is well known that the identification of a stellar disc in an early-type galaxy, particularly when based on the galaxy’s photometric properties, is subject to inclination effects. As predicted by Carter (1987), this problem is largely overcome with kinematic analyses (e.g. Franx, Illingworth & Heckman 1989; Nieto et al. 1991; Rix & White 1992; Cinzano & van der Marel 1993; D’Onofrio et al. 1995; Graham et al. 1998, and the ATLAS^{3D} survey, Cappellari et al. 2011a), which allow one to determine the presence of a rotationally supported component

in a way nearly insensitive to projection effects (McElroy 1983; Cappellari et al. 2007; Emsellem et al. 2007). Yet, identifying the radial extent of an early-type galaxy’s disc with respect to the spheroidal component can still be subtle. Studying both the surface brightness profiles and the ellipticity profiles of early-type galaxies in the Virgo cluster – including those with elliptical (E), spindle and lenticular (S0) isophotes – Liller (1966) drew attention to the observation that many of the galaxies displayed ‘characteristics intermediate between those of type E and type S0’, and she classified them as ‘ES’ galaxies. Building on this and other investigations of ellipticity profiles (e.g. Strom & Strom 1978; di Tullio 1979), Michard (1984) used the classification ‘S0-like’ for these early-type galaxies with humped ellipticity profiles, dominated by a somewhat edge-on disc at intermediate radii. Nieto, Capaccioli & Held (1988) identified two dozen such spheroid-dominated early-type galaxies, whose discs do not prevail at large radii, and referred to them as ‘disk ellipticals’ (or ‘disky ellipticals’; Simien & Michard 1990). However, as noted by Nieto et al. (1988), unless the

* E-mail: gsavorgn@astro.swin.edu.au

orientation of the disc is favourable (i.e. somewhat edge-on), it can be missed. The same is true when searching for pointy isophotes that are shaped by the combination of the spheroid and a near edge-on disc (e.g. Carter 1978, 1987; Bender & Moellenhoff 1987; Ebneter et al. 1987; Jedrzejewski 1987a; Bender 1988; Bijaoui, Marchal & Michard 1989).

Today, most early-type galaxies are classified as ‘fast rotators’ (Emsellem et al. 2011; Scott et al. 2014), that is, they are rapidly rotating within their half-light radius. The exact definition of a fast rotator can be found in Emsellem et al. (2007), although the most recent literature (e.g. Arnold et al. 2011; Romanowsky & Fall 2012; Arnold et al. 2014) prefers the use of the term ‘central fast rotator’ to emphasize the fact that this classification pertains to the kinematic properties of a galaxy only within its half-light radius. Thanks to their more extended kinematic maps, Arnold et al. (2014) revealed that some of the central fast rotators continue to be fast rotating at large radii, whereas other central fast rotators become slow rotating in their outer regions.¹ Unfortunately, such extended kinematic maps are not yet available for large numbers of galaxies in the local Universe. Nevertheless, the ellipticity profile of a galaxy’s isophotes can help identify the extent of a stellar disc in an early-type galaxy.

In general, stellar discs are intrinsically flat and close to circular (e.g. Andersen et al. 2001; Andersen & Bershady 2002); their apparent ellipticity, dictated by their inclination to our line of sight, is fixed. Spheroids are often rounder than the observed projection on the sky of their associated discs, thus their average ellipticity is often lower than that of their disc. An ellipticity profile that increases with radius can be ascribed to an inclined disc that becomes progressively more important at large radii, whereas a radial decrease of ellipticity signifies the opposite case. This approach can be taken to the next level by inspecting the isophotes for discy structures (e.g. Carter 1978, 1987; Bender & Moellenhoff 1987; Capaccioli 1987; Jedrzejewski 1987a) and checking the velocity line profiles for asymmetry (e.g. Franx & Illingworth 1988; Bender 1990; Rix & White 1992; Scorsa & Bender 1995, and references therein; Scorsa 1998).

Building on the investigations in works such as Liller (1966), Jedrzejewski (1987a) and Rix & White (1990), the toy model shown in Fig. 1 illustrates the typical ellipticity profile ($\epsilon = 1 - b/a$, where b/a is the ratio of minor-to-major axis length) and the specific angular momentum profile ($\lambda = \langle R|V| \rangle / (R\sqrt{V^2 + \sigma^2})$, where R is the semimajor-axis radius, V is the mean velocity and σ is the velocity dispersion; Emsellem et al. 2007) of: (1) a lenticular galaxy, comprised of a large-scale disc which dominates the light at large radii over a relatively smaller encased bulge, i.e. a disc-dominated central fast rotator that continues to be fast rotating beyond one half-light radius; (2) a ‘discy elliptical’ galaxy (Michard 1984; Nieto et al. 1988) composed of an intermediate-scale disc embedded in a relatively larger spheroid which dominates the light at large radii, i.e. a spheroid-dominated central fast rotator that becomes slow rotating beyond 1–2 half-light radii; and (3) an elliptical galaxy with an additional nuclear stellar disc, i.e. a (spheroid-dominated) slow rotator. This sequence is analogue to that illustrated in fig. 2 of Cappellari et al. (2011b), although here we emphasize the correspondence

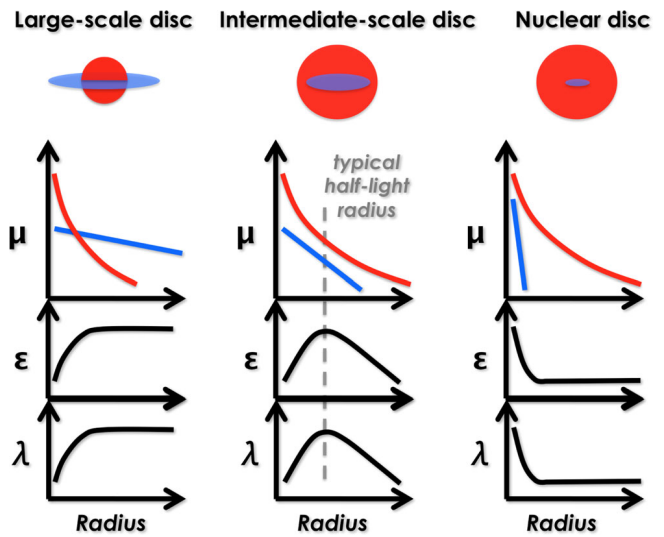


Figure 1. Illustration of the spheroid/disc decomposition of the one-dimensional surface brightness profile, μ , the ellipticity profile, ϵ , and the specific angular momentum profile, λ , for the three prototype early-type galaxy sub-classes. In the flux decompositions, the spheroid (or bulge) and the disc are shown with the red and blue colour, respectively. The left-hand panel shows a disc-dominated central fast rotator (lenticular galaxy), composed of a bulge encased in a large-scale disc. The right-hand panel displays a spheroid-dominated slow rotator (elliptical) with (an optional) nuclear stellar disc. The middle panel presents a spheroid-dominated central fast rotator with an intermediate-sized disc embedded in the spheroid.

between the spheroid/disc decomposition of the surface brightness profile and the ‘shape’ of the ellipticity profile (assuming that the disc inclination is not close to face-on) and also the specific angular momentum profiles.

While some recent studies have correctly distinguished between large- and intermediate-scale discs, and modelled them accordingly (e.g. Kormendy & Bender 2012; Krajnović et al. 2013), intermediate-scale discs have been missed by many galaxy modellers of late, who have labelled as ‘unphysical’ (Allen et al. 2006) those spheroid/disc decompositions in which the disc does not dominate over the spheroid at large radii as is observed with spiral galaxies. This has led to the rejection of many early-type galaxy decompositions similar to that illustrated in the top middle panel of Fig. 1. Unsurprisingly, studies affected by this bias have not obtained spheroid/disc decompositions with a spheroid-to-total ratio larger than 0.6–0.8 (e.g. Gadotti 2008; Head et al. 2014; Méndez-Abreu & CALIFA Team 2015; Querejeta et al. 2015).

As mentioned before, an isophotal analysis allows one to identify the presence and the radial extent of a disc in an early-type galaxy only when the disc has a certain level of inclination. On the other hand, a kinematic analysis has the advantage of being virtually insensitive to inclination effects, but cannot help one determine the radial extent of a disc if the kinematic data are limited within one half-light radius. Therefore, the best results are obtained when photometry and kinematics are combined together.

In this paper, we focus on the increasingly overlooked occurrence of intermediate-scale discs in galaxies with directly measured black hole masses. We report on the photometric and kinematical signatures of these intermediate-sized stellar discs, and the impact they have on the (black hole mass)-to-(spheroid stellar mass) ratio which is used to constrain galaxy evolution models. In Section 2, we present a detailed photometric analysis of three galaxies with intermediate-scale discs (Mrk 1216, NGC 1332, and NGC 3115)

¹ As pointed out by Cappellari et al. (2011a), while all of the disk ellipticals from Bender, Saglia & Gerhard (1994) are fast rotators, the complement is not true because weak discs only impact the isophotal shape if the discs have orientations close to edge-on, whereas their rotational signature can still be detected when they have a near face-on orientation. Of course if a disc is face-on, then the galaxy will not be classified as a fast rotator.

and we briefly describe another five galaxies with intermediate-scale discs (NGC 821, NGC 1271, NGC 1277, NGC 3377, and NGC 4697) already modelled by us elsewhere in the literature. We compare our photometric analysis with the kinematical information available from the literature, and explain the differences between our galaxy models and past decompositions. In Section 3, we explore the important implications this has for the (black hole mass)–(spheroid stellar mass) diagram. Finally, in Section 4 we briefly discuss our results in terms of galaxy evolution.

2 INTERMEDIATE-SCALE DISC GALAXIES

Three examples of galaxies with intermediate-scale discs are Mrk 1216, NGC 1332, and NGC 3115. In the following section, we present a photometric analysis of these three galaxies, and we compare our results with the kinematical analysis available from the literature for Mrk 1216 and NGC 3115. For the galaxies NGC 1332 and NGC 3115, we used $3.6\text{ }\mu\text{m}$ images obtained with the InfraRed Array Camera (IRAC) onboard the *Spitzer Space Telescope*. For the galaxy Mrk 1216, we used an archived *Hubble Space Telescope* (*HST*) image taken with the Wide Field Camera 3 (WFC3) and the near-infrared *F160W* filter (*H* band). Our galaxy decomposition technique is extensively described in Savorgnan & Graham (2015). Briefly, the galaxy images were background-subtracted, and masks for contaminating sources were created. The one-dimensional point spread function (PSF) was characterized using a Gaussian profile for the *HST* observation and a Moffat (1969) profile for the *Spitzer* observations. We performed an isophotal analysis of the galaxies using the *IRAF*² task *ellipse*³ (Jedrzejewski 1987b). The galaxy isophotes were modelled with a series of concentric ellipses, allowing the ellipticity, the position angle and the amplitude of the fourth harmonic to vary with radius. The decomposition of the surface brightness profiles was performed with software written by G. Savorgnan and described in Savorgnan & Graham (2015). We modelled the light profiles with a combination of PSF-convolved analytic functions, using one function per galaxy component.

2.1 NGC 3115

The presence of a disc in the central fast rotator NGC 3115 (e.g. Strom et al. 1977; Nieto et al. 1988; Scorsa & Bender 1995) is obvious due to its edge-on orientation (Fig. 2). Less obvious is the radial extent of this disc if one only relies on a visual inspection of the galaxy image. The ellipticity profile (Fig. 2) is consistent with the presence of an intermediate-scale disc. Moreover, the kinematics of NGC 3115 (Arnold et al. 2011) also disprove the presence of a large-scale disc, because the galaxy is rapidly rotating only

² *IRAF* is the Image Reduction and Analysis Facility, distributed by the National Optical Astronomy Observatory, which is operated by the Association of Universities for Research in Astronomy under cooperative agreement with the National Science Foundation.

³ Our analysis was performed before *isofit* (Ciambur 2015) was conceived or available. After *isofit* was recently developed and implemented in *IRAF*, we employed it to re-extract the surface brightness profiles of the galaxies NGC 1332 and NGC 3115. We then repeated the analysis and checked that this change does not significantly alter our results. In fact, although *isofit* provides a more accurate description of the isophotes in the presence of an inclined disc, the discs of NGC 1332 and NGC 3115 are relatively faint compared to the spheroidal components, therefore the differences between the light profile obtained with *ellipse* and that obtained with *isofit* are small for these two galaxies.

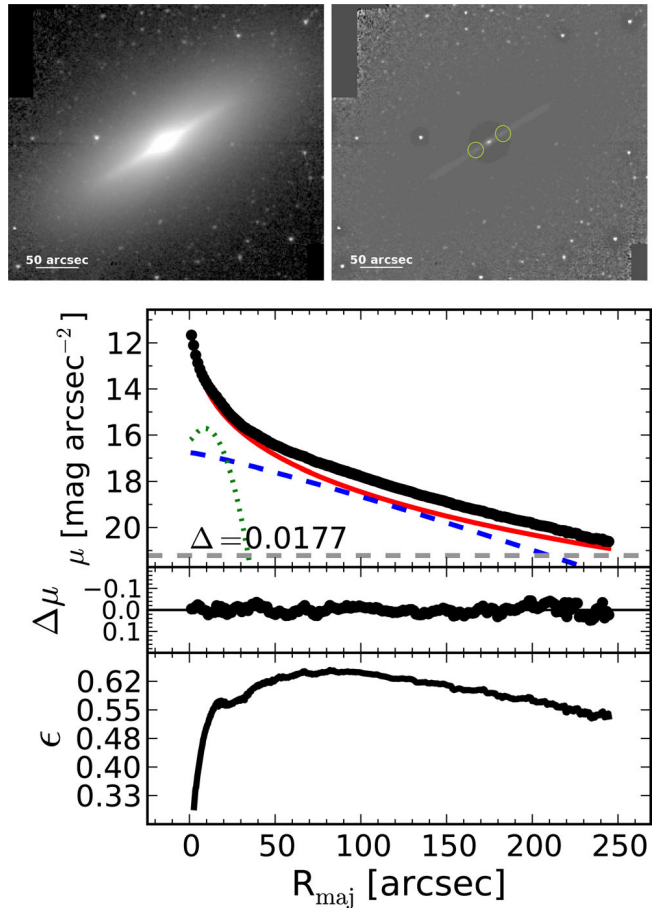


Figure 2. NGC 3115. The top panels are the *Spitzer*/IRAC $3.6\text{ }\mu\text{m}$ image (left) and its unsharp mask (right), obtained by dividing the image by a Gaussian-smoothed version of itself. In the unsharp mask, the green circles indicate the position of the two brighter spots associated with the edge-on nuclear ring. The bottom plots display the best-fitting model of the surface brightness profile, μ , and the ellipticity profile, ϵ , along the major axis, R_{maj} . The black points are the observed data, which extend out to five galaxy half-light radii ($\sim 5\text{ arcsec} \times 50\text{ arcsec}$). The colour lines represent the individual (PSF-convolved) model components: red solid = Sérsic (spheroid), blue dashed = Sérsic (disc), green dotted = Gaussian ring. The residual profile (data-model) is shown as $\Delta\mu$. The horizontal grey dashed line corresponds to an intensity equal to three times the root mean square of the sky background fluctuations. Δ denotes the root mean square scatter of the fit in units of mag arcsec^{-2} .

within two galaxy half-light radii ($\sim 2\text{ arcsec} \times 50\text{ arcsec}$), and the rotation significantly drops at larger radii. The unsharp mask of NGC 3115 (Fig. 2) betrays the presence of a faint edge-on nuclear ring, which can also be spotted as a small peak in the ellipticity profile (at semimajor-axis length $R_{\text{maj}} \sim 15\text{ arcsec}$). Such rings are common in early-type galaxies (e.g. Michard & Marchal 1993). The spheroidal component of NGC 3115 is well described with a Sérsic (1963) profile. The highly inclined intermediate-scale disc is better fitted with an $n < 1$ Sérsic profile (the Sérsic index n regulates the curvature of the Sérsic profile) rather than with an exponential function, as explained by Pastrav et al. (2013). The nuclear ring is modelled with a Gaussian function.

In comparison, Läsker, Ferrarese & van de Ven (2014a) fit NGC 3115 with a bulge + disc + envelope, and measured a bulge half-light radius of 3.9 arcsec and a bulge-to-total ratio of 0.12 . We describe this galaxy using a spheroid + intermediate-scale

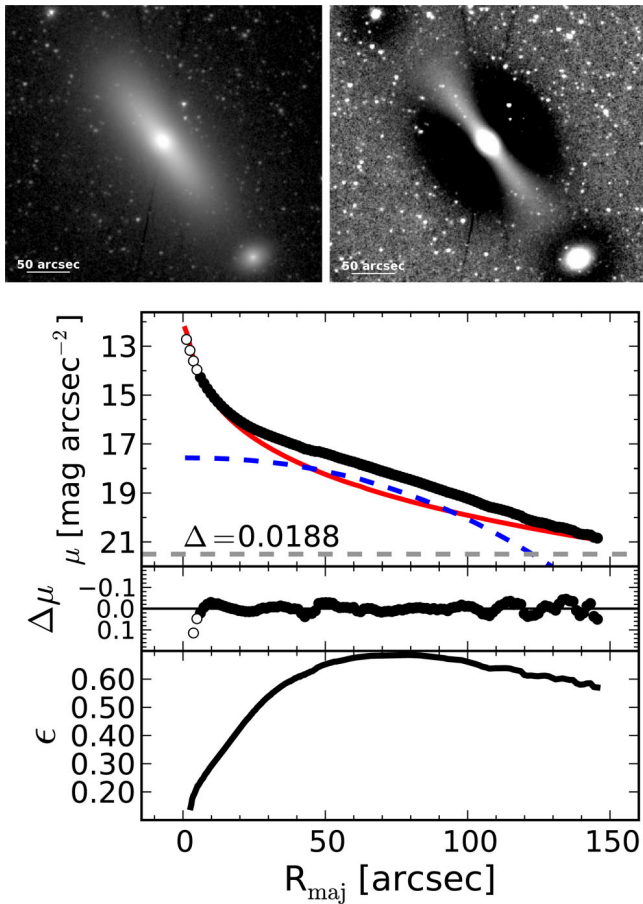


Figure 3. NGC 1332. Similar to Fig. 2. The surface brightness profile extends out to seven galaxy half-light radii ($\sim 7 \text{ arcsec} \times 20 \text{ arcsec}$). The empty points are data excluded from the fit.

disc + nuclear ring, and obtain a spheroid half-light radius of 43.6 arcsec and a spheroid-to-total ratio of 0.85. We have used both kinematical information and ellipticity profiles, together with the surface brightness profile, to obtain a physically consistent and meaningful model.

2.2 NGC 1332

The morphology of NGC 1332 (Fig. 3) is very similar to that of NGC 3115, with the ellipticity profile indicating the presence of an intermediate-scale disc, although in this case no nuclear component is evident. We were not able to find any extended kinematic profile or map for this galaxy in the literature. The data within the innermost 6 arcsec were excluded from the fit because, according to our galaxy decomposition, they are possibly affected by the presence of a partially depleted core. The surface brightness profile of NGC 1332 is well described with a Sérsic-spheroid plus an $n < 1$ Sérsic disc. Our galaxy decomposition suggests that NGC 1332 is a spheroid-dominated galaxy, with a spheroid-to-total ratio of 0.95.

Rusli et al. (2011) did not identify the restricted extent of the intermediate-scale disc, as revealed by the ellipticity profile, and proposed a model featuring a Sérsic bulge and a large-scale exponential disc, with a spheroid-to-total ratio of 0.43. Based on their bulge/disc decomposition, they concluded that NGC 1332 is a disc-dominated lenticular galaxy which is displaced from the (black hole mass)–(spheroid luminosity) correlation of Marconi & Hunt (2003) by an order of magnitude along the black hole mass direction. How-

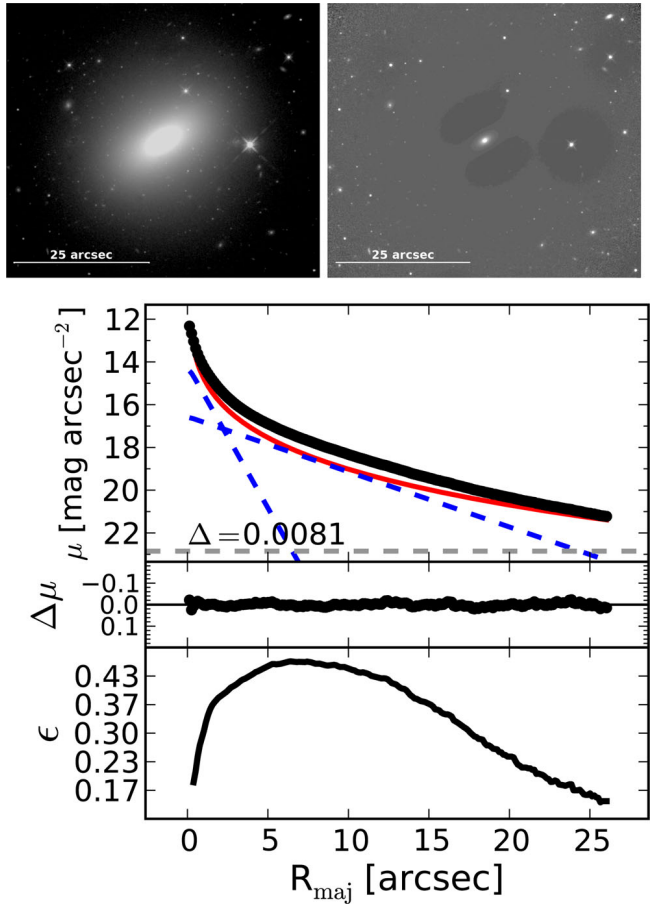


Figure 4. Mrk 1216. Similar to Fig. 2. The top panels are the *HST*/WFC3 *F160W* image (left) and its unsharp mask (right). The surface brightness profile extends out to five galaxy half-light radii ($\sim 5 \text{ arcsec} \times 5 \text{ arcsec}$). The colour lines represent the individual (PSF-convolved) model components: red solid = Sérsic (spheroid), blue dashed = exponential (nuclear and intermediate-scale disc).

ever, in Section 3 we show that, according to our decomposition, NGC 1332 lies within the 1σ scatter about the (black hole mass)–(spheroid stellar mass) correlation for early-type galaxies. We also note that the majority of galaxies with an elevated stellar velocity dispersion ($\sigma > 270 \text{ km s}^{-1}$) are core-Sérsic galaxies (Graham et al. 2003; Ferrarese et al. 2006; Dullo & Graham 2014), i.e. they have a partially depleted core which has been identified from high-resolution photometric data. NGC 1332 has $\sigma = 320 \text{ km s}^{-1}$, but, based on their decomposition of *HST* imaging, Rusli et al. (2011) did not find a core in this galaxy. However, our galaxy decomposition (Fig. 3) suggests that NGC 1332 is in fact a core-Sérsic galaxy. Since we did not use high-resolution photometric data, we refrain from a firm conclusion, but we caution that a re-analysis of the *HST* data – by taking into account the correct radial extent of the intermediate-scale disc – may indeed reveal the presence of a depleted core in this galaxy.

2.3 Mrk 1216

Although the disc in the central fast rotator Mrk 1216 is not immediately apparent from the image (Fig. 4), the velocity map (Yıldırım et al. 2015) reveals the presence of a fast rotating component within three galaxy half-light radii ($\sim 3 \text{ arcsec} \times 5 \text{ arcsec}$). The ellipticity

profile (Fig. 4), which extends out to five half-light radii, indicates the presence of an intermediate-scale disc. In addition, a nuclear disc is identified from the change in slope of the ellipticity profile ($R_{\text{maj}} \sim 1-2$ arcsec), from the unsharp mask, and from a clear feature in the $B4$ fourth harmonic profile (not shown here). We modelled the surface brightness profile of Mrk 1216 (Fig. 4) with a Sérsic-spheroid, an intermediate-sized exponential disc, and a nuclear exponential disc.

2.4 Other galaxies

Our models with an intermediate-sized disc embedded within a larger spheroidal component, plus an additional nuclear component when one is present, match the observed light distribution, and explain both the extended kinematic maps (when available; Arnold et al. 2014) and the ellipticity profiles, of five additional galaxies for which a direct measurement of their central supermassive black hole mass is available: NGC 821; NGC 1271; NGC 1277; NGC 3377; and NGC 4697. Our isophotal analysis and galaxy decompositions for NGC 1271 and NGC 1277 will be presented in Graham, Savorgnan & Ciambur (in preparation) and Graham et al. (2015a), respectively, while the galaxies NGC 821, NGC 3377, and NGC 4697 have been analysed in Savorgnan & Graham (2015).

2.4.1 NGC 1271

Walsh et al. (2015b) explored a three-component decomposition for the central fast rotator NGC 1271 and identified the galaxy bulge with the innermost of the three components, having a half-light radius of 0.61 arcsec and a bulge-to-total flux ratio of 0.23; our model features a spheroid + intermediate-scale disc, with a spheroid half-light radius of 3.3 arcsec and a spheroid-to-total flux ratio of 0.67.

2.4.2 NGC 1277

van den Bosch et al. (2012) proposed a model for the central fast rotator NGC 1277 with a bulge + disc + nuclear source + envelope, which gives a bulge half-light radius of 0.9 arcsec and a bulge-to-total flux ratio of 0.24; our model consists of a spheroid + intermediate-scale disc + nuclear component, and produces a spheroid half-light radius of 6.0 arcsec and a spheroid-to-total flux ratio of 0.79.

2.4.3 NGC 3377

Läsker et al. (2014a) modelled the central fast rotator NGC 3377 (e.g. Jedrzejewski 1987a; Scorsa & Bender 1995) with a bulge + nuclear disc + disc + envelope, and obtained a bulge half-light radius of 10.1 arcsec and a bulge-to-total flux ratio of 0.35; our model with a spheroid + intermediate-scale disc + nuclear disc returns a spheroid half-light radius of 61.8 arcsec and a spheroid-to-total flux ratio of 0.94.

2.4.4 NGC 821

Läsker et al. (2014a) decomposed the central fast rotator NGC 821 into a bulge + disc + envelope, and measured a bulge half-light radius of 3.8 arcsec and a bulge-to-total flux ratio of 0.19; our decomposition consists of a spheroid + intermediate-scale disc,

with a spheroid half-light radius of 36.5 arcsec and a spheroid-to-total flux ratio of 0.79.

2.4.5 NGC 4697

While NGC 4697 (e.g. Davies 1981; Carter 1987; Jedrzejewski, Davies & Illingworth 1987) was explicitly referred to as a ‘fast rotator’ by Capaccioli (1987) and Petrou (1981), it is only a central fast rotator and it represents an ‘extreme’ case. Läsker et al. (2014a) fit this galaxy with a bulge + nuclear source + disc + envelope, and obtained a bulge half-light radius of 6.3 arcsec and a bulge-to-total flux ratio of 0.08; we described NGC 4697 using a spheroid + intermediate-scale disc + nuclear disc model, and measured a spheroid half-light radius of 239.3 arcsec and a spheroid-to-total flux ratio of 0.89.

Past models that ‘forcedly’ described intermediate-scale disc galaxies using an inner bulge encased within a large-scale disc commonly required the addition of an extended envelope or halo to account for the outer portion of the spheroid. Such three-component models (bulge + disc + envelope) typically reduce the spheroid luminosity by a factor of 3–4, and underestimate the size of the spheroid by a factor of 6–10, although more ‘extreme’ cases can be found.

3 THE BLACK HOLE–SPHEROID CORRELATION

Inaccurate measurements of the spheroid-to-total ratio of galaxies can impact galaxy scaling relations. Recently, a handful of galaxies with intermediate-scale discs have been claimed to host overmassive black holes, i.e. the mass of their central supermassive black hole has been reported to be significantly larger than what is expected from the galaxy’s spheroid luminosity (or stellar mass). This is the case for the galaxies Mrk 1216 (for which only an upper limit on its black hole mass has been published; Yıldırım et al. 2015), NGC 1271 (Walsh et al. 2015b), NGC 1277 (van den Bosch et al. 2012; Walsh et al. 2015a; Yıldırım et al. 2015) and NGC 1332 (Rusli et al. 2011). In addition to these, the elliptical galaxy NGC 4291 has also been claimed to be an $\sim 3.6\sigma$ outlier above the (black hole mass)–(spheroid mass) scaling relation (Bogdán et al. 2012). Obviously, having both the black hole mass and the spheroid mass correct is important for placing systems in the (black hole mass)–(spheroid mass) diagram.

At present, for early-type galaxies, the spheroid luminosity and the galaxy luminosity can be used to predict the black hole mass with the same level of accuracy⁴ (Savorgnan et al. 2015). If a galaxy hosts a black hole that is overmassive compared to expectations from the spheroid luminosity, but whose mass is normal compared to expectations from the galaxy luminosity, one should wonder whether the spheroid luminosity might have been underestimated due to an inaccurate spheroid/disc decomposition. Indeed, none of the five galaxies just mentioned (Mrk 1216, NGC 1271, NGC 1277,

⁴ Note that Läsker et al. (2014b) reported that the spheroid luminosity and the galaxy luminosity are equally good tracers of the black hole mass irrespective of the galaxy morphological type, but their sample of 35 galaxies contained only 4 spiral galaxies. However, using a sample of 45 early-type and 17 spiral galaxies, Savorgnan et al. (2015) shows that, when considering all galaxies irrespective of their morphological type, the correlation of the black hole mass with the spheroid luminosity is better than that with the galaxy luminosity.

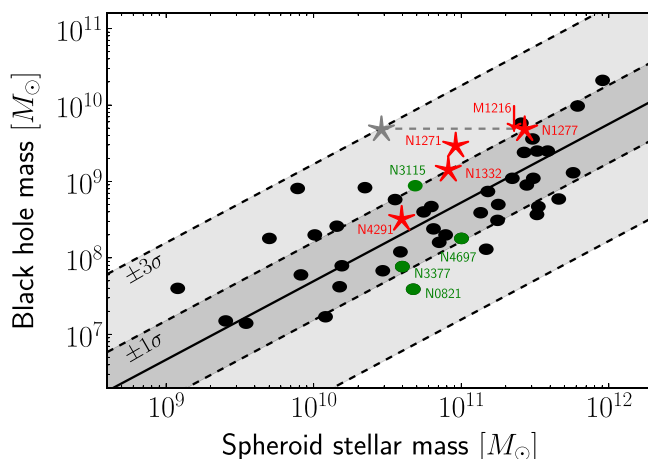


Figure 5. Black hole mass plotted against spheroid stellar mass for 45 + 3 early-type galaxies (from Savorgnan et al. 2015). The black solid line is the bisector linear regression for all galaxies except Mrk 1216, NGC 1271, and NGC 1277. The dashed lines mark the 1σ and 3σ deviations, where σ (0.51 dex) is the total rms scatter about the correlation in the black hole mass direction. The red symbols mark five galaxies that were claimed to be extreme outliers in this diagram: four intermediate-scale disc galaxies (Mrk 1216, NGC 1271, NGC 1277, and NGC 1332) and one elliptical galaxy (NGC 4291). All five reside well within a 3σ deviation from the correlation when using their correct spheroid mass. For NGC 1277, we show the previously reported spheroid stellar mass (van den Bosch et al. 2012) in grey. The green colour is used to show the location of four additional intermediate-scale disc galaxies mentioned in Section 2.

NGC 1332, and NGC 4291) is a noticeable outlier in the (black hole mass)–(galaxy luminosity) diagram. In Fig. 5, we show the location of these five galaxies in the updated (black hole mass)–(spheroid stellar mass) diagram for early-type galaxies from Savorgnan et al. (2015). Fig. 5 was populated using the galaxy decomposition technique shown here and extensively described in Savorgnan & Graham (2015). Briefly, we obtained *Spitzer*/IRAC 3.6 μ m images for 45 early-type galaxies which already had a dynamical detection of their black hole mass. We modelled their one-dimensional surface brightness profiles with a combination of analytic functions, using one function per galaxy component. Spheroid luminosities were converted into stellar masses using individual, but almost constant mass-to-light ratios (~ 0.6 ; Meidt et al. 2014).

In Fig. 5, we show the galaxies Mrk 1216, NGC 1271, and NGC 1277, which were not a part of the original sample of 45 early-type galaxies. For the galaxy NGC 1271, we use the black hole mass measurement and the stellar mass-to-light ratio obtained by Walsh et al. (2015b). For the galaxy NGC 1277, we use the black hole mass measurement obtained by Walsh et al. (2015a) and the stellar mass-to-light ratio obtained by Martín-Navarro et al. (2015). Note that for NGC 1277, we recover a spheroid stellar mass of $2.7 \times 10^{11} M_\odot$, in agreement with the value of $\approx 1.2 \times 10^{11} M_\odot$ obtained by Emsellem (2013) from his multi-Gaussian expansion models.⁵ For the galaxy Mrk 1216, we use the upper limit on the black hole mass and the stellar mass-to-light ratio obtained by Yıldırım et al. (2015). For the first time, Fig. 5 reveals that when the four intermediate-scale disc galaxies Mrk 1216, NGC 1271, NGC 1277, NGC 1332, and the

elliptical galaxy NGC 4291 are properly modelled, they no longer appear as extreme outliers above the (black hole mass)–(spheroid stellar mass) correlation for early-type galaxies, i.e. they all reside well within a 3σ deviation from the correlation.

4 ORIGIN OF COMPACT MASSIVE GALAXIES

Acknowledging the correct structure of galaxies with intermediate-scale discs is important to properly understand their origin. According to the current paradigm of cosmological structure evolution, the genesis of massive early-type galaxies is characterized by two distinct phases: ‘*in situ*’ and ‘*ex situ*’. The first phase takes place in a young Universe (within its first 4 Gyr), when cold gas inflows produced short and intense bursts of star formation that created compact and dense conglomerates of stars with high-velocity dispersion (e.g. Prieto, Jimenez & Haiman 2013). These naked and compact conglomerates, named ‘red nuggets’ (Damjanov et al. 2009), have been observed at high redshift with half-light sizes of 1–2 kpc (Daddi et al. 2005; Trujillo et al. 2006; van Dokkum et al. 2008). In the second phase (last 10 Gyr), discs and stellar envelopes were accreted around these primordial conglomerates and the external parts of today’s galaxies assembled on scales of 2–20 kpc (e.g. Driver et al. 2013).

Today’s Universe is populated by an abundance of compact, massive spheroids, with the same physical properties – mass and compactness – as the high-redshift red nuggets (Graham, Dullo & Savorgnan 2015b). Some of these local compact massive spheroids are encased within a large-scale disc, that is to say they are the bulges of some lenticular and spiral galaxies. Over the last 10 Gyr, their spheroids have evolved by growing a relatively flat disc (e.g. Pichon et al. 2011; Danovich et al. 2012; Stewart et al. 2013) – rather than a three-dimensional envelope – which has increased the galaxy size but preserved the bulge compactness. Of course, some lenticular/ES galaxies may have been built from mergers (e.g. Querejeta et al. 2015, and references therein). The other compact massive spheroids of today’s Universe belong to some galaxies with intermediate-scale discs. Indeed, Mrk 1216, NGC 1271, NGC 1277, NGC 1332, and NGC 3115 are all local compact intermediate-scale disc galaxies with purely old (> 10 Gyr) stellar populations. These galaxies have undergone the lowest degree of disc growth.

In addition to the observational clues as to the actual physical components in galaxies with intermediate-scale discs, one can reason on other grounds as to why these compact galaxies are not comprised of an inner bulge plus large-scale disc plus outer envelope. If they were such three-component systems, then one would have two possibilities. The first possibility is that these galaxies were already fully assembled 10 Gyr ago; this would explain their old stellar populations, but it would also imply that their discs and envelopes had already formed during the first 4 Gyr of the Universe, in disagreement with the current cosmological picture. The second possibility is that only their inner bulges (with sizes of 0.1–0.2 kpc, according to past decompositions) originated in the first 4 Gyr and they subsequently accreted a substantial disc and envelope. If this was correct, then we would observe high-redshift, star-like, naked bulges with stellar masses within a factor of a few times the currently observed red nuggets but sizes which are 10 times smaller. However, a dramatically different expectation is reached if one considers these galaxies today as spheroid-dominated systems with an intermediate-scale disc; in this case, both the galaxy size and the spheroid size are compact (1–2 kpc). This implies that, among the local descendants of the high-redshift red nuggets, the compact

⁵ In Emsellem (2013), readers will find a clever discussion of the problematics associated with the definition and the identification of the ‘bulge’ component in a galaxy.

intermediate-scale disc galaxies have undergone the lowest degree of disc growth. That is, the bulk of a compact intermediate-scale disc galaxy quickly assembled ‘*in situ*’ in a very young Universe and experienced very little evolution over the last 10 Gyr.

5 SUMMARY AND CONCLUSIONS

Early-type galaxies display a broad distribution of spheroid-to-total flux ratios (e.g. Cappellari et al. 2011b), going from disc-less, ‘pure’ elliptical galaxies (slow rotators) to disc-dominated lenticular galaxies (central fast rotators that continue to be fast rotating also beyond one half-light radius). In between these two extremes lie galaxies with intermediate-scale discs (spheroid-dominated central fast rotators that become slow rotating in their outer regions), i.e. discs of kiloparsec size that remain ‘embedded’ within the spheroidal component of the galaxy and do not dominate the galaxy light at large radii as large-scale discs do. While this is likely known to some readers, the surge of papers presenting galaxy decompositions which are not aware of this reality has created a pressing need for this reminder. We have shown that the light distribution of galaxies with intermediate-scale discs can be accurately described with a simple spheroid + disc (+optional nuclear component) model, without the need for the addition of a bright envelope component.

Our decompositions correctly reproduce both the photometric (surface brightness and ellipticity profiles) and kinematic (specific angular momentum profile) properties of nine intermediate-scale disc galaxies. Four of these nine galaxies (Mrk 1216, NGC 1271, NGC 1277, NGC 1332) and one additional elliptical galaxy (NGC 4291) had previously been claimed to be extreme outliers in the (black hole mass)–(spheroid mass) diagram. However, here we have demonstrated that, when correctly modelled, these five galaxies all reside well within the scatter of the correlation, i.e. they do not host overmassive black holes. This serves to strengthen the (black hole mass)–(spheroid mass) relation, and rules out the need for exotic formation scenarios.

ACKNOWLEDGEMENTS

This research was supported by Australian Research Council funding through grant FT110100263. GS is grateful to Matteo Fossati, Luca Cortese and Giuseppe Gavazzi for useful comments and discussion. The publication of this paper would not have been possible without the invaluable support of Chris Blake and Duncan Forbes. We warmly thank our anonymous referee for their very careful review of our paper, and for the comments, corrections and suggestions that ensued. This work is based on observations made with the IRAC instrument (Fazio et al. 2004) on-board the *Spitzer Space Telescope*, which is operated by the Jet Propulsion Laboratory, California Institute of Technology under a contract with NASA, and also on observations made with the NASA/ESA *HST*, and obtained from the Hubble Legacy Archive, which is a collaboration between the Space Telescope Science Institute (STScI/NASA), the Space Telescope European Coordinating Facility (ST-ECF/ESA) and the Canadian Astronomy Data Centre (CADC/NRC/CSA). This research has made use of the GOLDMine data base (Gavazzi et al. 2003) and the NASA/IPAC Extragalactic Database (NED) which is operated by the Jet Propulsion Laboratory, California Institute of Technology, under contract with the National Aeronautics and Space Administration.

REFERENCES

- Allen P. D., Driver S. P., Graham A. W., Cameron E., Liske J., de Propris R., 2006, MNRAS, 371, 2
 Andersen D., Bershady M. A., 2002, in Athanassoula E., Bosma A., Mujica R., eds, ASP Conf. Ser. Vol. 275, Disks of Galaxies: Kinematics, Dynamics and Peturbations. Astron. Soc. Pac., San Francisco, p. 39
 Andersen D. R., Bershady M. A., Sparke L. S., Gallagher J. S., III, Wilcots E. M., 2001, ApJ, 551, L131
 Arnold J. A., Romanowsky A. J., Brodie J. P., Chomiuk L., Spitler L. R., Strader J., Benson A. J., Forbes D. A., 2011, ApJ, 736, L26
 Arnold J. A. et al., 2014, ApJ, 791, 80
 Bender R., 1988, A&A, 193, L7
 Bender R., 1990, A&A, 229, 441
 Bender R., Moellenhoff C., 1987, A&A, 177, 71
 Bender R., Saglia R. P., Gerhard O. E., 1994, MNRAS, 269, 785
 Bijaoui A., Marchal J., Michard R., 1989, in Corwin H. G., Jr, Bottinelli L., eds, World of Galaxies (Le Monde des Galaxies), p. 250
 Bogdán Á. et al., 2012, ApJ, 753, 140
 Capaccioli M., 1987, in de Zeeuw P. T., ed., Proc. IAU Symp. 127, Structure and Dynamics of Elliptical Galaxies. Reidel, Dordrecht, p. 47
 Capaccioli M., Piotto G., Rampazzo R., 1988, AJ, 96, 487
 Cappellari M. et al., 2007, MNRAS, 379, 418
 Cappellari M. et al., 2011a, MNRAS, 413, 813
 Cappellari M. et al., 2011b, MNRAS, 416, 1680
 Carter D., 1978, MNRAS, 182, 797
 Carter D., 1987, ApJ, 312, 514
 Ciambur B. C., 2015, ApJ, 810, 120
 Cinzano P., van der Marel R. P., 1993, in Danziger I. J., Zeilinger W. W., Kjær K., eds, Eur. South. Obs. Conf. Workshop Proc. Vol. 45, Structure, Dynamics and Chemical Evolution of Elliptical Galaxies, p. 105
 D’Onofrio M., Zaggia S. R., Longo G., Caon N., Capaccioli M., 1995, A&A, 296, 319
 Daddi E. et al., 2005, ApJ, 626, 680
 Damjanov I. et al., 2009, ApJ, 695, 101
 Danovich M., Dekel A., Hahn O., Teyssier R., 2012, MNRAS, 422, 1732
 Davies R. L., 1981, MNRAS, 194, 879
 di Tullio G. A., 1979, A&AS, 37, 591
 Djorgovski S. B., 1985, PhD thesis, California Univ.
 Driver S. P., Robotham A. S. G., Bland-Hawthorn J., Brown M., Hopkins A., Liske J., Phillipps S., Wilkins S., 2013, MNRAS, 430, 2622
 Dullo B. T., Graham A. W., 2014, MNRAS, 444, 2700
 Ebneter K., Davis M., Jeske N., Stevens M., 1987, BAAS, 19, 681
 Emsellem E., 2013, MNRAS, 433, 1862
 Emsellem E. et al., 2007, MNRAS, 379, 401
 Emsellem E. et al., 2011, MNRAS, 414, 888
 Fazio G. G. et al., 2004, ApJS, 154, 10
 Ferrarese L. et al., 2006, ApJS, 164, 334
 Franx M., Illingworth G. D., 1988, ApJ, 327, L55
 Franx M., Illingworth G., Heckman T., 1989, ApJ, 344, 613
 Gadotti D. A., 2008, MNRAS, 384, 420
 Gavazzi G., Boselli A., Donati A., Franzetti P., Scodéglio M., 2003, A&A, 400, 451
 Graham A. W., Colless M. M., Busarello G., Zaggia S., Longo G., 1998, A&AS, 133, 325
 Graham A. W., Erwin P., Trujillo I., Asensio Ramos A., 2003, AJ, 125, 2951
 Graham A. W., Durrel M., Savorgnan G. A. D., Batcheldor D., Watson B., Medling A., Scott N., Marconi A., 2015a, ApJ, Submitted
 Graham A. W., Dullo B. T., Savorgnan G. A. D., 2015b, ApJ, 804, 32
 Head J. T. C. G., Lucey J. R., Hudson M. J., Smith R. J., 2014, MNRAS, 440, 1690
 Jedrzejewski R. I., 1987a, in de Zeeuw P. T., ed., Proc. IAU Symp. 127, Structure and Dynamics of Elliptical Galaxies. Reidel, Dordrecht, p. 37
 Jedrzejewski R. I., 1987b, MNRAS, 226, 747
 Jedrzejewski R. I., Davies R. L., Illingworth G. D., 1987, AJ, 94, 1508
 Kormendy J., Bender R., 2012, ApJS, 198, 2
 Krajnović D. et al., 2013, MNRAS, 432, 1768
 Läsker R., Ferrarese L., van de Ven G., 2014a, ApJ

- Läsker R., Ferrarese L., van de Ven G., Shankar F., 2014b, ApJ
Liller M. H., 1966, ApJ, 146, 28
McElroy D. B., 1983, ApJ, 270, 485
Marconi A., Hunt L. K., 2003, ApJ, 589, L21
Martín-Navarro I., La Barbera F., Vazdekis A., Ferré-Mateu A., Trujillo I., Beasley M. A., 2015, MNRAS, 451, 1081
Meidt S. E. et al., 2014, ApJ, 788, 144
Méndez-Abreu J., CALIFA Team 2015, in Cenarro A. J., Figueras F., Hernández-Monteagudo C., Trujillo Bueno J., Valdvielso L., eds, Proceedings of the XI Scientific Meeting of the Spanish Astronomical Society, Highlights of Spanish Astrophysics VIII. Teruel, p. 268
Michard R., 1984, A&A, 140, L39
Michard R., Marchal J., 1993, A&AS, 98, 29
Moffat A. F. J., 1969, A&A, 3, 455
Nieto J.-L., Capaccioli M., Held E. V., 1988, A&A, 195, L1
Nieto J.-L., Bender R., Arnaud J., Surma P., 1991, A&A, 244, L25
Pastrav B. A., Popescu C. C., Tuffs R. J., Sansom A. E., 2013, A&A, 553, A80
Petrou M., 1981, MNRAS, 196, 933
Pichon C., Pogosyan D., Kimm T., Slyz A., Devriendt J., Dubois Y., 2011, MNRAS, 418, 2493
Prieto J., Jimenez R., Haiman Z., 2013, MNRAS, 436, 2301
Querejeta M., Eliche-Moral M. C., Tapia T., Borlaff A., Rodríguez-Pérez C., Zamorano J., Gallego J., 2015, A&A, 573, A78
Rix H.-W., White S. D. M., 1990, ApJ, 362, 52
Rix H.-W., White S. D. M., 1992, MNRAS, 254, 389
Romanowsky A. J., Fall S. M., 2012, ApJS, 203, 17
Rusli S. P., Thomas J., Erwin P., Saglia R. P., Nowak N., Bender R., 2011, MNRAS, 410, 1223
Savorgnan G. A. D., Graham A. W., 2015, ApJ, preprint ([arXiv:1511.07446](https://arxiv.org/abs/1511.07446))
Savorgnan G. A. D., Graham A. W., Marconi A., Sani E., 2015, ApJ, preprint ([arXiv:1511.07437](https://arxiv.org/abs/1511.07437))
Scorza C., 1998, in Aguilar A., Carraminana A., eds, IX Latin American Regional IAU Meeting, Focal Points in Latin American Astronomy. p. 117
Scorza C., Bender R., 1995, A&A, 293, 20
Scott N., Davies R. L., Houghton R. C. W., Cappellari M., Graham A. W., Pimbblet K. A., 2014, MNRAS, 441, 274
Sérsic J. L., 1963, Bull. Argentina Assoc. Astron., 6, 41
Simien F., Michard R., 1990, A&A, 227, 11
Stewart K. R., Brooks A. M., Bullock J. S., Maller A. H., Diemand J., Wadsley J., Moustakas L. A., 2013, ApJ, 769, 74
Strom S. E., Strom K. M., 1978, AJ, 83, 732
Strom K. M., Strom S. E., Jensen E. B., Moller J., Thompson L. A., Thuan T. X., 1977, ApJ, 212, 335
Trujillo I. et al., 2006, MNRAS, 373, L36
van den Bosch R. C. E., Gebhardt K., Güttekin K., van de Ven G., van der Wel A., Walsh J. L., 2012, Nature, 491, 729
van Dokkum P. G. et al., 2008, ApJ, 677, L5
Walsh J. L., van den Bosch R. C. E., Gebhardt K., Yıldırım A., Richstone D. O., Güttekin K., Husemann B., 2015a, preprint ([arXiv:1511.04455](https://arxiv.org/abs/1511.04455))
Walsh J. L., van den Bosch R. C. E., Gebhardt K., Yıldırım A., Güttekin K., Husemann B., Richstone D. O., 2015b, ApJ, 808, 183
Yıldırım A., van den Bosch R. C. E., van de Ven G., Husemann B., Lyubanova M., Walsh J. L., Gebhardt K., Güttekin K., 2015, MNRAS, 452, 1792

This paper has been typeset from a TeX/LaTeX file prepared by the author.

8

Final Remarks and Future Perspectives

In this thesis, we explored scaling relations between the supermassive black hole mass and various properties of the host spheroid, in the pursuit of a more profound understanding of the co-evolution between SMBHs and their host galaxies. A summary of our principal findings and some additional considerations are presented here. This Chapter incorporates also some promising future research directions.

In Chapter 2 (Savorgnan et al., 2013), we compared the results obtained by four independent studies (Graham & Driver, 2007a; Sani et al., 2011; Vika et al., 2012; Beifiori et al., 2012) that attempted photometric decompositions of similar samples of galaxies with a direct measurement of the black hole mass. In many cases we found a large discrepancy between the spheroid Sérsic index measurements obtained by different studies for the same galaxy, either due to a significantly different choice of model components or to other various systematic effects. By rejecting the most discrepant Sérsic index measurements and averaging the remaining ones, we were able to recover a strong $M_{\text{BH}} - n_{\text{sph}}$ correlation, which was not found using the individual datasets of three of the four aforementioned studies. From this we concluded that some of their galaxy decompositions were not accurate. Chapter 2 emphasises the importance of a correct, physically motivated selection of model components and cautions against the several systematics that can affect galaxy decomposition.

Chapter 3 (Savorgnan & Graham, 2016b) was dedicated to the careful multicomponent decomposition of 66 galaxies with a direct measurement of the black hole mass. We followed the same approach as Laurikainen et al. (2005) in selecting the components for each galaxy

model. *A priori* identification of the galaxy components was done on the basis of several different indicators such as the analysis of the isophotal parameters, the inspection of unsharp masks, complementary information extracted from the literature, and – most importantly – from the galaxy kinematics. A joint photometric-kinematic approach (e.g. Krajnović et al. 2013; Arnold et al. 2014) turned out to play a decisive role for the robustness of our galaxy modelling. Upon examining central (Emsellem et al., 2011; Scott et al., 2014) and more extended (Arnold et al., 2014) velocity maps and comparing kinematic and photometric signatures of stellar discs, we were able to securely identify the presence and the radial extent of such discs. We observed a wide range of spheroid-to-disc ratios in early-type galaxies, going from parsec-sized nuclear discs, to kiloparsec-sized intermediate- and large-scale discs, in agreement with the findings of Krajnović et al. (2013). Comparison of our results with those obtained by previous studies indicates that multicomponent models (as opposed to simple bulge/disc models) are necessary to derive reliable structural parameters, confirming previous results (e.g. Laurikainen et al. 2005, 2007, 2010; Läsker et al. 2014a; Salo et al. 2015). In general, the best-fit parameters obtained with 1D and 2D decomposition techniques for the same galaxy are consistent with each other, i.e. no systematic effects were noticed between 1D and 2D modelling. However, our practical experience led us to prefer the 1D decomposition technique. Advantages associated with the 1D technique are a higher convergence rate for the fits, the wealth of information contained in the 1D isophotal analysis, and the easier interpretation of the 1D residuals. We caution against the dangerous practice of identifying unsubtracted galaxy components from the residual image of a 2D fit. As an additional warning, given the level of detail to which our galaxy decompositions were carried out, we do not consider it possible for current automatic routines to reproduce our human-supervised analysis.

In our 1D galaxy decomposition code, the minimisation routine is based on the Levenberg-Marquardt algorithm, which is known to be one of the fastest algorithms available, but is also prone to “get trapped” into local minima of the chi-squared distribution. As a future project, it would be interesting to implement in the code different minimisation algorithms, such as those available in `Imfit` (Erwin, 2015), and test their performance. It would also be beneficial to create a procedure to estimate the systematic uncertainties associated with the best-fit parameters from the fit itself, without the need to resort to decompositions performed by other authors as we did in this work. One of the issues associated with multicomponent decomposition is the risk of “overfitting”, i.e. having a model with more components (or parameters) than what is actually

needed. Information theory and Bayes analysis provide us with a number of methods to estimate the maximum number of parameters required by a model to fit a given dataset, such as the Akaike (1974) Information Criterion that was used in Chapter 5. One could check whether or not these methods agree with our human-supervised selection of “physically motivated” model components. Our structural analysis of galaxies confirmed the usefulness of a joint photometric-kinematic approach, especially when extended (i.e. $> 1R_e$, Arnold et al. 2014) kinematic maps are available. Future galaxy decomposition studies will be able to take advantage from the large datasets of on-going Integral Field Spectroscopy surveys (e.g. SAMI, Croom et al. 2012, and MaNGA, Law & MaNGA Team 2014). Finally, we note that Ciambur (2015) recently developed the IRAF task `isofit`, which allows the user to perform a more sophisticated isophotal analysis of galaxies than the task `ellipse` in the presence of an inclined disc. Our isophotal analysis was carried out before `isofit` was conceived or available, but future studies will be able to use it.

In Chapter 4 (Savorgnan et al., 2016), we used our dataset to derive and explore the $M_{\text{BH}} - L_{\text{gal}}$ and $M_{\text{BH}} - L_{\text{sph}}$ (or $M_{\text{BH}} - M_{*,\text{sph}}$) diagrams. When considering all galaxies, irrespective of their morphological type, the $M_{\text{BH}} - L_{\text{sph}}$ correlation has a lower level of intrinsic scatter than the $M_{\text{BH}} - L_{\text{gal}}$ correlation. However, when considering only early-type galaxies (elliptical+lenticular), L_{gal} and L_{sph} correlate equally well with M_{BH} . Läsker et al. (2014b) found the same level of intrinsic scatter in their $M_{\text{BH}} - L_{\text{gal}}$ and $M_{\text{BH}} - L_{\text{sph}}$ diagrams for all galaxies because their sample was highly biased towards early-type objects (among their 35 galaxies, only four are spirals). Our subsample of Sérsic spheroids defines a less steep $M_{\text{BH}} - L_{\text{sph}}$ sequence (with a log-slope of 1.53 ± 0.20) than previously reported (2.73 ± 0.55 , Graham & Scott 2013). Looking at the spheroids with Sérsic index $n_{\text{sph}} < 2$, we did not observe any systematic offset from the $M_{\text{BH}} - L_{\text{sph}}$ correlation traced by spheroids with $n_{\text{sph}} > 2$, in disagreement with the claims of Sani et al. (2011). However, this might be due to our sample selection and this result might change once reasonable number of galaxies with low-mass black holes ($M_{\text{BH}} \lesssim 10^6 M_\odot$) will be added to the $M_{\text{BH}} - L_{\text{sph}}$ diagram (see Ciambur et al. *in preparation*). We identified two distinct trends in the $M_{\text{BH}} - M_{*,\text{sph}}$ diagram, that is, a *red sequence* of early-type (elliptical+lenticular) galaxies following $M_{\text{BH}} \propto M_{*,\text{sph}}^{1.04 \pm 0.10}$ and a dramatically steeper *blue sequence* of late-type (spiral) galaxies following $M_{\text{BH}} \propto M_{*,\text{sph}}^{2-3}$. This is in agreement with the near-linear $M_{\text{BH}} - L_{\text{sph}}$ (or $M_{\text{BH}} - M_{*,\text{sph}}$) correlation measured by previous studies that used galaxy samples dominated by high-mass early-type objects (e.g. Magorrian et al. 1998; Marconi & Hunt 2003;

Häring & Rix 2004; Gültekin et al. 2009; Sani et al. 2011; Beifiori et al. 2012; Erwin & Gadotti 2012; Vika et al. 2012), and it gives reason as to why other studies, whose galaxy samples gave a better representation of the late-type population with low-mass ($M_{\text{BH}} \lesssim 10^8 M_{\odot}$) black holes, obtained a correlation steeper than linear or noticed super-linear deviations at the low-luminosity end of the diagram (e.g. Laor 1998, 2001; Wandel 1999; Salucci et al. 2000; Ryan et al. 2007). An interesting exception has been the under-linear $M_{\text{BH}} \propto L_{\text{sph}}^{0.75 \pm 0.10}$ relation measured by Läske et al. (2014b), who attributed the smaller log-slope of the correlation to the reduction of bulge luminosities derived from their multicomponents fits and to the type of linear regression algorithm used. It is worth mentioning that, among our 17 spiral galaxies, at least 12 host a Seyfert nucleus. Wandel (1999) and Ryan et al. (2007) had previously noted that a linear $M_{\text{BH}} - M_{*,\text{sph}}$ relation systematically overestimates the $M_{\text{BH}}/M_{*,\text{sph}}$ ratio in Seyfert galaxies. In effect, the sample of ≈ 140 low-redshift AGNs with virial black hole masses $10^5 \lesssim M_{\text{BH}}/M_{\odot} \lesssim 2 \times 10^6$ collected by Graham & Scott (2015) appears to be the low-mass continuation of the $M_{\text{BH}} - M_{*,\text{sph}}$ sequence traced by our spiral galaxies. Finally, we note that our estimate of the normalization of the $M_{\text{BH}} - M_{*,\text{sph}}$ relation for early-type galaxies is the largest ever reported: $M_{\text{BH}}/M_{*,\text{sph}}$ is $\approx 0.7\%$ using our dataset, whereas it is as low as $\approx 0.5\%$ in Scott et al. (2013) and Kormendy & Ho (2013), and even lower in previous studies. A recalibration of the $M_{\text{BH}} - M_{*,\text{sph}}$ normalization has important consequences for semi-analytical models and simulations of galaxy evolution that include black hole growth, and it also affects calculations of gravitational waves background from SMBH binary coalescence (e.g. Shannon et al. 2015; Shankar et al. 2016). However, it is important to keep in mind the warnings of Merritt (2013a; see also Ferrarese & Merritt 2000; Merritt & Ferrarese 2001b,a; Valluri et al. 2004; Ferrarese & Ford 2005), who cautioned that the majority of stellar-dynamics based black hole mass measurements are likely to have been overestimated by a factor of 3 to 4 due to an insufficient spatial resolution of the sphere-of-influence of black holes. His concern seems to be confirmed by the very recent findings of Shankar et al. (2016), who argued that the current sample of directly measured black hole masses is highly biased by the fact that their detectability is subject to the requirement of spatially resolve their gravitational sphere-of-influence. This selection effect allows us to see only the upper envelope of the “true” black hole mass correlations, artificially increasing the normalization of the $M_{\text{BH}} - \sigma_*$ correlation by a factor of ≈ 3 and even more dramatically that of the $M_{\text{BH}} - M_{*,\text{sph}}$ correlation. New black hole mass measurements obtained with the extraordinary spatial resolution of the next generation 30-meter class telescopes will help shed light on this

point.

In Chapter 5 (Savorgnan, 2016), we analysed the $L_{\text{sph}} - n_{\text{sph}}$ and $M_{\text{BH}} - n_{\text{sph}}$ diagrams and found that in the former early- and late-type galaxies split into two separate correlations, whereas in the latter relation all galaxies – irrespective of their morphological type – define a single correlation. Our $M_{\text{BH}} - L_{\text{sph}}$ and $M_{\text{BH}} - n_{\text{sph}}$ diagrams show consistent amount of intrinsic scatter, in agreement with the results from Graham & Driver (2007a). The present dataset allows one to explore also the correlation of black hole mass with spheroid central surface density, $\mu_{0,\text{sph}}$, and spheroid deprojected central stellar density, $\rho_{*,0,\text{sph}}$.

In Chapter 6, we focused on the $M_{\text{BH}} - \sigma_*$ diagram and in particular on the over-massive black holes that have been reported to exist at the high-mass end of the correlation. Volonteri & Ciotti (2013) explained the presence of the outlying black holes as a natural consequence of the fact that their host Central Cluster Galaxies (CCGs) have experienced more dry mergers than any other galaxy, since dry mergers are expected to increase the black hole mass and “conserve” the stellar velocity dispersion. We tested and disproved this scenario for 23 core-Sérsic galaxies, using the ratio between black hole mass and stellar mass deficit as a proxy for the number of dry mergers experienced by a galaxy (Merritt, 2006b). This was confirmed by a second test using the central kinematic classification of 37 galaxies. Our analysis suggests that the merger history of the CCGs hosting over-massive black holes in the $M_{\text{BH}} - \sigma_*$ diagram is not exceptional, therefore these galaxies should be considered as legitimate members of the $M_{\text{BH}} - \sigma_*$ correlation. An alternative possibility for the CCGs is that their partially depleted cores have been replenished by stars, globular clusters and nuclear star clusters acquired from minor dry mergers, where the accreted satellite galaxies did not host a massive black hole. However, high-resolution cosmological simulations seem to favour an “inside-out” formation scenario for early-type galaxies, where minor mergers only contribute to the build-up of the external envelope of high-mass galaxies (e.g. Wellons et al. 2016). It should also be noted that evidence is accumulating against the “naive” assumption that low-mass galaxies do not host any central massive black hole (e.g. Baldassare et al. 2015; Graham et al. 2016a).

Finally, in Chapter 7, we tackled the issue of the over-massive black holes in the $M_{\text{BH}} - M_{*,\text{sph}}$ diagram. We showed that the intermediate-scale discs of the galaxies Mrk 1216 (Yıldırım et al.,

2015), NGC 1271 (Walsh et al., 2015), NGC 1277 (van den Bosch et al., 2012), and NGC 1332 (Rusli et al., 2011) had been confused with large-scale discs and incorrectly modelled as such. This led to a considerable underestimation of their spheroid luminosity, which caused them to appear as extreme outliers above the $M_{\text{BH}} - M_{*,\text{sph}}$ correlation of local early-type galaxies. Furthermore, at least one of these galaxies had its black hole mass overestimated by one order of magnitude (NGC 1277, e.g. Graham et al. 2016b). Graham et al. (2015) showed that, while the majority of the high-redshift compact massive spheroids have evolved into today's bulges of lenticular and early-type spiral galaxies (see also Graham 2013), i.e. they have accreted a large-scale stellar disc, a few of them (such as Mrk 1216, NGC 1271, NGC 1277, NGC 1332, and NGC 3115) have only accreted an intermediate-scale stellar disc. The spheroidal components of the galaxies Mrk 1216, NGC 1271, NGC 1277, NGC 1332, and NGC 3115 have the same structural properties (compactness), stellar mass ($\approx 10^{11} M_{\odot}$), high stellar velocity dispersion ($\approx 300 \text{ km s}^{-1}$) and purely old stellar population as the $z \approx 2$ compact massive spheroids (e.g. Daddi et al. 2005; Trujillo et al. 2006; van Dokkum et al. 2008; Damjanov et al. 2009), i.e. they experienced negligible evolution over the last 10 Gyr. If also their black holes have had little or no mass accretion since $z = 2$, assuming that the $M_{\text{BH}} - M_{*,\text{sph}}$ relation was already in place 10 Gyr ago, these five spheroids provides us with a fossil record of the correlation at $z = 2$. The fact that the five spheroids lie within $\lesssim 1\sigma$ above the $z = 0$ correlation can be used as a constraint for the evolution with redshift of the $M_{\text{BH}} - M_{*,\text{sph}}$ normalization (assuming no evolution with redshift of the log-slope of the correlation). Furthermore, knowing that their intermediate-scale discs have been accreted over the last 10 Gyr and that their disc-to-total ratios are typically small ($\lesssim 20\%$), one can deduce that the location of these five galaxies in the $M_{\text{BH}} - M_{*,\text{gal}}$ diagram (where $M_{*,\text{gal}}$ is the galaxy stellar mass) is roughly the same as that at $z = 2$. Therefore, finding a larger number of local galaxies with the same characteristics as the aforementioned five would be helpful to study the redshift evolution of the $M_{\text{BH}} - M_{*,\text{sph}}$ and $M_{\text{BH}} - M_{*,\text{gal}}$ relations. The Hobby-Eberly Telescope Massive Galaxy Survey (HETMGS, van den Bosch et al. 2015) has identified a few of these rare objects such as Mrk 1216, NGC 1271, NGC 1277, and NGC 1281 (Yıldırım et al., 2016), although the last galaxy still lacks an accurate photometric decomposition; more of them might be yet to be found in the HETMGS database. Saulder et al. (2015) selected 76 compact massive galaxies with high stellar velocity dispersion within $0.05 < z < 0.2$ from the Sloan Digital Sky Survey (SDSS, Abazajian et al. 2009) and proposed them as candidate survivors of the $z = 2$ compact massive spheroids.

However, it should be noted that their criterion of high mass and compactness relies on the *galaxy* properties rather than the *spheroid* properties, therefore a number of these candidates might not be real descendants of the $z = 2$ population¹. The same concern holds for the simulated compact massive galaxies of Wellons et al. (2016). It would be interesting to perform photometric decompositions for the observed 76 compact massive galaxies of Saulder et al. (2015) and for those simulated by Wellons et al. (2016), to select only those with compact massive *spheroids*. Kormendy et al. (2011) and Kormendy & Ho (2013) argued that black holes correlate only with the remnants of major mergers, i.e. classical bulges and elliptical galaxies, and that the growth of the most massive black holes happened by means of a co-evolution with their host galaxies via a series of mergers and AGN feedback. The universality of this picture is contradicted by galaxies like Mrk 1216, NGC 1271, NGC 1277, NGC 1332, and NGC 3115. These galaxies have classical bulges and host some of the most massive black holes known ($10^9 \lesssim M_{\text{BH}}/\text{M}_{\odot} \lesssim 10^{10}$), but they are not the product of major mergers like the majority of today's massive elliptical galaxies. In effect, these galaxies have conserved their 10 Gyr old compact massive spheroids because they had little or no evolution since $z \approx 2$; note that $z \approx 3$ is the epoch that corresponds to the highest cosmic merger rate for galaxies more massive than $10^{10} \text{ M}_{\odot}$ (e.g. Conselice et al. 2008).

Keep looking up.

¹Some candidates might be lenticular galaxies with compact *galaxy* sizes and large disc-to-total ratios, therefore their spheroids would be significantly less massive than the $z = 2$ red nuggets.

Bibliography

- Abazajian, K. N., Adelman-McCarthy, J. K., Agüeros, M. A., et al. 2009, ApJS, 182, 543
- Akaike, H. 1974, Automatic Control, IEEE Transactions, 19, 716
- Akritas, M. G., & Bershady, M. A. 1996, ApJ, 470, 706
- Alexander, T., & Natarajan, P. 2014, Science, 345, 1330
- Aller, M. C., & Richstone, D. O. 2007, ApJ, 665, 120
- Andredakis, Y. C., Peletier, R. F., & Balcells, M. 1995, MNRAS, 275, 874
- Arnold, J. A., Romanowsky, A. J., Brodie, J. P., et al. 2014, ApJ, 791, 80
- Bañados, E., Venemans, B. P., Morganson, E., et al. 2014, AJ, 148, 14
- Baldassare, V. F., Reines, A. E., Gallo, E., & Greene, J. E. 2015, ApJL, 809, L14
- Begelman, M. C., Blandford, R. D., & Rees, M. J. 1980, Nature, 287, 307
- Beifiori, A., Courteau, S., Corsini, E. M., & Zhu, Y. 2012, MNRAS, 419, 2497
- Berrier, J. C., Davis, B. L., Kennefick, D., et al. 2013, ApJ, 769, 132
- Bogdán, Á., Forman, W. R., Zhuravleva, I., et al. 2012, ApJ, 753, 140
- Buitrago, F., Trujillo, I., Conselice, C. J., et al. 2008, ApJL, 687, L61
- Burkert, A., & Tremaine, S. 2010, ApJ, 720, 516

- Caon, N., Capaccioli, M., & D'Onofrio, M. 1993, MNRAS, 265, 1013
- Cappellari, M., Emsellem, E., Krajnović, D., et al. 2011, MNRAS, 413, 813
- Carollo, C. M., Cibinel, A., Lilly, S. J., et al. 2014, ArXiv e-prints, arXiv:1402.1172
- Carr, B. J., & Hawking, S. W. 1974, MNRAS, 168, 399
- Carrasco, E. R., Conselice, C. J., & Trujillo, I. 2010, MNRAS, 405, 2253
- Carter, D. 1987, ApJ, 312, 514
- Ciambur, B. C. 2015, ApJ, 810, 120
- Cimatti, A., Nipoti, C., & Cassata, P. 2012, MNRAS, 422, 62
- Cinzano, P., & van der Marel, R. P. 1993, in European Southern Observatory Conference and Workshop Proceedings, ed. I. J. Danziger, W. W. Zeilinger, & K. Kjär, Vol. 45, 105
- Ciotti, L., Lanzoni, B., & Volonteri, M. 2007, ApJ, 658, 65
- Clark, P. C., Glover, S. C. O., Klessen, R. S., & Bromm, V. 2011, ApJ, 727, 110
- Colpi, M. 2014, Space Science Reviews, 183, 189
- Colpi, M., Callegari, S., Dotti, M., & Mayer, L. 2009, Classical and Quantum Gravity, 26, 094029
- Conselice, C. J., Rajgor, S., & Myers, R. 2008, MNRAS, 386, 909
- Croom, S. M., Lawrence, J. S., Bland-Hawthorn, J., et al. 2012, MNRAS, 421, 872
- Croton, D. J., Springel, V., White, S. D. M., et al. 2006, MNRAS, 365, 11
- Daddi, E., Renzini, A., Pirzkal, N., et al. 2005, ApJ, 626, 680
- Damjanov, I., McCarthy, P. J., Abraham, R. G., et al. 2009, ApJ, 695, 101
- Davies, R. L., Efstathiou, G., Fall, S. M., Illingworth, G., & Schechter, P. L. 1983, ApJ, 266, 41
- De, T., Chattopadhyay, T., & Chattopadhyay, A. K. 2014, PASA, 31, e047

- de Jong, R. S. 1996, A&AS, 118, 557
- de Souza, R. E., Gadotti, D. A., & dos Anjos, S. 2004, ApJS, 153, 411
- de Vaucouleurs, G. 1948, Annales d'Astrophysique, 11, 247
- D'Onofrio, M., Capaccioli, M., & Caon, N. 1994, MNRAS, 271, 523
- D'Onofrio, M., Zaggia, S. R., Longo, G., Caon, N., & Capaccioli, M. 1995, A&A, 296, 319
- Dotti, M., Sesana, A., & Decarli, R. 2012, Advances in Astronomy, 2012, 940568
- Dressler, A. 1989, in IAU Symposium, Vol. 134, Active Galactic Nuclei, ed. D. E. Osterbrock & J. S. Miller, 217
- Driver, S. P., Robotham, A. S. G., Bland-Hawthorn, J., et al. 2013, MNRAS, 430, 2622
- Dullo, B. T., & Graham, A. W. 2014, MNRAS, 444, 2700
- Einstein, A. 1915, Sitzungsberichte der Königlich Preußischen Akademie der Wissenschaften (Berlin), Seite, 844
- . 1939, Annals of Mathematics, 40, 922
- Emsellem, E. 2013, MNRAS, 433, 1862
- Emsellem, E., Cappellari, M., Krajnović, D., et al. 2007, MNRAS, 379, 401
- . 2011, MNRAS, 414, 888
- Erwin, P. 2015, ApJ, 799, 226
- Erwin, P., & Gadotti, D. A. 2012, Advances in Astronomy, 2012, 4
- Erwin, P., & Sparke, L. S. 2003, ApJS, 146, 299
- Faber, S. M., Dressler, A., Davies, R. L., Burstein, D., & Lynden-Bell, D. 1987, in Nearly Normal Galaxies. From the Planck Time to the Present, ed. S. M. Faber, 175–183
- Fabian, A. C. 1999, MNRAS, 308, L39
- . 2012, ARAA, 50, 455

- Fabian, A. C., Iwasawa, K., Reynolds, C. S., & Young, A. J. 2000, PASP, 112, 1145
- Fabricius, M. H., Coccato, L., Bender, R., et al. 2014, MNRAS, 441, 2212
- Fan, L., Fang, G., Chen, Y., et al. 2013, ApJL, 771, L40
- Fan, X., Strauss, M. A., Schneider, D. P., et al. 2003, AJ, 125, 1649
- Feoli, A., & Mancini, L. 2009, ApJ, 703, 1502
- Feoli, A., & Mele, D. 2005, International Journal of Modern Physics D, 14, 1861
- Ferrarese, L. 2002, ApJ, 578, 90
- . 2006, Observational Evidence for Supermassive Black Holes, ed. F. Haardt, V. Gorini, U. Moschella, & M. Colpi, 1–62
- Ferrarese, L., & Ford, H. 2005, Space Science Reviews, 116, 523
- Ferrarese, L., & Merritt, D. 2000, ApJL, 539, L9
- Ferré-Mateu, A., Mezcua, M., Trujillo, I., Balcells, M., & van den Bosch, R. C. E. 2015, ApJ, 808, 79
- Franx, M., Illingworth, G., & Heckman, T. 1989, ApJ, 344, 613
- Gadotti, D. A. 2008, MNRAS, 384, 420
- Gaskell, C. M. 2010, in American Institute of Physics Conference Series, Vol. 1294, American Institute of Physics Conference Series, ed. D. J. Whalen, V. Bromm, & N. Yoshida, 261–261
- Gebhardt, K., & Thomas, J. 2009, ApJ, 700, 1690
- Gebhardt, K., Bender, R., Bower, G., et al. 2000, ApJL, 539, L13
- Genzel, R., Eisenhauer, F., & Gillessen, S. 2010, Reviews of Modern Physics, 82, 3121
- Gerhard, O. E., & Binney, J. J. 1996, MNRAS, 279, 993
- Ghez, A. M., Salim, S., Weinberg, N. N., et al. 2008, ApJ, 689, 1044
- Graham, A. W. 2007, MNRAS, 379, 711

- . 2012, ApJ, 746, 113
- . 2013, Elliptical and Disk Galaxy Structure and Modern Scaling Laws, ed. T. D. Oswalt & W. C. Keel, 91
- . 2016a, Galactic Bulges, 418, 263
- . 2016b, Galactic Bulges, 418, 263
- Graham, A. W., Ciambur, B. C., & Soria, R. 2016a, ApJ, 818, 172
- Graham, A. W., Colless, M. M., Busarello, G., Zaggia, S., & Longo, G. 1998, A&AS, 133, 325
- Graham, A. W., & Driver, S. P. 2005, PASA, 22, 118
- . 2007a, ApJ, 655, 77
- . 2007b, MNRAS, 380, L15
- Graham, A. W., Driver, S. P., Allen, P. D., & Liske, J. 2007, MNRAS, 378, 198
- Graham, A. W., Dullo, B. T., & Savorgnan, G. A. D. 2015, ApJ, 804, 32
- Graham, A. W., Durré, M., Savorgnan, G. A. D., et al. 2016b, ApJ, 819, 43
- Graham, A. W., Erwin, P., Caon, N., & Trujillo, I. 2001, ApJL, 563, L11
- Graham, A. W., Erwin, P., Trujillo, I., & Asensio Ramos, A. 2003, AJ, 125, 2951
- Graham, A. W., & Guzmán, R. 2003, AJ, 125, 2936
- Graham, A. W., & Prieto, M. 1999, Ap&SS, 269, 653
- Graham, A. W., & Scott, N. 2013, ApJ, 764, 151
- . 2015, ApJ, 798, 54
- Graham, A. W., & Worley, C. C. 2008, MNRAS, 388, 1708
- Greif, T. H., Springel, V., White, S. D. M., et al. 2011, ApJ, 737, 75
- Gültekin, K., Richstone, D. O., Gebhardt, K., et al. 2009, ApJ, 698, 198
- Häring, N., & Rix, H.-W. 2004, ApJL, 604, L89

- Heger, A., Fryer, C. L., Woosley, S. E., Langer, N., & Hartmann, D. H. 2003, ApJ, 591, 288
- Hirschmann, M., Khochfar, S., Burkert, A., et al. 2010, MNRAS, 407, 1016
- Ho, L. C., Filippenko, A. V., & Sargent, W. L. W. 1997, ApJS, 112, 315
- Hopkins, P. F., Bundy, K., Murray, N., et al. 2009, MNRAS, 398, 898
- Jahnke, K., & Macciò, A. V. 2011, ApJ, 734, 92
- Jiang, L., Fan, X., Vestergaard, M., et al. 2007, AJ, 134, 1150
- Jiang, Y.-F., Greene, J. E., & Ho, L. C. 2011, ApJL, 737, L45
- Kautsch, S. J., Grebel, E. K., Barazza, F. D., & Gallagher, III, J. S. 2006, A&A, 445, 765
- Kelly, B. C. 2007, ApJ, 665, 1489
- Khochfar, S., & Burkert, A. 2006, A&A, 445, 403
- Khosroshahi, H. G., Wadadekar, Y., & Kembhavi, A. 2000, ApJ, 533, 162
- Kormendy, J. 1982, ApJ, 257, 75
- Kormendy, J., Bender, R., & Cornell, M. E. 2011, Nature, 469, 374
- Kormendy, J., & Ho, L. C. 2013, ARAA, 51, 511
- Kormendy, J., & Kennicutt, Jr., R. C. 2004, ARAA, 42, 603
- Kormendy, J., & Richstone, D. 1995, ARAA, 33, 581
- Krajnović, D. 2015, in IAU Symposium, Vol. 311, IAU Symposium, ed. M. Cappellari & S. Courteau, 45–48
- Krajnović, D., Cappellari, M., de Zeeuw, P. T., & Copin, Y. 2006, MNRAS, 366, 787
- Krajnović, D., Emsellem, E., Cappellari, M., et al. 2011, MNRAS, 414, 2923
- Krajnović, D., Alatalo, K., Blitz, L., et al. 2013, MNRAS, 432, 1768
- Kriek, M., van Dokkum, P. G., Franx, M., et al. 2008, ApJ, 677, 219
- Laor, A. 1998, ApJL, 505, L83

- . 2001, ApJ, 553, 677
- Läsker, R., Ferrarese, L., & van de Ven, G. 2014a, ApJ, 780, 69
- Läsker, R., Ferrarese, L., van de Ven, G., & Shankar, F. 2014b, ApJ, 780, 70
- Lauer, T. R., Faber, S. M., Richstone, D., et al. 2007, ApJ, 662, 808
- Laurikainen, E., Peletier, R., & Gadotti, D. 2016, Galactic Bulges, 418, doi:10.1007/978-3-319-19378-6
- Laurikainen, E., Salo, H., & Buta, R. 2005, MNRAS, 362, 1319
- Laurikainen, E., Salo, H., Buta, R., & Knapen, J. H. 2007, MNRAS, 381, 401
- Laurikainen, E., Salo, H., Buta, R., Knapen, J. H., & Comerón, S. 2010, MNRAS, 405, 1089
- Law, D. R., & MaNGA Team. 2014, in American Astronomical Society Meeting Abstracts, Vol. 223, American Astronomical Society Meeting Abstracts #223, 254.31
- Lupi, A., Haardt, F., Dotti, M., et al. 2016, MNRAS, 456, 2993
- Lynden-Bell, D. 1969, Nature, 223, 690
- . 1978, Phys. Scr, 17, 185
- Madau, P., Haardt, F., & Dotti, M. 2014, ApJL, 784, L38
- Magorrian, J., Tremaine, S., Richstone, D., et al. 1998, AJ, 115, 2285
- Malin, D. F., & Zealey, W. J. 1979, Sky and Telescope, 57, 354
- Malkan, M. A. 1983, ApJ, 268, 582
- Maller, A. H., Katz, N., Kereš, D., Davé, R., & Weinberg, D. H. 2006, ApJ, 647, 763
- Marconi, A., & Hunt, L. K. 2003, ApJL, 589, L21
- Matković, A., & Guzmán, R. 2005, MNRAS, 362, 289
- Mayer, L. 2009, in APS April Meeting Abstracts
- McConnell, N. J., Ma, C.-P., Gebhardt, K., et al. 2011, Nature, 480, 215

- McConnell, N. J., Ma, C.-P., Murphy, J. D., et al. 2012, ApJ, 756, 179
- McLure, R. J., Pearce, H. J., Dunlop, J. S., et al. 2013, MNRAS, 428, 1088
- McNamara, B. R., & Nulsen, P. E. J. 2012, New Journal of Physics, 14, 055023
- Melia, F., & McClintock, T. M. 2015, ArXiv e-prints, arXiv:1511.05494
- Merritt, D. 2006a, Reports on Progress in Physics, 69, 2513
- . 2006b, ApJ, 648, 976
- . 2013a, Dynamics and Evolution of Galactic Nuclei
- . 2013b, Classical and Quantum Gravity, 30, 244005
- Merritt, D., & Ferrarese, L. 2001a, in Astronomical Society of the Pacific Conference Series, Vol. 249, The Central Kiloparsec of Starbursts and AGN: The La Palma Connection, ed. J. H. Knapen, J. E. Beckman, I. Shlosman, & T. J. Mahoney, 335
- Merritt, D., & Ferrarese, L. 2001b, ApJ, 547, 140
- Michard, R. 1984, A&A, 140, L39
- Miller, M. C., & Colbert, E. J. M. 2004, International Journal of Modern Physics D, 13, 1
- Milosavljević, M., & Merritt, D. 2001, ApJ, 563, 34
- Miyoshi, M., Moran, J., Herrnstein, J., et al. 1995, Nature, 373, 127
- Montgomery, C., Orchiston, W., & Whittingham, I. 2009, Journal of Astronomical History and Heritage, 12, 90
- Moriondo, G., Giovanardi, C., & Hunt, L. K. 1998, A&AS, 130, 81
- Mortlock, D. J., Warren, S. J., Venemans, B. P., et al. 2011, Nature, 474, 616
- Naab, T., Johansson, P. H., & Ostriker, J. P. 2009, ApJL, 699, L178
- Nesvadba, N. P. H., Lehnert, M. D., Eisenhauer, F., et al. 2006, ApJ, 650, 693
- Nieto, J.-L., Bender, R., Arnaud, J., & Surma, P. 1991, A&A, 244, L25

- Nieto, J.-L., Capaccioli, M., & Held, E. V. 1988, A&A, 195, L1
- Novak, G. S., Faber, S. M., & Dekel, A. 2006, ApJ, 637, 96
- Ostriker, J. P., & Ciotti, L. 2005, Royal Society of London Philosophical Transactions Series A, 363, 667
- Park, D., Kelly, B. C., Woo, J.-H., & Treu, T. 2012, ApJS, 203, 6
- Pasham, D. R., Strohmayer, T. E., & Mushotzky, R. F. 2014, Nature, 513, 74
- Peng, C. Y. 2007, ApJ, 671, 1098
- Peng, C. Y., Ho, L. C., Impey, C. D., & Rix, H.-W. 2002, AJ, 124, 266
- . 2010, AJ, 139, 2097
- Peterson, B. M. 1993, PASP, 105, 247
- Pota, V., Graham, A. W., Forbes, D. A., et al. 2013, MNRAS, 433, 235
- Press, W. H., Teukolsky, S. A., Vetterling, W. T., & Flannery, B. P. 1992, Numerical recipes in FORTRAN. The art of scientific computing
- Reynolds, C. S., & Nowak, M. A. 2003, Physics Reports, 377, 389
- Richstone, D., Ajhar, E. A., Bender, R., et al. 1998, Nature, 395, A14
- Rix, H.-W., & White, S. D. M. 1990, ApJ, 362, 52
- . 1992, MNRAS, 254, 389
- Rusli, S. P., Thomas, J., Erwin, P., et al. 2011, MNRAS, 410, 1223
- Rusli, S. P., Thomas, J., Saglia, R. P., et al. 2013, AJ, 146, 45
- Ryan, C. J., De Robertis, M. M., Virani, S., Laor, A., & Dawson, P. C. 2007, ApJ, 654, 799
- Sadoun, R., & Colin, J. 2012, MNRAS, 426, L51
- Salo, H., Laurikainen, E., Laine, J., et al. 2015, ApJS, 219, 4
- Salpeter, E. E. 1964, ApJ, 140, 796

- Salucci, P., Ratnam, C., Monaco, P., & Danese, L. 2000, MNRAS, 317, 488
- Salucci, P., Szuszkiewicz, E., Monaco, P., & Danese, L. 1999, MNRAS, 307, 637
- Sani, E., Marconi, A., Hunt, L. K., & Risaliti, G. 2011, MNRAS, 413, 1479
- Saulder, C., van den Bosch, R. C. E., & Mieske, S. 2015, A&A, 578, A134
- Savorgnan, G., Graham, A. W., Marconi, A., et al. 2013, MNRAS, 434, 387
- Savorgnan, G. A. D. 2016, ArXiv e-prints, arXiv:1603.01910
- Savorgnan, G. A. D., & Graham, A. W. 2015, MNRAS, 446, 2330
- . 2016a, MNRAS, 457, 320
- . 2016b, ApJS, 222, 10
- Savorgnan, G. A. D., Graham, A. W., Marconi, A., & Sani, E. 2016, ApJ, 817, 21
- Scharwächter, J., Combes, F., Salomé, P., Sun, M., & Krips, M. 2016, MNRAS, 457, 4272
- Scott, N., Davies, R. L., Houghton, R. C. W., et al. 2014, MNRAS, 441, 274
- Scott, N., Graham, A. W., & Schombert, J. 2013, ApJ, 768, 76
- Seigar, M. S., Kennefick, D., Kennefick, J., & Lacy, C. H. S. 2008, ApJL, 678, L93
- Sérsic, J. L. 1963, Boletin de la Asociacion Argentina de Astronomia La Plata Argentina, 6, 41
- . 1968, Atlas de galaxias australes
- Shahbaz, T. 1999, Journal of Astrophysics and Astronomy, 20, 197
- Shankar, F., Bernardi, M., Sheth, R. K., et al. 2016, ArXiv e-prints, arXiv:1603.01276
- Shannon, R. M., Ravi, V., Lentati, L. T., et al. 2015, Science, 349, 1522
- Sheth, K., Regan, M., Hinz, J. L., et al. 2010, PASP, 122, 1397
- Shields, G. A. 1978, Nature, 272, 706
- Silk, J., & Rees, M. J. 1998, A&A, 331, L1

- Simard, L. 1998, in Astronomical Society of the Pacific Conference Series, Vol. 145, Astronomical Data Analysis Software and Systems VII, ed. R. Albrecht, R. N. Hook, & H. A. Bushouse, 108
- Simien, F., & de Vaucouleurs, G. 1986, *ApJ*, 302, 564
- Snyder, G. F., Hopkins, P. F., & Hernquist, L. 2011, *ApJL*, 728, L24
- Soltan, A. 1982, *MNRAS*, 200, 115
- Stacy, A., Greif, T. H., & Bromm, V. 2012, *MNRAS*, 422, 290
- Thorne, K. S. 1994, Black holes and time warps: Einstein's outrageous legacy
- Toft, S., van Dokkum, P., Franx, M., et al. 2007, *ApJ*, 671, 285
- Tombesi, F., Cappi, M., Reeves, J. N., & Braito, V. 2012, *MNRAS*, 422, L1
- Trakhtenbrot, B., Urry, C. M., Civano, F., et al. 2015, *Science*, 349, 168
- Tremaine, S., Gebhardt, K., Bender, R., et al. 2002, *ApJ*, 574, 740
- Trujillo, I., Conselice, C. J., Bundy, K., et al. 2007, *MNRAS*, 382, 109
- Trujillo, I., Erwin, P., Asensio Ramos, A., & Graham, A. W. 2004, *AJ*, 127, 1917
- Trujillo, I., Feulner, G., Goranova, Y., et al. 2006, *MNRAS*, 373, L36
- Tundo, E., Bernardi, M., Hyde, J. B., Sheth, R. K., & Pizzella, A. 2007, *ApJ*, 663, 53
- Turk, M. J., Abel, T., & O'Shea, B. 2009, *Science*, 325, 601
- Valluri, M., Merritt, D., & Emsellem, E. 2004, *ApJ*, 602, 66
- van den Bosch, R. C. E., Gebhardt, K., Gültekin, K., et al. 2012, *Nature*, 491, 729
- van den Bosch, R. C. E., Gebhardt, K., Gültekin, K., Yıldırım, A., & Walsh, J. L. 2015, *ApJS*, 218, 10
- van der Marel, R. P. 2004, Coevolution of Black Holes and Galaxies, 37
- van Dokkum, P. G., Franx, M., Kriek, M., et al. 2008, *ApJL*, 677, L5

- Vika, M., Driver, S. P., Cameron, E., Kelvin, L., & Robotham, A. 2012, MNRAS, 419, 2264
- Volonteri, M., & Bellovary, J. 2012, Reports on Progress in Physics, 75, 124901
- Volonteri, M., & Ciotti, L. 2013, ApJ, 768, 29
- Walsh, J. L., van den Bosch, R. C. E., Gebhardt, K., et al. 2015, ApJ, 808, 183
- Wandel, A. 1999, ApJL, 519, L39
- Wellons, S., Torrey, P., Ma, C.-P., et al. 2016, MNRAS, 456, 1030
- Wolfe, A. M., & Burbidge, G. R. 1970, ApJ, 161, 419
- Wu, X.-B., Wang, F., Fan, X., et al. 2015, Nature, 518, 512
- Yıldırım, A., van den Bosch, R. C. E., van de Ven, G., et al. 2015, MNRAS, 452, 1792
- . 2016, MNRAS, 456, 538
- Zel'dovich, Y. B., & Novikov, I. D. 1964, Doklady Akad. Nauk. SSSR, 158, 811
- Zirm, A. W., van der Wel, A., Franx, M., et al. 2007, ApJ, 656, 66

List of publications

In addition to my six lead-author papers that constitute the main body of this thesis, as a result of my PhD project, I participated in the following publications:

- Shankar, F., Bernardi, M., Sheth, R. K., Ferrarese, L., Graham, A. W., **Savorgnan, G. A. D.**, Allevato, V., Marconi, A., Laesker, R., Lapi, A.
Selection bias in dynamically-measured super-massive black hole samples: its consequences and the quest for the most fundamental relation
Submitted to *MNRAS*.
- Graham, A. W., Durré, M., **Savorgnan, G. A. D.**, Medling, A. M., Batcheldor, D., Scott, N., Watson, B., Marconi, A.
A Normal Supermassive Black Hole in NGC 1277
ApJ, 819, 43, 2016.
- Graham, A. W., Dullo, B., **Savorgnan, G. A. D.**
Hiding in Plain Sight: An Abundance of Compact Massive Spheroids in the Local Universe
ApJ, 804, 32. 2015.